ΙΔΡΥΜΑ ΤΕΧΝΟΛΟΓΙΑΣ ΚΑΙ ΕΡΕΥΝΑΣ

Διιδρυματικό Πρόγραμμα Μεταπτυχιακών Σπουδών

«Μοριακή-Κυτταρική Βιολογία και Βιοτεχνολογία»

Biomedical Research Institute BRI-FORTH

Master thesis title:

# "Effect of graphene and graphene oxide on human pluripotent stem cells and vascular cells"

«Διατριβή Μεταπτυχιακής Ειδίκευσης»

Master Student's name: Athanasia Zoi Pappa, Biologist

Supervisors: Carol Murphy and Theodoros Fotsis

University Campus of Ioannina, 45110 Ioannina, Greece, (Carol Murphy's lab, Biomedical Research Institute, Foundation for Research and Technology – Hellas, University of Ioannina).

Ioannina 2022

## Acknowledgments

First and foremost, I am extremely grateful to my supervisors, Dr. Carol Murphy and Prof. Theodoros Fotsis for their invaluable advice, continuous support, and patience during my Master thesis. Their immense knowledge and plentiful experience have encouraged me in all the time of my academic research and daily life. I would like to extend my sincere thanks to Dr. Maria Markou for her assistance at every stage of the research project. Her thoughtful comments and recommendations were crucial for the accomplishment of this dissertation. Moreover, I would like to special thank Dr. Sofia Bellou for her contribution to my thesis with the light sheet microscopy images and our valuable scientific discussions. I would like to offer my special thanks to Dr. Eleni Bagkli for her support on the statistical analysis of the results illustrated in the present thesis. I would like to express my gratitude to Dr. Christos Gkogkas for providing valuable suggestions.

I would like to express my sincere gratitude to Inter-institutional Interdepartmental Program of Postgraduate Studies “Molecular and Cellular Biology and Biotechnology” committee and its coordinator Stathis Frillingos for accepting me as a part of this Master programme.

I would like to thank my friends, lab mates, colleagues and research team – Elena, Manolis, Sofia, Katerina and Aristea for a cherished time spent together in the lab, and in social settings. It is their help and support that have made my study in Ioannina a wonderful time. Finally, my appreciation also goes out to my family and real friends for their encouragement, motivation and support all through my studies. Without their tremendous understanding in the past year, it would be impossible for me to complete my study.

## Index

## *LIST OF FIGURES*

## *LIST OF TABLES*

## *ABBREVIATIONS*

PSC – pluripotent stem cells

hESCs – human embryonic stem cells

hiPSCs – human induced pluripotent stem cells

ASCs – adult stem cells

2D /3D – 2 dimension / 3 dimension

NP – nanoplatelets

SMCs – smooth muscle cells

cSMCs – contractile smooth muscle cells

sSMCs – synthetic smooth muscle cells

VSMCs – vascular smooth muscle cells

ECs – endothelial cells

ADSC – adipose derived stem cell

ECM – extracellular matrix

HUVECs - human umbilical vein endothelial cells

G2, G9 and GO – Graphene type 2, 9 and Graphene oxide

PCL - ε-poly(caprolactone)

PLGA - poly(lactic-co-glycolic) acid

PLA - poly(lactic acid)

VPCs – Vascular Progenitor Cells, $CD34^{+}$VPCs

Lamp1 – Lysosomal-associated membrane protein 1

CD63 – (Lamp 3) Lysosomal-associated membrane protein 3

SMA – smooth muscle actin

***Summary***

The present study constitutes a translational application of graphene nanoplatelets in tissue engineering and regenerative medicine, aiming at developing a graphene containing vascularised brain organoid. Therefore, we focused on the effect of graphene on the cell types which would constitute the vascularised organoid. The cells were: human pluripotent stem cells (PSCs, H1), pluripotent stem cells differentiated to vascular progenitor cells ($CD34^+$VPCs), ECs (umbilicial vein ECs, HUVECs) and mural cells (vascular smooth muscle cells, VSMCs). The role of graphene on neural cells was not addressed in this study.

An initial screening of 9 types of graphene, differing in diameter, was performed using HUVECs to select the optimum graphene nanoparticle size and surface area. HUVECs were selected as we considered them to be a very sensitive cell type. Following the screening, three graphene types were selected for analysis in the other cell types mentioned above, graphene 30 micron (G2), 1.5 micron (G9) and graphene oxide (GO). The reasoning behind the choice of graphene size was that the 1.5 micron and 30 micron nanoparticle were devoid of side effects on proliferation, in addition the 30 micron size would not be internalised avoiding potential damage to intracellular organelles and being more of a scaffold to which cells might attach. GO offers an altered surface charge and a wide range of nanoparticle sizes.

The 3 graphene types selected (G2, G9 and GO) were then tested regarding their effects on the proliferation of PSCs, $CD34^+$VPCs and VSMCs cells. Our results indicated that 1 μg/ml of G2, G9 and GO did not alter cell proliferation, even though the $CD34^+$ VPCs showed some sensitivity at this concentration. Likewise, the same concentration of graphenes did not alter the pluripotency marker OCT3/4 and did not affect the differentiation of H1 hPSCs to $CD34^+$VPCs. With respect to VSMCs, we have developed a differentiation protocol that generates synthetic (sSMCs) and contractile (cSMCs) phenotypes. These phenotypes were stable in 1 μg/ml of G2, G9 and GO undergoing no transition between phenotypes when analysed using the appropriate markers (a-SMA, calponin and SM22). Testing graphene nanomaterials in more complex assays indicated that G2 nanoplatelets did not internalise, as expected, whereas the G9 and GO ones did and were identified in lysosomes that appeared to be not compromised, however this requires more experiments. Regarding other assays, G2, G9 and GO did not alter vascular organoid formation at 1 μg/ml, whereas functional analysis of vascular organoids sprouting (sSMCs/ $CD34^+$VPCs and cSMCs / $CD34^+$VPCs), revealed that graphene bears an angiogenic potential since it increased the number, length, and network depth of the developing sprouts.

In conclusion, based on the above results, and the fact that we consider it better to select a graphene type which is not internalised, the optimal graphene type and size that should be further used is type 2 (30μm diameter) at 1 μg/ml.

## *Περίληψη*

Η παρούσα εργασία αποτελεί μια μελέτη της εφαρμογής των νανοσωματιδίων γραφενίου στη μηχανική των ιστών και την αναγεννητική ιατρική με σκοπό την ανάπτυξη ενός αγγειοποιημένου οργανοειδούς εγκεφάλου που περιλαμβάνει γραφένιο. Γι' αυτό το λόγο, εστιάσαμε στην επίδραση του γραφενίου στις επιμέρους κυτταρικές σειρές που απαρτίζουν το αγγειοποιημένο οργανοειδές. Τα κύτταρα που χρησιμοποιήσαμε ήταν τα εξής: πολυδύναμα ανθρώπινα βλαστικά κύτταρα (PSCs, H1), πολυδύναμα βλαστικά διαφοροποιημένα προς ανώριμα ενδοθηλιακά (CD34+ κύτταρα), ώριμα ενδοθηλιακά (HUVECs) και τοιχωματικά κύτταρα (αγγειακά λεία μυϊκά κύτταρα, VSMCs). Ο ρόλος του γραφενίου στα νευρικά κύτταρα δεν διερευνήθηκε σε αυτή τη μελέτη.

Με σκοπό την επιλογή των κατάλληλων τύπων γραφενίου που θα εξεταστούν περαιτέρω στην παρούσα εργασία, πραγματοποιήσαμε μία διαλογή 9 τύπων γραφενίου, που διέφεραν σε ειδική επιφάνεια και διάμετρο, και στη συνέχεια τα προσθέσαμε σε καλλιέργεια ώριμων ενδοθηλιακών κυττάρων. Από τη διαλογή, καταλήξαμε σε 3 τύπους, τύπος 2 (30 μm διάμετρος-G2), τύπος 9 (1.5 μm διάμετρος-G9) και οξείδιο του γραφενίου (GO), βασιζόμενοι στην ανασταλτική τους δράση ως προς τον κυτταρικό πολλαπλασιασμό των παραπάνω κυτταρικών σειρών.

Οι τρεις τύποι γραφενίου που επιλέχθηκαν (G2, G9 and GO) δοκιμάστηκαν στη συνέχεια ως προς την επίδρασή τους στον κυτταρικό πολλαπλασιασμό των PSCs, CD34+ και VSMCs κυττάρων. Τα αποτελέσματά μας έδειξαν ότι η συγκέντρωση 1 μg/ml των G2, G9 and GO δεν είχε αρνητική επίδραση αν και τα CD34+ κύτταρα έδειξαν κάποια ευαισθησία ως προς αυτή τη συγκέντρωση. Αντίστοιχα, η ίδια συγκέντρωση των G2, G9 and GO δεν επηρέασε την έκφραση του δείκτη πολυδυναμίας OCT3/4 αλλά ούτε και τη διαφοροποίηση των H1 hPSCs προς CD34+ cells. Αναφορικά με τα VSMCs, αναπτύξαμε ένα πρωτόκολλο διαφοροποίησης για την παραγωγή συνθετικών (sSMCs) και συσταλτών (cSMCs) φαινοτύπων. Αυτοί οι φαινότυποι παρέμειναν σταθεροί στο 1 μg/ml των G2, G9 and GO ενώ δεν παρατηρήθηκε κάποια αλληλομετατροπή μεταξύ τους, εξετάζοντας τα επίπεδα έκφρασης των κατάλληλων δεικτών (a-SMA, calponin and SM22). Η πραγματοποίηση πιο περίπλοκων δοκιμασιών έδειξε ότι τα G2 νανοσωματίδια δεν εσωτερικεύονται, όπως αναμενόταν, αν και το G9 και GO συσσωρεύτηκαν στα λυσοσώματα. Σχετικά με άλλες αναλύσεις, τα G2, G9 and GO δεν επέδρασαν στη δημιουργία αγγειακών οργανοειδών στο 1 μg/ml, αν και η ανάλυση της λειτουργικότητας των αγγειακών οργανοειδών (sSMCs/ $CD34^{+}$ και cSMCs/$CD34^{+}$), αποκάλυψε ότι το γραφένιο φέρει ένα αγγειογενετικό δυναμικό με αυξημένες τις τιμές στον αριθμό, μήκος και βάθος του αγγειακού δικτύου των αναπτυσσόμενων εκβλαστήσεων.

Συμπερασματικά, βασιζόμενοι στα παραπάνω αποτελέσματα και στο γεγονός ότι θεωρούμε καλύτερο να επιλέξουμε κάποιον τύπο γραφενίου ο οποίος δεν εσωτερικεύεται, έχει το βέλτιστο τύπο

και μέγεθος και θα μπορούσε να αναλυθεί περαιτέρω είναι ο τύπος 2 (30μm διάμετρος) στη συγκέντρωση 1 μg/ml.

## *Abstract*

Brain organoids constitute a novel research approach because (i) they partially mimic early neurodevelopment, (ii) they are useful in developing disease models, and (iii) they can be used as powerful tools for drug testing. Moreover, vascularisation of brain organoids has been shown to increase nutrient and oxygen supply decreasing cell death, thereby establishing a critical role for the communication between the vasculature and neuronal cells for the proper neuronal differentiation, migration, and maturity. We have, recently, succeeded in generating vascularised brain organoids using endothelial and mural cells.

In the present work, we investigated the employment of advanced graphene nanomaterials as scaffolds to provide an improved interaction between the cells of the brain organoids. Indeed, graphene and graphene oxide (GO) nanoplatelets exhibit unique biocompatibility, flexibility and electrical conductivity properties allowing graphene to act as an excellent scaffold for promoting neurogenesis and angiogenesis. Therefore, the overall goal is to generate a vascularised graphene-containing brain organoid. The focus of our research is the vascular component of the organoid, i.e. endothelial and mural cells. Before assembling the vascularised graphene-containing brain organoid, we established the optimal type, size, and concentration of graphene for use employing pluripotent stem cells, endothelial cells, mural cells, and vascular organoids. We tested the effect of graphene on (i) the expression of pluripotent stem cell marker OCT3/4, (ii) the mitotic potential of endothelial and mural cells, (iii) the expression of mural cell phenotype markers (calponin, a-SMA and SM22), and (iv) finally the formation and sprouting of vascular organoids. Our results define the type and concentration of graphene which can now be used for the generation of vascularised brain organoids.

## 1.1 Stem Cells

### *1.1.1 Embryonic Stem Cells*

Stem cells are versatile cells that can be distinguished by two defining characteristics: self-renewability and differentiation to specialized cell types for the regeneration/self-repair of various tissues and organs in the human body (Rashid and Alexander, 2013). Stem cells can be derived from a wide range of tissues, including bone marrow, adipose, skeletal muscle, and placenta. Stem cells exist both in embryos and adult tissues. Their classification depends on the variety of tissues they can differentiate to.

**Totipotent stem cells** have the ability to divide and differentiate towards every cell line that constitutes the whole organism. Totipotency represents the highest differentiation potential and allows cells to form both embryo and extra-embryonic structures. One example of a totipotent cell is a zygote formed after egg fertilization. These specific cells can then differentiate either into any of the three germ layers or construct a placenta. After approximately 4 days, the blastocyst's inner cell mass becomes a structure which constitutes a source of pluripotent cells.

**Pluripotent stem cells (PSCs)** can differentiate into cells of all germ layers but not to extraembryonic structures, such as the placenta. ESCs are pluripotent and are harvested from the inner cell mass of preimplantation embryos. Another example is induced pluripotent stem cells (iPSCs)(Takahashi & Yamanaka, 2006)(Rashid & Alexander, 2013) discovered by Shinya Yamanaka's group (Takahashi & Yamanaka, 2006). By enforcing the expression of just a few defined transcription factors, differentiated adult mammalian cells can be reprogrammed to become pluripotent (Bellin et al., 2012). Significantly, the process does not require the destruction of developing embryos. They derive from the patient's own cells, they are autologous and no longer generate any risk of immune rejection. In terms of phenotype and behavior, iPSCs closely resemble ESCs (Liang & Zhang, 2012)(Bellin, Marchetto, Gage, & Mummery, 2012). They either remain in an undifferentiated condition for an indefinite period, or differentiate into any cells of the three cellular layers of endoderm (e.g. hepatocytes, pancreatic β cells, and lung epithelium), mesoderm (e.g., bone cells and cartilage cells), and ectoderm (e.g., neural cells) (G. Y. Chen, Pang, Hwang, Tuan, & Hu, 2012a). One of the methods to evaluate their differentiation potential and spectrum is the teratoma formation assay.

**Multipotent stem cells** have a narrower spectrum of differentiation than PSCs, but they can specialise in distinct cells of specific cell lineages(Fujita & Fukuda, 2014; Ohnuki & Takahashi, 2015). An example

is an haematopoietic progenitor stem cell, which can generate several types of blood cells (Zakrzewski et al., 2019)

**Oligopotent stem cells** can differentiate into several cell types. For instance, myeloid stem cell can divide into white blood cells but not red blood cells (Zakrzewski et al., 2019)

**Unipotent stem cells** are characterized by the narrowest differentiation capabilities and a special property of dividing repeatedly. Their latter property set them a promising candidate for therapeutic use in regenerative medicine.

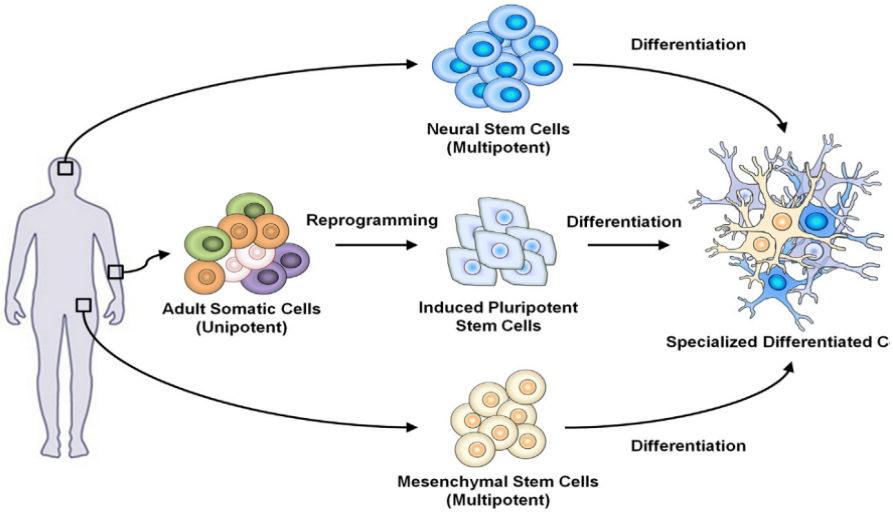


**Figure 1.1.** Categorization of stem cells. Stem cells can be classified into two groups: (1) pluripotent stem cells and (2) multipotent stem cells. Pluripotent stem cells consist of embryonic stem cells (ESCs) and induced pluripotent stem cells (iPSCs). iPSCs are generated by nuclear reprogramming of adult somatic cells. Like ESCs, iPSCs properties such as indefinite growth in the culture without a loss of pluripotency and the ability to differentiate into all types of somatic cells in the body. Source: Kenry et al., 2018

Regulating stem cell fate has become one of the most important topics in regenerative tissue engineering and medicine. A key factor to this control is the knowledge on various agents affecting stem cell functions. Generally, stem cell responses, such as attachment, proliferation, and differentiation into certain lineages, are significantly dependent on a multitude of physical, chemical, and environmental factors, specifically substrate topography, extracellular matrices (ECMs), stem cell-growth factor/chemical inducer interactions, and stem cell substrate interactions (Hall & Watt, 1989) (Engler, Sen, Sweeney, & Discher, 2006) (Kommireddy, Sriram, Lvov, & Mills, 2006). Consequently, it is crucial the development of effective physical platforms such as scaffolds or nanoplatelets for the specific control of these environmental factors.

Stem cells play an important role in the human body because of their ability for continual growth and renewal. Many groundbreaking therapies in the field of regenerative medicine and tissue engineering depend on the stem cell control. Intensive research has been carried out on stem cells to understand the myriad of environmental factors that organize their complex molecular and cellular events. Some representative studies target therapies based on bone marrow-derived mesenchymal stem cells (MSCs), induced pluripotent stem cells (iPSCs), and neural stem cells (Terraciano et al., 2007).

In order to be useful in therapy, stem cells must be converted into specific cell types. A key factor in successful regenerative medicine is the understanding of the signaling pathways for differentiation. In directed differentiation, it is common to mimic signals that are received by cells when they undergo successive stages of development. Through the manipulation of the culture conditions, it is likely to restrict specific differentiation pathways and induct others. However, achieving a similar effect *in vivo* is challenging and requires multiple growth factors and stable culture conditions that will allow the promotion of enhanced differentiation of ESCs/hiPSCs into functional and desired tissues (Zakrzewski et al., 1996). There are numerous protocols for the methods of forming progenitors of cells of each of germ layers, such as cardiomyocytes (Burridge & Zambidis, 2013), hepatocytes, renal cells (Kadzik & Morrisey, 2012), lung cells (Wichterle, Lieberam, Porter, & Jessell, 2002) (Spence et al., 2011), motor neurons (Oldershaw et al., 2010), intestinal cells, or chondrocytes.

### *1.1.2 Adult Stem Cells*

Whereas embryonic stem cells are isolated from mammalian embryos in the blastocyst stage during the embryonic development, adult stem cells constitute a group of tissue-specific cells of the postnatal organism into which they are committed to differentiate(Körbling & Estrov, 2003; Young & Black, 2004). With respect to the treatment of trauma and disease, adult precursor cells can be very useful for therapies including autologous transplantation. Precursor cells can be isolated from newborn to geriatric adults, including patients waiting for treatment. The use of autologous precursor cells overcomes the inherent mortality associated with HLA mismatches that require the use of immunosuppressant drugs. Adult stem cells can be harvested from a small biopsy of easily accessible tissues, such as skeletal muscle or dermis(Weissman, 2000; Young & Black, 2004). One paradigm of a source of adult stem cells is the marrow which contains at least three discrete stem cell populations; haematopoietic stem cells (HSCs), mesenchymal stem/stromal cells (MSCs) and endothelial progenitor cells (EPCs).

HSCs are found rarely, with a frequency of 1 in $10^4$ to 1 in $10^5$ among bone marrow cells. Other examples of ASCs are the peritrabecular tissues in cancellous bone, cartilage, muscle, fat and pericytes—mostly known as connective tissue stem cells, most of which are multipotent.(Alison &

Islam, 2009; Graf, 2002). In the case of the small intestine, stem cells are identified in a postulated stem cell niche around the crypt base. The intestinal subepithelial myofibroblasts and their secreted basement membrane factors are proven to form and maintain the stem cell niche, and thereby play an important role in epithelial cell function (Table 1). A characteristic example of the adult stem cell is the hematopoietic system which is formed as a hierarchic system with multipotent, self-renewing stem cells at the top, committed progenitor cells in the middle, and lineage-restricted precursor cells, that generate finally differentiated cells, at the bottom (Quesenberry et al., 2002). However, this paradigm of stem-cell differentiation restricted to its organ-specific lineage is questioned by the suggestion that adult stem cells, maintain a previously unrecognized degree of developmental plasticity that allows them to differentiate across boundaries of lineage, tissue, and germ layer. The results of recent studies of the plasticity of adult stem cells, which contradict the dogma that the differentiation and commitment of adult stem cells are restricted to their own tissue, are the subject of intense discussion.

Table 1.1 Adult human multipotent stem cells and their cell commitment through differentiation Source: Körbling et al., 2003

| Cell Type | Tissue-Specific Location | Cells or Tissues Produced |
|---|---|---|
| Hematopoietic stem cells | Bone marrow, peripheral blood | Bone marrow and blood lymphohematopoietic cells |
| Mesenchymal stem cells | Bone marrow, peripheral blood | Bone, cartilage, tendon, adipose tissue, muscle, marrow stroma, neural cells |
| Neural stem cells | Ependymal cells, astrocytes (subventricular zone) of the central nervous system | Neurons, astrocytes, oligodendrocytes |
| Hepatic stem cells | In or near the terminal bile ductules (canals of Hering) | Oval cells that subsequently generate hepatocytes and ductular cells |
| Pancreatic stem cells | Intraislet, nestin-positive cells, oval cells, duct cells | Beta cells |
| Skeletal-muscle stem cells or satellite cells | Muscle fibers | Skeletal muscle fibers |
| Stem cells of the skin (keratinocytes) | Basal layer of the epidermis, bulge zone of the hair follicles | Epidermis, hair follicles |
| Epithelial stem cells of the lung | Tracheal basal and mucus-secreting cells, bronchiolar Clara cells, alveolar type II pneumocyte | Mucous and ciliated cells, type I and II pneumocytes |
| Stem cells of the intestinal epithelium | Epithelial cells located around the base of each crypt | Paneth's cells, brush-border enterocytes, mucus-secreting goblet cells, enteroendocrine cells of the villi |

The hierarchical aspect doesn't seem to be the dominant explanation (Blau et al., 2001; Weissman, 2000).

### 1.1.3 Induced Pluripotent Stem Cells

In 2006, a major technological breakthrough in science and medicine was accomplished following the discovery that cells with a gene expression profile and developmental potential similar to embryonic stem cells (ESCs) can be generated from mouse somatic cells (such as fibroblasts) by applying a cocktail of four different transcription factors (J. Yu et al., 2007). These cells were named as induced pluripotent stem cells (iPSCs), and the four factors — OCT4, SOX2, KLF4 and c-MYC — were called "Yamanaka factors". After one year of experimenting, two research groups independently published and supported the generation of iPSCs from human fibroblasts (Takahashi et al., 2007; Takahashi & Yamanaka, 2006)(Shi et al., 2016). In order to circumvent the safety issues that arose from harboring integrated exogenous sequences in the target cell genome, a large number of modified genetic methods have been developed and produced iPSCs with potentially lower risks. Some of the advances deriving from the generation of human iPSCs are that constitute an attractive alternative due to the accuracy of the human diseases' recapitulation (especially by using those with particular genetic conditions). Moreover, iPSCs are generated from easily accessible cell types, such as skin fibroblasts and blood cells, from diverse patients(Kimbrel & Lanza, 2015). Their distinctive intrinsic properties of self-renewal and capacity to differentiate into nearly every cell type in the body, make the patient-specific iPSCs able to provide disease-associated cells and a variety of different cell types that were until recently inaccessible, such as neurons and cardiomyocytes (Shi et al., 2016).

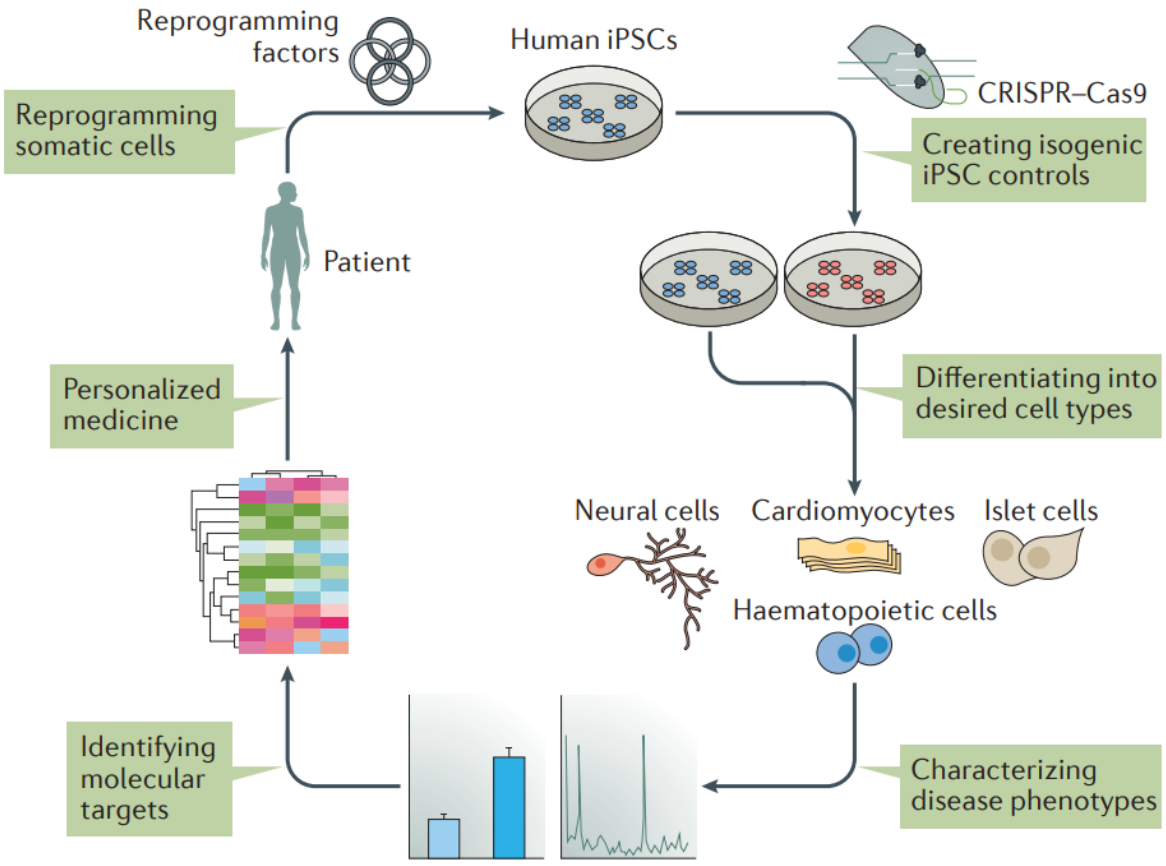


**Figure 1.2**. Schematic diagram depicting the human iPSC-derived disease modeling. Source: (Shi et al., 2016)

## 1.2 Organoids

### *1.2.1 Organoids, Tissue Engineering and Regenerative Medicine*

Over the recent years, stem cell research has obtained tremendous scientific attention due to the clinical applications stem cells have in modern cell therapy and drug discovery (Nishikawa, Jakt, & Era, 2007) (Bellin et al., 2012). This special interest has formed the driving force for the development of tissue engineering and regenerative medicine to extend to new horizons (Takahashi & Yamanaka, 2006) (Rashid & Alexander, 2013). More specifically, in the past decade, the field of tissue engineering has been combined with stem cell biology. These areas had one common component: the regeneration of living tissues and organs. In 1999, William Haseltine, then the Scientific Founder and Chief Executive Officer of Human Genome Sciences, invented the term "regenerative medicine," in order to incorporate the areas of tissue engineering, cell biology, nuclear transfer, and materials science under one defining term (Atala, 2012; Hasetine, 1999). Regenerative medicine involves a variety of biomaterials which include both natural and synthetic matrices (commonly called "scaffolds") and biological components (living cells) to improve or repair the functions of damaged tissues. The

increasing demand for organ and tissue transplants stimulated investigations on the regenerative properties of cells.

One of the restrictions of using cell-based techniques to organ replacement has been the inherent challenge of growing specific cell types in large quantities. Even in case of the liver, which carries a high regenerative capacity *in vivo*, cell growth and expansion *in vitro* may be tough. By identifying and isolating progenitor cells from a tissue, as well as by exploring the conditions under which differentiation and/or self-renewal is promoted, it has been possible to surpass some of the obstacles that previously limited cell expansion *in vitro*. However, conventional 2D cell culture faces some limitations regarding cell-cell interaction, lack of cellular organization, and the difference from the real *in vivo* scenario. All of the above could be improved by the use of a more advanced 3D cell culture (Y. Chen et al., 2011).

### *1.2.2 Organoids: Definitions – Characteristics*

Organoid technology offers the advantage to connect the field of conventional two-dimensional cell line culture and the vivo models (Xu et al., 2018). Regarding terminology, organoids are in vitro-derived structures that undergo some level of self-organization and resemble, at least partly, in vivo tissues and organs(di Lullo & Kriegstein, 2017). An advantage that derives from the use of the organoids is that they can more accurately predict drug responses, and act as a suitable platform for drug screening, along with efficacy evaluation and pharmacokinetics analysis. Moreover, organoid technology can also be implemented to investigate the possible optimized treatment strategies for personalised medicine. Despite that, organoid generation is an innovative strategy for regenerative medicine and transplantation, overcoming the lack of healthy donor tissue and inherent immunological rejection by establishing isogenic organoids from patient microbiopsies.

Well-designed fabrication of organoids is nowadays able to mimic *in vitro* cytoarchitecture and the *in vivo* functionalities of an organ. In this condition, PSCs self-organise into 3D organoids whose characteristics can be summarized in four points:

1. Two or more interacting cell types
2. 3D multi-cellular structure
3. Self-organisation of multiple distinct cell phenotypes into specific supra-cellular structures found in organs
4. Functional properties resembling the corresponding *in vivo* tissue. (Kim et al., 2020).

Furthermore, it has been demonstrated that 3D culture systems and organoids can be retained in culture for long timeframes (in some cases up to 1 year) (Lancaster & Knoblich, 2014) and can be expanded after dissociation and following re-plating, enabling the formation of clonal cultures

(Calandrini et al., 2020; Sachs et al., 2018). Studies on intestinal tissue engineering have shown that when extracellular matrix (ECM) scaffolds and protein factors are adequately supplied, epithelial cells of the small intestine,(Dekkers et al., 2013; Gonzalez et al., 2013; Mahe et al., 2013; Nakamura & Sato, 2018; Tuÿsüz et al., 2017), colon,(Sato et al., 2009) and fetal intestine (Fordham et al., 2013; Mustata et al., 2013) of mice and humans, are organized into unique three-dimensional (3D) structures with an efficient expansion of their stem cell populations.

A more complicated form of organoids generated by spatially organizing multiple cell types, called assembloids, enable deeper insights into tissue architecture and function. In order to achieve a more precise reflection of an in vivo tissue, the complexity of these organoids should be elevated. Assembloids constitute a relatively direct approach for incorporating various cell lines by mixing them before generating the organoids. Strategies like this have been implemented to generate brain organoids with vasculature-like structures (Vogt, 2021). Another example of 3D cell organization are the spheroids. In this case, different types of human cells which normally grow as monolayers or suspension cultures are examined for their property to form and grow as spheroids.(Carlsson et al., 1983). The production of multicellular spheroids can be initiated either by stimulating single cells to directly generate spherical colonies through proliferation, or by inducing cell aggregation first with subsequent growth of the aggregates. The former method is mainly applied in screening experiments testing the cellular capacity for colony formation in semisolid agar (Mueller-Klieser, 1987).

However, it is important to mention the drawbacks of the 3D organoid model use in tissue engineering. First of all, their generation and development require extended culture time due to cellular immaturity, they present challenges in microscopy, they f**ace the inadequate mass flow of nutrients and oxygen due to the diffusion-limited environment, and it is tough to maintain the required aseptic conditions** (Dhandayuthapani et al., 2011). Furthermore, the 3D culture of spheroids presents limitations during analysis such as spatial analysis concerns due to the structure, requirement of fixation for histology analysis and reliability of tissue construct in terms of drug response (Simon et al., 2016). However, the obstacle of cellular instability and immaturity could be overcome by the incorporation of scaffolds into a 3-D cellular culture or more efficiently the assembly of the vasculature.

### *1.2.3 Organoids: Generation*

Engineering organoids mainly focus on developing a proper microenvironment for cells and overcoming the challenges resembling the complexity of the cell niche. There are several methods developed for the generation of organoids each of which facilitate different applications.

1) Use of 3D spheroids as intermediate building blocks to form the final organoid. The progress of 3D spheroid technologies enables new paths for organoid engineering as it allows us to generate more

complex cell aggregates, including rods, tori, and honeycombs, with a combination of hydrogels. However, these areas must be exploited further. Still, in organoid systems, Matrigel based cell spheroids are widely used due to their excellent biomimetic capabilities *in vitro*(Unagolla & Jayasuriya, 2022).

2) Bioreactors which include a dynamic 3D cell culture platform can be implemented in various distinct organoid-related applications, including the expansion of diverse cell types such as PSCs, generation of 3D organoids etc.

3) Microfluidics enables dynamic culture conditions with the help of automation by providing constant inflow and outflow of medium and nutrients through microchannels and further facilitate the long-term expansion of organoids.

4) Bioprinting can be used to pattern the living cell incorporated into biomimetic hydrogel matrices and other biophysical cues resembling the *in vivo* systems.

5) Vascularization. The formation and the assembly of vascular networks in a larger organoid system poses a major challenge to tissue engineering applications. More specifically, one strategy is a scaffold-based system, where the vascular network is generated through a 3D modeling process, such as bioprinting. Another parameter that enhances the expansion of the angiogenic network is the addition of the proangiogenic biomolecules, such as platelet-derived growth factors (PDGFs), vascular endothelial growth factor (VEGF), and basic fibroblast growth factors (bFGFs) for rapid generation of vascular networks or angiogenesis.

6) Organ-on-a-chip platforms: This method constitutes the most integrated approach since it achieves not only the microenvironmental control but also it models the tissue-tissue and multiorgan interaction while reducing the variability(Unagolla & Jayasuriya, 2022). The development of the organ-on-chip system is a combination of all the previously discussed techniques, including microarray systems, bioreactors, 3D bioprinting, and vascularization(Zisch et al., 2003).

**Brain organoids:** A well-studied example of organoid generation and application research is brain organoids which have been developed as an evolution from previous research on the culture of embryoid bodies. Embryoid bodies form large multicellular aggregates of pluripotent stem cells that are capable of undergoing developmental processes similar to those of the pregastrulation embryo in vivo (di Lullo & Kriegstein, 2017). Brain organoids are hPSC-derived organoids that self-assemble to form an organized architecture, composed of progenitor, neuronal and glial cell types, resembling the fetal human brain (Jo et al., 2016; Kadoshima et al., 2013; Lancaster et al., 2013; Mariani et al., 2015; Pasca et al., 2015; Qian et al., 2016). These organoids may contain areas recapitulating different areas of the brain, often referred to as “brain organoids” or “cerebral organoids,” mirroring the broad presence of human brain regions in vivo(Bagley et al., 2017; Kadoshima et al., 2013)

Brain organoids can be formed via guided methods, where small molecules and growth factors are implemented during the differentiation process to instruct hPSCs and generate cells and tissues representative of certain brain regions, such as the cerebral cortex, hippocampus, and midbrain, etc(Qian et al., 2019). The human brain consists of diverse cell types from the neuroectodermal lineage such as progenitors, neurons, around 250 neuronal sub-types, glial cells, oligodendrocytes, microglia, and vascular cells, that are mostly recruited during embryonic development(Agboola et al., 2021). This technology can imitate embryonic organ development and human diseases, genetic disorders, and in some cases, cancers. Patient-derived hiPSCs have been extensively investigated for their potential to model neurodevelopmental brain disorders(Agboola et al., 2021). Regarding these applications, brain organoids have been modeled for the investigation of the mechanisms underlying autism spectrum disorders (ASD), where the transcriptome of ASD is compared with a control dataset of human brain transcriptomes from the embryonic stage until adulthood(Kang et al., 2011a). Another example of the brain organoids' applications is the Alzheimer's disease (AD) which demonstrates great promise in exhibiting amyloid-β deposition and hyperphosphorylation of tau protein(Fan et al., 1995.; Hernández et al., 2021; Jo et al., 2016). In Parkinson's disease (PD) a long-term neurodegenerative disease that affects mainly the motor system the research focuses on the neurodegeneration of dopaminergic neurons (DA neurons) found at the midbrain (Kang et al., 2011b).

### *1.2.4 Organoids: Prevascularisation*

A major problem that tissue engineering has to deal with, is the cell death related to tissue construct expansion and finally *in vivo* implantation (Koç & Gerson, 2003). In order for tissue engineering to surpass the tissue thickness limit of 100–200 μm, it must overcome the challenge of generating functional blood vessels to supply cells with oxygen and nutrients and to remove byproducts (Jain et al., 2005). One alternative to this, is vascularisation of engineered tissue constructs before transplantation by the induction of angiogenesis.

The journey of this trial began back to 2010. Baptista et al. proceeded with the implantation the vascular network scaffold into the liver of mice. It was observed that there was a position that endothelial cells aggregated (Baptista et al., 2011). Clearly, the typical vascular endothelium and liver epithelium could be recognized, which is reported as the first successful development of a bioengineered liver that has advanced the transformation of the medical field. In 2012, Quint et al. (Quint et al., 2012) repeated the previous process by using human PSCs and ECs with SMCs, which were observed to exhibit a vascular network structure.

A study from Levenberg et al. showed the potential of success of such an approach by engineering three-dimensional vascularized skeletal muscle constructs from myoblasts, fibroblasts and endothelial cells (Levenberg et al., 2005). It was observed that in vitro pre-vascularisation of the tissue constructs

eliminated apoptosis of cells upon implantation in three different sites in mice: subcutaneous, intramuscular and intra-abdominal. Thus, there should be noted the significance of each component of vasculature in angiogenesis of both in vivo and in vitro systems (tissue constructs). The developmental process of angiogenesis is described as the generation of new blood vessels from an existing vascular mold.

Recent studies on brain organoid vascularisation demonstrated an improvement on the quality of brain organoids due to apoptosis and stress reduction, and nutrients transport, a model that recapitulates the human brain more closely(M. A. Lancaster et al., 2016; Mansour et al., 2018). Notably, the continuous endothelium of the vascular component helps the maintenance of the structural and functional integrity of the brain, so vascularisation is critical for improving this model for usage(J. Yu, 2020).

### *1.2.5 Organoids: Microfluidics (Connection to the Flow)*

Organoids are described as complex 3D structures that exhibit architectures and properties closely resembling those of *in vivo* organs and develop from stem cells or organ-specific progenitors through a self-organisation process (Clevers, 2016; Lancaster & Knoblich, 2014; Rossi et al., 2018). As referred above, one of the biggest challenges that scientists face while developing mature organoids is the restricted nutrient supply, gas exchange and waste removal at the interior of the organoids. The average diameter of organoids achieved in the majority of the studies is usually up to 3 mm (Eicher, Berns, & Wells, 2018)(Akkerman, BioEssays, & 2017, 2017) complexity as observed in the case of adult human brain. Thus, an important obstacle of nutrient supply was able to get overcome due to the technology of microfluidics(Yu, Hunziker, & Choudhury, 2019).

The field of microfluidics, which involves manipulating fluids in channels with size of tens of micrometers, has recently come into existence (Whitesides, 2006). Microfluidics has an impact on multidisciplinary scientific fields ranging from optics and information technology to chemical synthesis and biological investigation. Yet, is still at an early stage of development. The variety of the implementations of microfluidic technologies are based on their useful properties. First of all, they are made to employ extremely low amounts of materials and reagents, and to perform separations and detections with high resolution and sensitivity, cheap cost, quick turnaround times, and small analytical device footprints (Manz et al., 1992). The most visible property of microfluidics is its small size, but it also makes use of less obvious qualities of fluids in microchannels, like laminar flow. It provides fundamentally new capacities for managing molecule concentrations in both space and time. Regarding its basic components and their contribution to the flow, there have been recognized three:

1) A department of reagents and samples introduction (probably as fluids)

2) Methods for circulating these fluids around on the chip surface, and for mixing them
3) Detectors instruments (e.g. components for purification of products for systems used in synthesis).(Stone, Stroock, & Ajdari, 2004)(Squires & Quake, 2005)(Beebe, Mensing, & Walker, 2002).

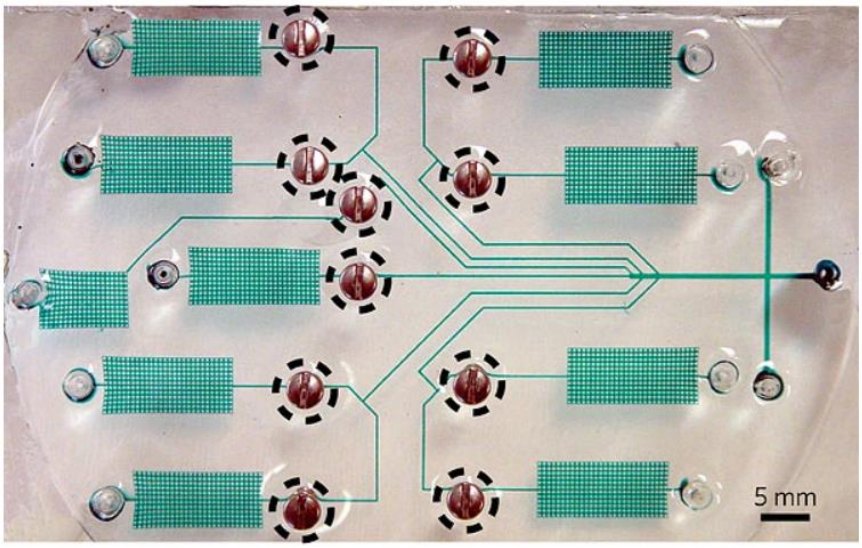


**Figure 1.4**. A simple microfluidic diagnostic device. Source: Whitesides et al., 2006

When it comes to applications in cell culture, microfluidics technology, provide controlled conditions with optimal levels of temperature, pH, nutrient and oxygen supply and waste removal (F. Yu, Deng,

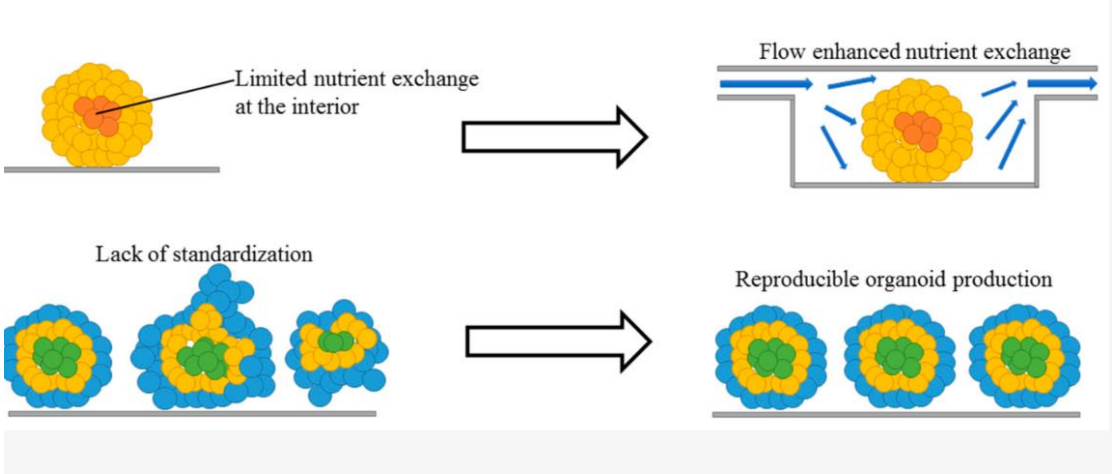


**Figure 1.5**. Because the inside of the organoid lacks adequate nutrient exchange, adding flow and enhancing nutrition and gas exchange will aid in the development of larger, more developed organoids. Future organoids production will be more repeatable thanks to improved geometrical confinement and environmental control, which are currently limitations of the organoid technology. Source: Yu, et al., 2019

et al., 2017a; F. Yu, Zhuo, et al., 2017). The progress of the microfluidic technology permits the generation of the organoids with specific structural and physiological features in a controlled manner (Choudhury et al., 2011). Moreover, when 3D cell culture is accompanied by microfluidic technology, it can be enhanced to become more complex organ-on-a-chip and organoid-on-a-chip models (Jang et al., 2013; Marsano et al., 2016). Microfluidic organs-on-a-chip platforms have the advantage to create a variety of biomimetic organ models, such as lung (Huh et al., 2010), liver, kidney (Jang et al.,

2013;Wang et al., 2017), heart (Marsano et al., 2016; F. Yu, Deng, et al., 2017b; F. Yu et al., 2018) and neural networks(Rossi et al., 2018; F. Yu et al., 2019). They are able to support the integration of multiple tissue compartments to simulate the physiology of the organs, and pursue pharmacokinetics predictions for candidate drugs. The development of multi-organ chips has captured the physiological complexity in the human body between different organs(Peyrin et al., 2011; Y. S. Zhang et al., 2016).

## 1.3 The contribution of scaffolds in tissue engineering

One of the key factors in making stem cell therapies effective and controlled is the ability to guide and enhance the proliferation and differentiation of stem cells into specific tissue/ organ (Dawson, et al., 2008) (Hwang, et al., 2008). The future of tissue engineering depends on three-dimensional -3D scaffolds created by novel promising biomaterials (Mao et al., 2015; Atala, 2009; Marx, 2015). Plenty of tissue engineering-based therapies such as wound healing and orthopedic applications have gained approval from Food and Drug Administration for clinical experiments and are commercially available (Bai, et al., 2019).

Scaffolds constitute necessary components for the regeneration of tissues in a 3D cell culture. Their wide range of applications in tissue engineering aims to provide a desirable micro-environment that allows neo-tissue to be generated properly for repairing and replacing damaged tissues or organs (Y. Chen, Zhou, & Li, 2011).

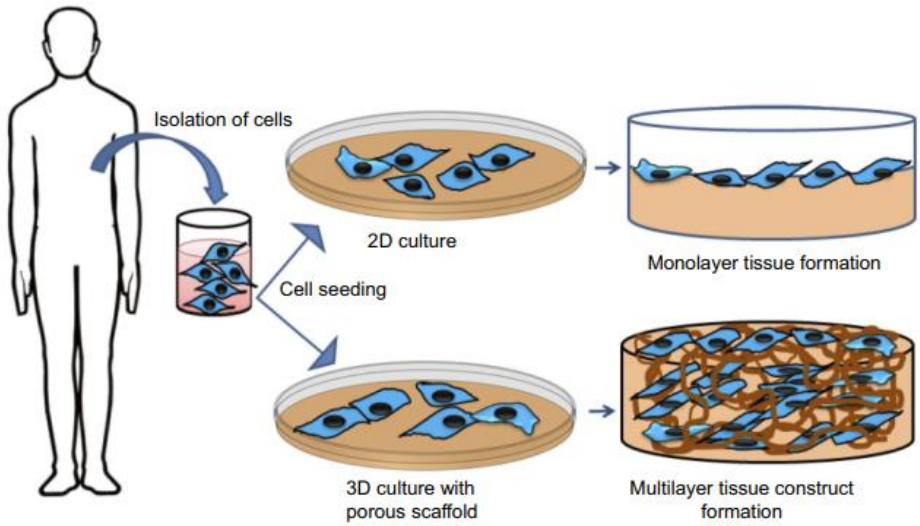


**Figure 1.6**. Schematic illustration of the 2D and 3D scaffolds when introduced in cell culture. (Bai et al., 2019)

From the mechanical aspect, scaffolds assist to eliminate external pressures and provide the developing tissue with structural support. Scaffold properties vary regarding polymer concentration, ligand density, porosity, structure, flexibility, and stiffness. Natural polymers such as collagen, gelatin, elastin, silk fibroin, chitosan (CS), chitin, fibrin, and fibrinogen due to their biocompatible properties,

are widely used for forming 3D scaffolds. From the biological aspect, scaffolds are structures that support the development of ECM and cell proliferation (Dhandayuthapani, Yoshida, Maekawa, & Kumar, 2011). A biologically active microenvironment including the cell–cell or cell–ECM interactions, that mimic the normal real-life physiological systems in accomplished through the generation of a 3-D organ model. Under this proper developmental condition, enables cells grow, differentiate and proliferate. Moreover, a surface architecture is available for supporting a variety of cell growth, differentiation, and proliferation processes (Carletti, et al., 2011).

Some more advantages of 3D tissue cultures containing scaffolds is that they offer a wider platform for therapeutic experimentations and drug discovery. The extended permeability of the scaffold is

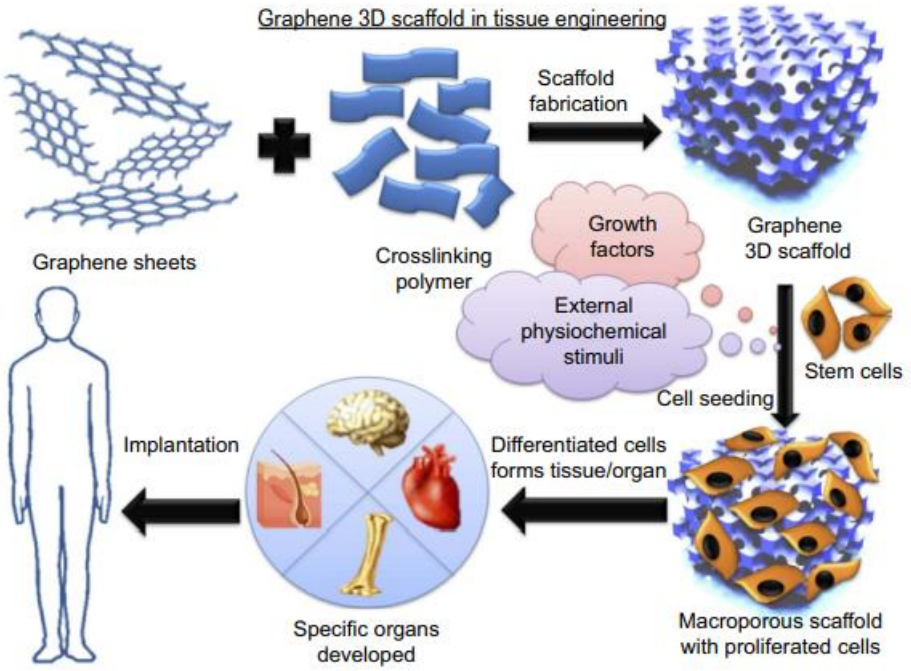


**Figure 1.7**. Schematic representation of 3D scaffolds Source: (Bai et al., 2019)

another factor, where the transfer of nutrients and support the removal of toxic by-products from the tissues is assisted. Gradually degradation of the scaffold material by allowing the takeover of the cells is another important factor to be taken into consideration to support the regenerative tissue (Hollister, et al., 2002) (Velasco, et al., 2015).

Successful tissue engineering requires optimization of scaffold stiffness for a given application and cell type(Levy-Mishali et al., 2009). It has been reported that substrate /scaffold properties, such as stiffness and nanostructure, also regulate cell response. Recently, studies have demonstrated substrate (2D) and (3D) stiffness to play an important role in differentiation, morphology, and spreading of various cell types(Sales et al., 2006; Thibault et al., 2007). Moreover, 3D scaffold stiffness revealed alteration in protein composition of focal adhesions,(Pelham et al., 1997) leading to changes

in mechanical contractile forces towards cells, which may lead to scaffold deformation(Huang et al., 2007).

In conclusion, scaffolds are formed to provide stable support, resisting cell contractile forces while preventing tissue degeneration / deformation. As referred above, (3D) scaffold function as extracellular matrix (ECM) in which cells originally reside, and the most likely to be used scaffold has been an ECM-resembling structure, which is composed of nanofibers(Ahn et al., 2012; Hinderer et al., 2016; Woo et al., 2007). Biopolymer scaffold's properties such as stiffness are crucial for the functional purpose of the desired engineered tissue, and can also regulate cell growth, differentiation, and organization during tissue formation(Huang et al., 2007). Another factor affecting the suitability of a scaffold in tissue engineering is its biodegradation rate. The biodegradation of new polymers in the implant field are often compared to polylactic glycolic acid -PLGA as this material has a well-established history of applications (e.g.nanotechnology, drug delivery systems, tissue engineering scaffolds as well as other implantable medical device concepts(Ghosal et al., 2022). In conclusion, a biomimetic and bioinspired approach to materials is one of the most promising scientific and technological challenges of the coming years. Bioinspired materials and systems, adaptive materials, nanomaterials, hierarchically structured materials, three-dimensional composites, materials compatible with ecological requirements, should get research priority in advanced technologies(Sanchez et al., 2005).

## 1.4 Graphene: types, properties and applicability in regeneration

### *1.4.1 Graphene*

Graphene as a nanoparticle belongs to the basic structure of graphite, which consists of a single layer of carbon atoms. It has been reported that its in-plane strength exceeds that of diamond. Consequently, it has become the most active research subject in all of condensed-matter physics today(Gerstner, 2010). In 2010, Professors Andre Geim and Konstantin Novoselov were awarded with the Nobel Prize in Physics, for being the first researchers to isolate and exhibit the properties of this remarkable material. The properties of graphene had been studied theoretically for decades, mainly due to the fact that it is the building block of both graphite and carbon nanotubes. In 2004, graphene was isolated for the first time via simple mechanical exfoliation by Novoselov, Geim and coworkers. They demonstrated field-effect transistors built from flakes of graphite just a few atomic-layers thick. These flakes that had been peeled off a block of highly oriented pyrolytic graphite using adhesive tape. After a short period, they succeeded in making single-layer graphene devices(Novoselov et al., 2005), and the electronic behavior they observed in these devices was profound. In this way, it was set the beginning on the enormous potential investigation(Geim & Novoselov, 2007).

Figure 1.8 shows different parameters affecting cell response to graphene-based particles in suspension. Graphene particles in suspension have the property to agglomerate and cover the cell surface, limiting nutrient supply and inducing oxidative stress. Small and well-dispersed graphene particles can enter cells and may interact with intracellular biomolecules. Depending on the synthesis method chosen, graphene with various physical characteristics is yielded, which may result in variations in the cellular response(Novoselov et al., 2004). Using mouse fibroblasts (L-929), Chen et al. established the cytocompatibility of a graphene sheet (H. Chen, et al., 2008).

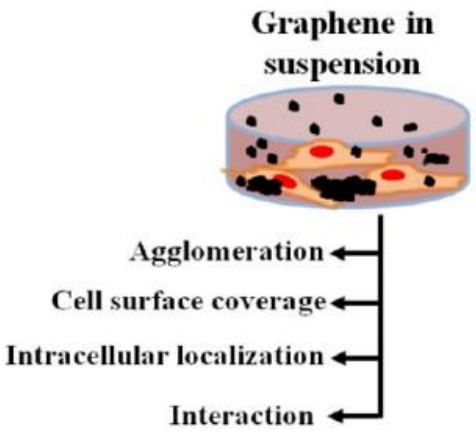


**Figure 1.8**. Schematic shows different parameters of graphene in suspension that are believed to influence cellular response Source: Kumar et al., 2015

Despite being a type of carbon allotrope, graphene has unique qualities that other carbon compounds, including benzene and other allotropes, do not. Consequently, graphene has offered numerous benefits for tissue engineering. Its remarkable qualities, including electrical conductivity, flexibility, and the ability to absorb protein and other low molecular weight molecules, may change how stem cells differentiate and how rapidly brain cells proliferate.

**Electrical Conductivity**: The electrical conductivity of a graphene substrate has an impact on proliferation, migration, and differentiation of nerve cells (N. Li et al., 2011). There are several techniques to alter the electrical properties of graphene, including stacking it in several layers, changing its geometric composition, and chemically treating it (Farokhzad et al., 2009).

**Elasticity**: One characteristic that makes graphene ideal in regenerative medicine is its superb elasticity. So far graphene has the highest Young's modulus compared to other identified substances. Its value is reported to be 0.1-1TPa (Bolotin et al., 2008). Due to its high elastic force, graphene remains unbroken and stably preserved. Without changing its properties graphene is bendable, which makes it convenient to be coated onto surfaces (Wu et al., 2009). This native elastic property of graphene is known to influence cell growth and its fate (Ryu & Kim, 2013).

**Adsorption of Proteins and Low Molecular Weight Substances:** One important feature of graphene that can be implemented for tissue engineering is its ability to adsorb protein and low molecular weight chemicals. Indeed, cells, for regulatory purposes secrete autocrine and paracrine factors to regulate their own growth and communicate with other cells. Such substances are adsorbed onto the surface of graphene and affect cell proliferation and differentiation (W. C. Lee et al., 2011). Ionic bonds and hydrophobic interactions are the main principles behind adsorption of proteins and low molecular weight substances on graphene surfaces (Utesch, et al., 2011) (Mücksch & Urbassek, 2011). The same mechanisms explain why trypsin (Xu et al., 2012), heparin (J. H. Ryu et al., 2011), lysozyme (Raffaini & Ganazzoli, 2010), and peptides (Sheng, Wang, & Chen, 2010) also bind to graphene oxide and graphite. Thus, via this property, graphene may exert considerable impact on cells.

**Cytotoxicity**: Nevertheless, in several reports, graphene has been responsible for causing cytotoxicity when introduced in cell culture (Liao, Lin, MacOsko, & Haynes, 2011a) (Sasidharan et al., 2011)(Y. Li et al., 2012). It is should be noted that, in most papers, the graphene and GO used for cytotoxicity assays and other biological effects assessments were pre-modified with polyethylene glycol (PEG), proteins, or other materials, which limited somehow the insight into the cellular uptake of the pristine graphene and GO (Mu et al., 2012)(Contreras-Torres et al., 2017a)(J. Yuan et al., 2012)(Akhavan, Ghaderi, & Akhavan, 2012)(Chang et al., 2011)(Liu, Robinson, Sun, & Dai, 2008). Mechanisms underlying the cytotoxic effect include plasma membrane damage (Sasidharan et al., 2011b) (Liao, et al., 2011)(Zhang et al., 2010)(Akhavan & Ghaderi, 2010)(Contreras-Torres et al., 2017), impairment of mitochondrial activity , induction of oxidative stress (Zhang et al., 2010) and DNA damage (J. Yuan et al., 2012). As a result, they were leading to apoptotic and/or necrotic cell death (Akhavan et al., 2012)(Chang et al., 2011)

In addition to the above, the main reason for much of the enthusiasm about graphene is its promising properties for new technology. The speed with which charge carriers move in graphene make it a distinguishable candidate to succeed silicon in high-speed computer chips. The co-existence of high conductivity, inherent flexibility and near-perfect optical transparency make it ideal for solar cells, touch-screen displays and similar large-area devices.

### *1.4.2 Graphene Oxide*

The promising properties of GO in bio-applications are determined from its special chemical structures and oxygen containing hydrophilic utilitarian bunches (Chung et al., 2013) (Dreyer, Park, Bielawski, & Ruoff, 2010). Many published pieces of evidence have reported that GO in the form of a suspension is more biocompatible than that of graphene or reduced graphene oxide. As a result, numerous cell studies have been performed on GO or GO-derived substrates or films for tissue engineering (Kumar

& Chatterjee, 2015). GO films influence cell expansion, morphology and guide stem cell differentiation due to the presence of hydrophilic oxygenated functional groups on its surface (W. C. Lee et al., 2011)(Tang et al., 2013). The presence of epoxide, hydroxyl, and carboxyl groups on the basal planes and edges of graphene/RGO enhances interaction and adsorption of serum proteins than those of graphene/RGO alone. Thus, GO is important for the effective cell attachment, proliferation, and differentiation that occurs during cellular interactions. It has many excellent properties when it comes to aqueous processability, amphiphilicity, ease of surface functionalization, surface enhanced Raman scattering property, and fluorescence quenching ability (Morozov et al., 2008) (C. Lee, Wei, Kysar, & Hone, 2008). The potential for GO-based composites as medical implant surfaces or as scaffolds (Tomioka et al., 2010) drug carriers, as bio-sensors (Elizabeth Stadler Ng et al., 2005) for vascular tissue engineering has also been explored. However, it has also been claimed that a GO-based composite can inhibit the growth of vascular smooth muscle cells (VSMCs)(Keyoumu et al., 2019)

As already mentioned, GO has proven to present a remarkable ability to adhere onto the surface of cell membrane and block the exchange of nutrients and oxygen, resulting in cell death (Heo et al., 2011). As a result, GO caused membrane damaging and lipid extraction due to the amphiphilic characteristics of GO. Once GO is internalized by living cells and accumulates in the cytoplasm and causes toxic effects (Lammel et al., 2013). Furthermore, intracellular GO causes the production of reactive oxygen species (ROS) and induces oxidative stress(Y. Li et al., 2012), apoptosis(Y. Li et al., 2012), and DNA damage(Akhavan et al., 2012).With the increasing use of GO in tissue engineering, it is important to understand its potential risks and further study the interactions between GO and surrounding cells. (Castro Neto, Guinea, Peres, Novoselov, & Geim, 2009)(Feng, Zhang, & Liu, 2011).

### *1.4.3 Graphene Internalisation*

According to previous results, NPs initially interact with the plasma membrane, often followed by their transfer into the cytoplasm (Fisichella et al., 2010; Ma et al., 2013; Treuel et al., 2013) via either clathrin-dependent or clathrin-independent endocytosis pathways (i.e. via caveolae), that might need the presence of membrane-severing GTPase dynamin (Carr & Rizo, 2010; Doherty & McMahon, 2009). However, the accurate pathways of cellular uptake of NPs have remained elusive (Carr & Rizo, 2010). Following cellular internalisation, NPs are delivered to the endolysosomal system (Cleal et al., 2013), where they may accumulate. Lysosomes play a significant role in cell physiology ranging from the degradation of malfunctional or aggregated proteins, through autophagy, or lipids to nutrient signaling and cell growth (Settembre et al., 2013). For instance, internalised growth factors like EGF are moved to late endosomes (Raiborg & Stenmark, 2009), which fuse with lysosomes to transfer their

intralumenal content for degradation (Luzio et al., 2010). Cellular uptake and accumulation of NPs directly affects the function of the endolysosomal system and their cell physiology in general.

Data from previous research have shown that dextran functionalised GO, when injected into mice, is distributed to various organs in which it can be still be found 4 h later (stomach, lung, kidney & intestine) (Rong et al., 2014). One more example of nanoscale graphene sheets (NGSs) processed with PEG demonstrate that are similarly distributed to various organs right after injection, but mainly accumulate in the liver and spleen. Lammel et al., worked on human hepatocellular carcinoma cell line Hep G2 where they investigated the interaction between the plasma membrane and the GO and carboxyl graphene (CXYG) nanoplatelets. Through TEM microscopy, they observed the internalisation and intracellular pathway of ultrathin sections of GO and CXYG-treated cells (Lammel, Boisseaux, Fernández-Cruz, & Navas, 2013a). GO and CXYG nanoplatelets were found to pierce through and mechanically disassembly the plasma membrane. At some of the sites where the nanoplatelets interacted with or penetrated through the plasma membrane, some highly-organized fibrillar structures were identified, resembling intermediate filament bundles (Lammel, Boisseaux, Fernández-Cruz, raphene& Navas, 2013b).

### *1.4.4 Applications of Graphene-Based Nanomaterial in Tissue Engineering*

Recently, graphene has emerged as an innovative nano-platform with promising potential for biomedical applications and translational research, such as tissue engineering and Regenerative Medicinee (Novoselov et al., 2004a) (L. Zhang & Webster, 2009) (W. C. Lee et al., 2011) and drug delivery (Dvir, Timko, Kohane, & Langer, 2011), because of its physical, chemical, and mechanical properties). Carbon-based nanomaterials pose an excellent platform for the development of 3D tissue engineering scaffolds (Minami et al., 2015)(Bolotin, Sikes, Jiang, et al., 2008). Many tissue engineering investigations have used carbon materials with different dimensions, such as fullerenes, carbon nanotubes, and graphite, because of their mechanical properties. These carbon nanomaterials are similar in size and shape to proteins found in the ECM, which is why they are considered to be physical analogs of ECM components (Martinelli et al., 2019; Minami et al., 2015). Carbon materials of different dimensions such as fullerenes, carbon nanotubes, and graphite were successfully employed in many tissue engineering investigations because of their mechanical properties (Minami et al., 2015; Akay, 2006). These carbon nanomaterials because of their similar dimensions they are resembling physical analogs of ECM components such as collagen fibers.

NPs in general, and especially graphene nanoplatelets (graphene nanoplatelets (GNP), which are short stacks of platelet-shaped graphene sheets) are shown to provide high regulation to properties of scaffolds such as enhancing their mechanical strength and providing regulated release of bioactive

agents (Park et al., 2012) (Pérez, Won, Knowles, & Kim, 2013)(Cheng, Tietjen, Saucier-Sawyer, & Saltzman, 2015)(Bahal et al., 2016)(Mi et al., 2016). Additionally, limiting factors included into the organoid formation such as low solubility, unstable bioactivity and short half-life of bioactive molecules (growth factors, cytokines, inhibitors, etc.), have brought out the NPs as one of the most suitable candidates for bioactive agent delivery and monitoring for applications (Park et al., 2012; Pérez et al., 2013; Cheng et al., 2015; Bahal et al., 2016; Mi et al., 2016). More specifically, graphene-based scaffolds have been applied in various medical applications including tissue engineering for the past few decades. Their preparation involves different synthesis approaches such as:

1) Covalent amide interactions by mixing graphene nanostructures with natural or synthetic polymers through gas foaming technique (ammonium bicarbonate as the porogen)
2) Graphene with different ratios of polymers and metal ions directed CVD process,
3) Self-assembled graphene foam (GF) mostly generated by hydrothermal synthesis and
4) Chemical etching (X. Li et al., 2016)(Kumar et al., 2015)(Jiang et al., 2014).

The progress of tissue engineering from 2D to 3D cultures introduced many concerns, which were suppressed by the excellent performance of graphene-based scaffolds. This issue was addressed due to graphene and graphene oxide (GO) aromatic scaffold nature. More specifically, they consist of potential compounds for promoting the cell behavior including attachment, growth, proliferation, and differentiation (Shadjou, et al., 2017)(Ryoo, et al., 2010)(Wang et al., 2011. Thanks to the biocompatibility at low concentration (Heo et al., 2011) and 2D nature with ultra-large surface area, graphene and GO have recently captured interests as cell culture substrates. Despite the promising outcomes about biomedical applications of graphene-related nanomaterials, there are still some concerns about the potential toxicity and biocompatibility of these nanoplatelets (Nair et al., 2015).

### *1.4.5 Graphene in Organoids:*

Graphene has very recently been added to organoids. Zhang and coworkers generated 3D bioprinted functional osteocyte bone organoids containing graphene to investigate mechanical loading (J. Zhang et al., 2022). Furthermore, Liu and coworkers generated human brain organoids containing GO. However, the high concentration used 50ug/ml was cytotoxic and altered lipid homeostasis through ER stress (X. Liu et al., 2022) underlying the importance of careful titration of the concentration and type of graphene used.

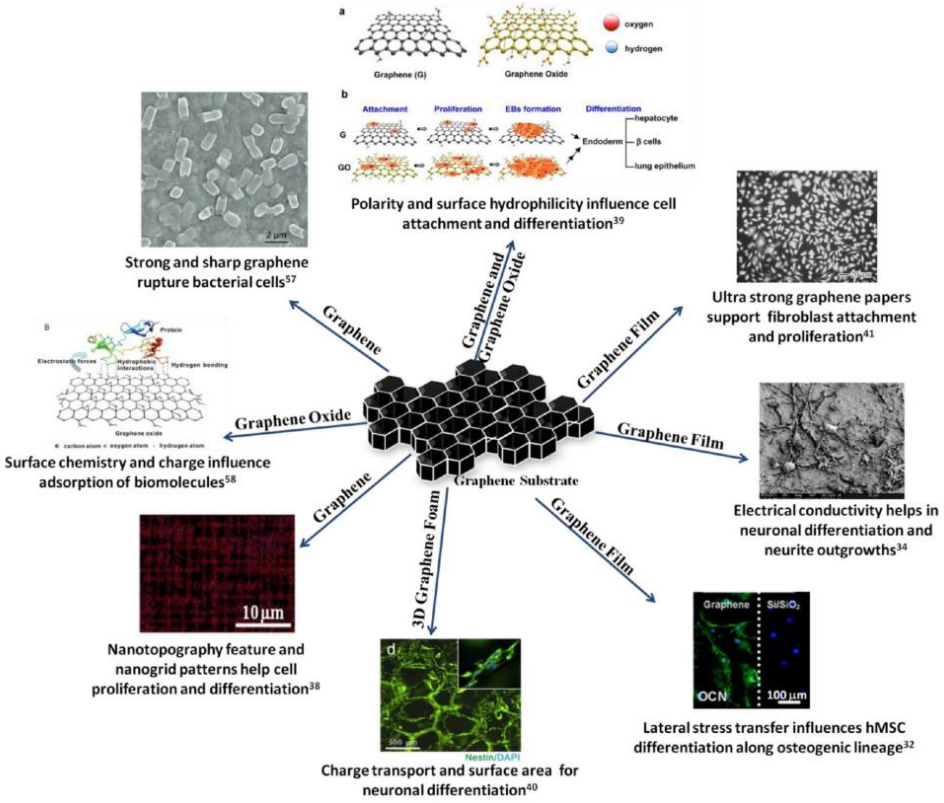


**Figure 1.9**. Utility of multifunctional properties of graphene-based substrates for various biomedical applications. Source: Kumar et al., 2016

## *2.Aim-importance*

The main goal of the present study is the development of a graphene containing vascularised brain organoid. Towards this direction, we performed an initial screening of 9 types of graphene, differing in diameter, surface area and concentration, on HUVECs to select the optimum graphene types regarding their effect on the cell proliferation. Later, we repeated cell growth assays using 3 candidate types for each of all vascular cell types assembling a vascularised brain organoid, to ensure the lack of cytotoxicity in any compartment. In addition, we needed to ensure that all cell types with which the

graphene would come into contact did not show any signs of cell phenotype or cell function alteration. These cell types include HUVECs, mural cells (both cSMCs and sSMCs), and human vascular progenitor cells differentiated from hESCs ($CD34^{+}$VPCs). In addition, we addressed the maintenance of the pluripotency state of the hESCs in presence of graphene. Even a minor change in cell fate commitment could result in the generation of an organoid unable to recapitulate the exact conditions of early human embryonic development. After gathering our first results, we examined the way graphene used in certain concentrations inhibits cell proliferation and the possibility that there is a specific internalization pattern. After incubating cSMCs with the 3 candidate graphene types and staining them with specific IF markers, we realized that there is a size-dependent manner of internalization which excludes the larger particles. At the same time, we brought all our observations together and generated vascular organoids where we investigated the effect of graphene nanoplatelets in the assembly and cell-cell interactions of this 3D structure. The ultimate goal of the present study was to evaluate the angiogenic potential of the vascular organoids when generated in the presence and absence of graphene. Our promising results are presented in detail in the following section. The effects of graphene on neural cells were addressed in a separate study.

## 3. Experimental procedures

### 3.1 H1 Embryonic Stem Cell Culture

H1 hESC line was purchased from Wicell Research Institute (Madison, WI, United States). hESCs were cultured on six-well tissue culture plates coated with hESC-qualified Matrigel (Corning, 354277) in mTeSRplus medium (StemCell Technologies, 05850) at 37◦C and 5% $CO_2$. Every 4–6 days, cells were passaged enzymatically using 1 mg/ml versene (Lonza – BE17-711E) for 2 min at 37°C. hESC colonies were then harvested, dissociated into small clumps and replated into Matrigel-coated 6-well plates.

**Pluripotency markers and graphene addition**

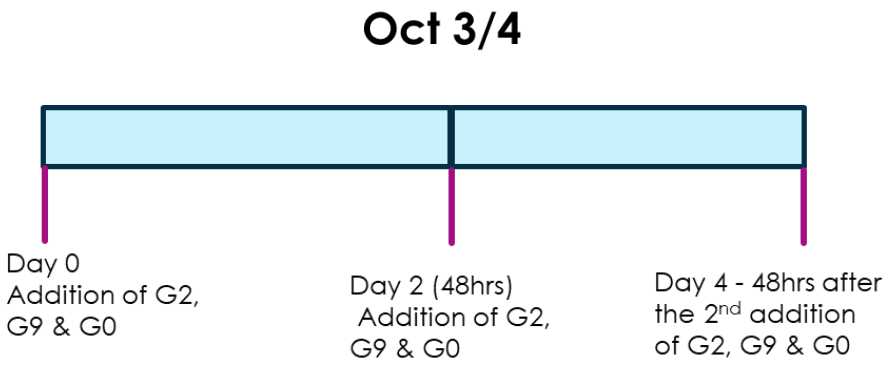


**Figure 3.1**. Schematic timeline of the total duration of the experimental process and the time points of graphene's addition

After the attachment of the H1 colonies and their morphology assessment (usually 24 hours), graphene and graphene oxide were introduced into the cell culture with a medium change. Graphene nanoplatelets were added in two different groups of concentrations. The first one included high concentrations of 5, 25 & 50 μg/ml and the second one was comprising of a lower one (1μg/ml). After 48 hours, the medium was removed carefully without discarding a portion of graphene. Then, the removed medium was centrifuged for 3 minutes at 13.200 rpm and the supernatant discarded. The pellet of graphene was diluted again with fresh mTESR plus and was added back to each well. In this way, it is reassured that the final concentration is not altered throughout the experiment. On day 4 (48 hours after the medium change), a lysis buffer was prepared and lysates were taken and processed according to the western blotting protocol and were checked for the expression of a characteristic pluripotency marker Oct 3/4. We performed a fluorescent-blot for a better visualisation of our antibodies on the Azzure imaging Biosystems. The antibodies that we used are Oct 3/4 and GapDH (Glyceraldehyde 3-phosphate dehydrogenase). The first one is a key regulator of pluripotent cells across mammalian species and the second one catalyzes an important energy-yielding step in carbohydrate metabolism. Its presence is ubiquitous in bone marrow, heart and 24 other tissues and as a result it is used as a loading. The results from both sets of conditions are displayed on Figure 4.4.

### *3.2 Human Umbilical Vein Endothelial Cells (HUVEC) isolation:*

Before the beginning of the isolation procedure, PBS, M199 PLAIN medium (Gibco, 31150-022) and FBS were incubated in a 37$^{o}$C waterbath. The umbilical veins were collected from the Gynecology Department of University hospital of Ioannina. Cords were washed twice with PBS which was preheated to 37$^{o}$C. Then, 3-way stops were attached to each side of the cord and were tied with surgical thread. After that, almost 15ml of collagenase (Worthington Biochemical) were added (750 ul in 50mL PBS) to each cord. The sealed cords were placed in waterbath for 12 min strictly. Then, the cord was opened at one end and the collagenase collected. 15-20 mL of M199 medium enriched with 10% FBS, 47μg/ml Endothelial Cell Growth Supplement (ECGS), 4,7U/ml heparin (Sigma, H-3149), 1% penicillin and 1% streptomycin were washed through the cord so that the majority of endothelial cells were detached and collected. The collected sample was centrifuged at 1100 rpm for 5 minutes. The supernatant was discarded and the pellet resuspended in Full HUVEC Medium. Cell populations from different cords were pooled and plated on collagen (Corning, 354236)-coated plates, which were incubated for 30 minutes at 37oc and then washed twice with PBS. ECs from human umbilical vein (HUVEC) were cultured in Full HUVEC Medium as follows: M199 (Gibco) medium supplemented with 20% fetal calf serum (FCS), 47 μg/ml endothelial cell growth supplement (ECGS), 4.7 μ/ml heparin (Sigma) and 1% penicillin-streptomycin as described (Bellou et al., 2012).

### *3.3 Differentiation and characterization of contractile and synthetic vascular smooth muscle cells from hESCs*

Both contractile and synthetic SMCs were generated using methods established in our lab (Markou et al., 2020). For contractile SMCs (cSMCs) generation, hESCs were plated on matrigel, cultured in contractile differentiation medium (CDM - 2,5% ADSC) consisting of basal medium (Lonza, PT-3273) supplemented with 2.5% FCS (Gibco, 10270-106) and glutamax (Gibco, 35050) for 9 days with daily medium changes. On day 9 cells were detached enzymatically using 0.05% Trypsin-EDTA (Gibco, 25300-054) and replated on gelatin (0.1% Gelatin-Millipore, ES-006-B) coated dishes and cultured in CDM until confluency (2–3 days). Medium was changed every second day. When 60-70% confluent, they were passaged again in a ratio of 1:2. One well was kept for the maintenance of the contractile phenotype using the CDM and the other proceeded with further differentiation towards the synthetic phenotype. There the medium changed from 2.5% ADSC to Synthetic Differentiation Medium - PM, which induces the synthetic phenotype. 48 hours later, the synthetic SMCs were generated. For the generation of the synthetic SMCs (sSMCs), cSMCs were seeded on gelatin coated dishes for 24 h and subsequently the medium was changed to either CDM supplemented with 2 ng/ml FGF2

(Immunotools, 11343623) or synthetic differentiation medium (SDM - Pericytic medium) for 48 h. SDM medium consisted of a basal medium (ScienCell, 1201-b) supplemented with 2% FCS, and a combination of growth factors (ScienCell, 1252) 2 ng/ml EGF, 2 ng/ml FGF2 and 2 ng/ml IGF-I (Markou et al., 2020).

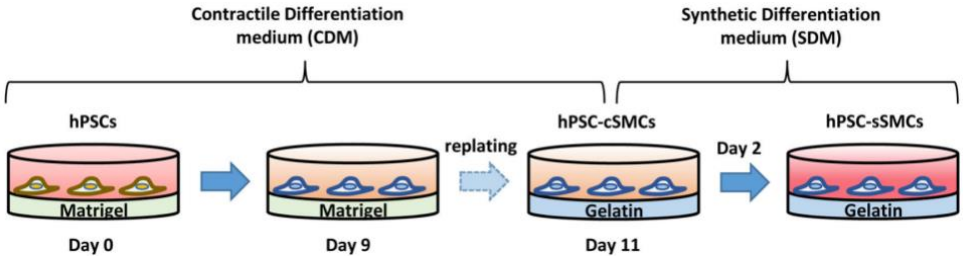


**Figure 3.2**. Differentiation of hPSCs to cSMCs and sSMCs. Overview of the differentiation procedure for 11 days

### *3.4 Smooth muscle protein markers*

According to previously described differentiation protocols in our lab, (Markou et al., 2020) when both cell types were generated, graphene nanoplatelets and graphene oxide were added to cell culture. Graphene derivatives (G2, G9 and GO) were introduced in each medium in various

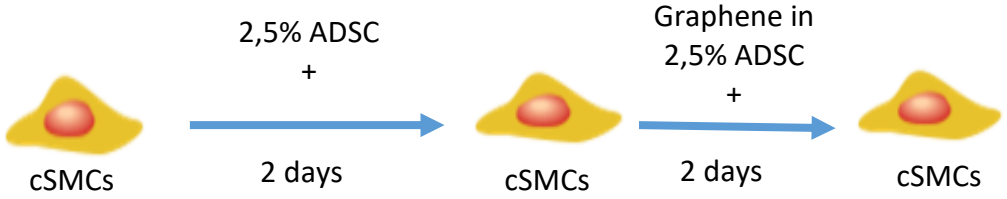


**Figure 3.3.** Schematic diagram of experimental process to generate cSMCs with the presence of graphene and assess the effect on the smooth muscle phenotype via western blotting

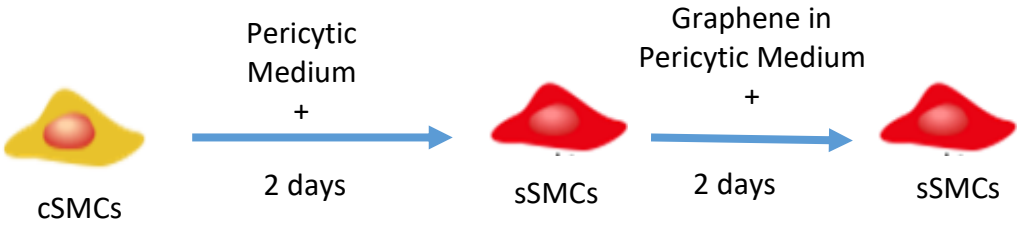


**Figure 3.4**. Schematic diagram of experimental process to generate sSMCs with the presence of graphene and assess the effect on the smooth muscle phenotype via western blotting.

concentrations for 48 hours. Lysates of both phenotypes were taken using the lysis buffer and analyzed by western blot analysis.

More specifically, we have developed an experimental process where cSMCs were expanded to passage 3 in gelatin-coated 12-well plates. The next day, they were assessed for their morphology and attachment, then the 2.5% ADSC medium was changed to pericytic medium to develop the synthetic phenotype. Cells were incubated with new medium for 48 hours and then when the phenotypical transition was accomplished, graphene was added in cell culture following a medium change. We used 4 graphene conditions (G2 1 μg/ml, G2 10 μg/ml, G9 1 μg/ml and GO 1 μg/ml). Graphene nanoplatelets remained in the cells for 48 hours. Then, supernatant was discarded, cells and lysates were taken using the lysis buffer. Lysates were processed and samples underwent a western blotting for the investigation of the graphene's effect on smooth muscle markers expression. At the same time, we examined graphene's effect on the phenotypic markers of cSMCs. In this case, diluted graphene was introduced in 2.5% ADSC medium. Graphs were generated from 3 independent biological repeats. Chemiluminescent detection was used for western blotting and proteins' expression was visualised via Azure Biosystems (USA). Images were collected, processed with Quantity One Analysis software (BIO-RAD) and then converted to band density values. Each value of SM markers was divided to the values of the loading protein and then they were normalised to control.

### *3.5 Differentiation and isolation of CD34+VPCs*

The differentiation of hESC towards CD34$^+$VPCs was developed under chemically determined conditions according to the protocol that has been described from our research team (Tsolis et al., 2016) a modified protocol from (Tan, Sriram, Rufaihah, Neoh, & Cao, 2013). The hESCs were cultured on Matrigel coated wells in mTeSRTM1 for 48 hrs. The mTESR Plus medium was (day 0) was replaced

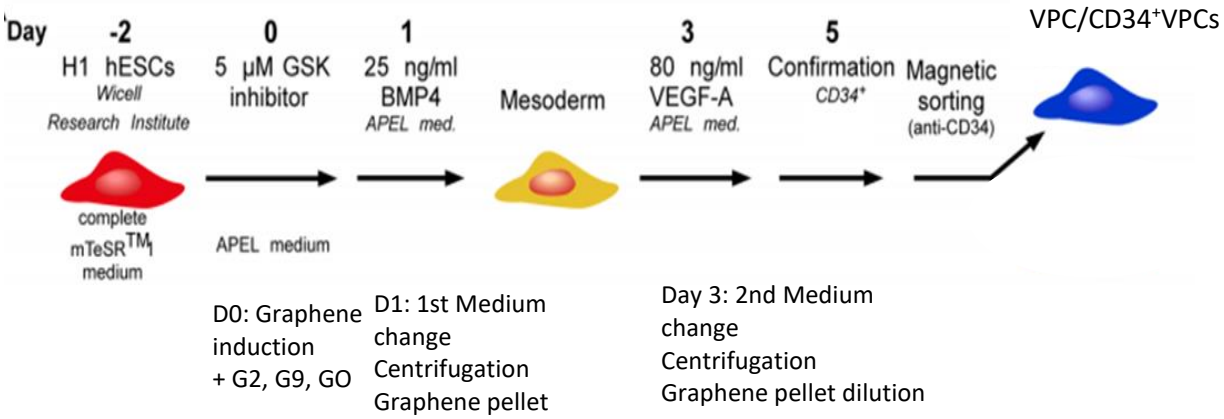


**Figure 3.5**. Schematic diagram depicting the chemically determined differentiation protocol for the generation of VPC/CD34$^+$ for an initial hESCs cell population

with Apel medium, which induces the differentiation towards ECs (Tsolis et al., 2016) containing CHIR, 5μM (Selleckchem, 99021) and 24 hours later another medium change was carried out with Apel medium containing 25ng/ml BMP4 (Gibco, PHC9534) for a further 48h. Afterwards, a third medium change followed where Apel was enriched with 80ng/ml VEGF (Immunotools, 11343663) for 48h. Finally, the hESC-VPC (Vascular Progenitor Cell) expressing the surface marker CD34 (25-35%) were isolated using the anti-CD34 immunomagnetic beads (EasySep Selection Kit, Stem Cell Technologies, 18056) The CD34+ cells were cultured in wells coated with 5μg/cm$^2$ fibronectin (Corning, 354008) in APEL medium enriched with 50ng/ml VEGF. When the cells reached confluency, they were re-cultured following trypsinization (Gibco, 25300-054) and were placed in wells covered with fibronectin in a 1:2 ratio. The differentiation protocol is shown in Figure 3.5. It was of great importance, to keep the concentration of graphene nanoplatelets stable throughout the experiment. The addition of graphene nanoplatelets was performed at day 0, which was diluted in APEL, enriched with CHIR, medium. Before each medium change, we collected the supernatant, while slightly moving the plate upwards, and we added the new APEL with the proper agent. Then, the collected medium was centrifuged at 1200 rpm for 1 minute, the supernatant was discarded and the medium was centrifuged once again. After this, we kept the pellet, diluted it in few μl of the new medium and added it to the cells.

### *3.6 Generation of Vascular Organoids/Spheroids*

Vascular organoids (consisting of hESC-contractile SMC and HUVECs) were created using methylcellulose (Sigma, M0512) and the hanging drop technique for 48 hours as previously described (Korff & Augustin, 1998). In brief, each vascular organoid was generated from 1,000 cells at a ratio of 1:9 hESC-SMCs: ECs in 10 μl solution (EGM-2 medium/methylcellulose solution:4:1), cultured in a hanging drop for 2 days at 37$^o$C and 5% $CO_2$.

### *3.7 Cell growth assay*

Cell growth was assessed by measuring the proliferation rate of cells when graphene derivatives were introduced in cell culture for 40 hours. By the time they reached, 80-90% confluency, cSMCs were expanded in vitro under standard conditions to passage 4 and then counted as single cells. In the present study we examined the effect of graphene on vascular cell lines (Results 4.2-4.4) and on H1 hESCs' cell proliferation (Appendix 6.1). Depending on the cell type, we placed cells in a 96-well plate (Corning, USA) which was coated either with matrigel, collagen or gelatin. All cells used were either infected with H2B-mCherry lentivirus or overexpressed the non targeted mcherry plasmid. This second alternative was achieved by targeting the mCherry ORF under the control of the actin promoter to the AAVS1 safe harbor locus in H1 ESCs (MI and MM unpublished results). The resulting cells exhibited a strong mCherry expression which was visualised by excitation at 561nm. The H1 mCherry cells were

differentiated to VPCs/CD34$^{+}$ and then they isolated as described above. We then used H1 hESCs constitutively expressing GFP also under the control of the actin promoter (A.P. unpublished results) to generate cSMCs and sSMCs which could be activated at 488nm. In this way, using mCherry VPCs/CD34$^{+}$ and GFP vSMCs we could later generate vascular organoids in the presence and absence of graphene and avoid the lengthy indirect immunofluorescence required when using unlabelled cells. After the placement of the cells into a gelatin-coated 96-well they were incubated (37$^{o}$C) for 24 hours. Then, graphene nanoplatelets were introduced in 5 different concentrations 1, 5, 10, 25 and 50 μg/ml in the proper medium for each cell line. After replacing the medium with the one containing the graphene, the plate was transferred into an empty space on the IncuCyte. The Incucyte® Live-Cell Analysis Systems are real-time quantitative live-cell imaging and analysis platforms that enable visualization and quantification of cell behavior over time, by automatically gathering and analyzing images around the clock within a standard laboratory incubator. This enables researchers to make time-lapsed, kinetic measurements from living cells over days and weeks thus providing insight into active biological processes in real time. Finally, the system was set up from IncuCyte ZOOM 2016B Software to take 4 pictures of all the selected wells every 4 hours.

### *3.8 Western Blot Analysis*

Protein extraction was performed from whole cell lysates using a lysis buffer containing (940μl of PBS 1x, 50μl 20% SDS, and 10μl PMSF) and quantified with a BCA Protein Assay kit (Thermo Scientific, 23225). Samples were prepared, subjected to SDS-PAGE, and blotted onto a nitrocellulose membrane, as previously described (Bellou et al., 2012). Specific proteins were detected following incubation with primary antibodies and peroxidase-conjugated secondary antibodies using the Azure documentation system. Alternatively, IRDyes were used as secondary antibodies, for the fluorescent blots. Quantification of band intensities was performed using Quantity One Analysis software (BIO-RAD).

Table 3.1. Primary and secondary antibodies used in the current thesis

| Antibody | Strand / Clone | Manufacturer |
|---|---|---|
| a-SMA | 1A4 | Dako, USA |
| Calponin | CALP | Dako, Denmark |
| SM22a | Polyclonal | Dako, Denmark |
| Nanog | Polyclonal | Cell Signaling, USA |
| Tubulin | E7 | DSHB, USA |
| a-GAPDH | Monoclonal | DSHB, USA |
| α-OCT4 | sc5279 | Santa Cruz, USA |
| CD34-PE | 4H11[APG] | Immunotools, Germany |
| α-Mouse HRP | Polyclonal | Thermo Fisher Scientific Inc., Netherlands |
| α-Rabbit HRP | Polyclonal | Jackson, ImmunoResearch Laboratories, USA |
| VE-cadherin | PEG (3) | |
| Alexa Fluor® 488 AffiniPure Donkey Anti-Mouse IgG (H+L) | Polyclonal | Jackson ImmunoResearch Laboratories, USA |
| Alexa Fluor® 488 AffiniPure Donkey Anti-Rabbit IgG (H+L) | Polyclonal | Jackson ImmunoResearch Laboratories, USA |
| Alexa Fluor® 594 AffiniPure Donkey Anti-Mouse IgG (H+L) | Polyclonal | Jackson ImmunoResearch Laboratories, USA |

### *3.9 Immunofluorescence*

***Adherent contractile SMCs***: Indirect immunofluorescence on adherent cells was performed as previously described (Bellou, 2012 #68) using primary and secondary antibodies. Initially, at approximately 50% confluency, cells were washed twice with PBS, fixed in 3.7% PFA (Sigma – P6148) for 15 min and quenched with 50mM $NH_4Cl$ (Sigma – A4514) for 15min. Subsequently, cells were permeabilised with 0.5% Triton X-100 (ThermoFisher Scientific – 10254583) for 4min, blocked in 10% FCS for 20min and incubated for 1 hour with primary antibodies. Next, cells were washed 3 times for

5min in PBS and incubated with secondary antibodies for 1 hour. Cells were washed 3 times for 5min in PBS and cell nuclei were stained using DRAQ5 (Sigma) for 10 minutes. In the case of phalloidin staining, after the incubation of the secondary antibodies, cells were washed 3 times for 5min in PBS and then phalloidin was added for 20 minutes. Then, cells were washed with PBS and mounted in moviol (EMD Millipore) and DABCO (Sigma), and images of nine fields were taken on a Leica TCS SP5 confocal microscope using HCX PL APO CS 40 × 1.25 OIL objective.

***3.10 Vascular organoids/spheroids:*** Vascular organoids or spheroids were fixed in 3.7% paraformaldehyde (Sigma – P6148) for 1 hour at RT, permeabilized with 0.2% Triton-X/0.9% gelatin solution for 1 h, and 0.5% Triton-X/0.9% gelatin solution for 15 min, and incubated with primary antibodies overnight at 4°C. The next day, the vascular organoids were washed 5x with 0.2% Triton-X and incubated with secondary antibodies for 1 h. After rinsing 5x with 0.2% Triton-X and incubation with Draq5 (Thermo Fisher Scientific) for 10 min, images were taken on a Leica TCS SP5 confocal microscope using HCX PL APO CS 40 × 1.25 OIL objective. At least 5 vascular organoids or spheroids were analyzed per experiment. Both vascular cell types were phenotypically characterized using cell-specific antibodies. For endothelial cell staining, we used VE-cadherin which constitutes a vascular endothelial cadherin playing an important role in maintaining a restrictive endothelial barrier. For the synthetic phenotype of the smooth muscle cells we stained with SM22, a cytoplasmic marker specialized in this type of cells. Afterwards, we incubated them with their secondary antibodies (Alexa 488 a-mouse for the VE-cadherin and Alexa 568 a-rabbit for SM22) and finally with Draq5 for nuclear staining.

The structure of vascular organoids was also evaluated by using an alternative way of fluorescent cells. In this case, we used contractile SMCs expressing the GFP protein and the CD34+ VPCs with the mcherry fluorescent protein which showed green and red colour respectively. In this way we overcame the restrictions of an insufficient infection or immunofluorescence staining.

### *3.11 In vitro Angiogenesis Assay*

Vascular organoids: Vascular organoids were plated on polymerized matrigel, in μ-Slide Angiogenesis plates (IBIDI) and cultured in EGM-2 medium (2 organoids/well). Media changes were performed every 2 days and organoid sprouting was observed daily. Images from at least 3 vascular organoids were taken on day 2 using a Leica TCS SP5 TIRF microscope. One day before the organoids transfer into matrigel (Corning, 354234), it was stored at 4°C in a box filled with ice, so that it would gradually thaw overnight. By the next day, 10μl of matrigel were placed carefully, without creating bubbles, into the μ-slide angiogenesis wells (IBIDI, 81501). The whole procedure was performed on ice, using cold pipette tips, in order to avoid matrigel's rapid polymerization before its placement into the wells. For the humidity's maintenance due to the small volumes used, the μ – Slide Angiogenesis plate (IBIDI)

was transferred into a larger plate (10 cm diameter) where a piece of wet paper was also introduced. The whole construct was then incubated at 37$^{o}$C for 60 min. Then, a vascular organoid was placed in every well along with 40µl EGM-2 medium. Medium change was carried out every 2 days, while the organoids were checked for their sprouts daily. Images were taken via the confocal Leica SP5 and the sprouting quantitation was performed with the Image J software.

### *3.12 Fluorescence-activated single cell sorting (FACS)*

This method is based on the characteristic scattering of light and fluorescence that every cell emits. CD34+ cells were enzymically removed with 0,05% Trypsin, transferred to new tubes with PBS enriched with 2% FBS and 1mM EDTA and were centrifuged for 5min at 1.200rpm. Afterwards, they were resuspended in the same dilution with final concentration 200.000 cells/40µl. Antibodies labeled with fluorescent dyes (FITC-Fluorescein isothiocyanate or PE-Phycoerythrin or APC-Allophycocyanin) were added to the 40µl mixture of cells and then incubated for 30min in absence of light. In the present study we used CD34- PE antibody. Consequently, 400µl PBS were added, cells were resuspended and then centrifuged for 5min at 1.600rpm. Then, the supernatant was discarded, cell pellet was diluted in 1ml PBS and transferred to a cone-like tube of 1,5ml suitable for the FACS machine, CyFlow (Partec, Münster, Germany). 20.000 incident were collected from every sample and their analysis was carried out using the FlowMax software.

### *3.13 H2B Lentivirus production*

HEK 293T were cultured in DMEM High (DMEM 31885 10% FCS, 1% P/S) and plated into 150 cm culture dishes for virus production. When 60- 70% confluent, cells were transfected with the following plasmids: (1) 15 µg psPAX2 (#12260, ADDGENE) (Trono Lab Packaging and Envelope Plasmids): plasmid which carries the pol and gag genes, expressing the viral enzymes and proteins of capsid which are responsible for the virus 73 packaging (2) 5 µg pMD2.G (VSV-G) (#12259, ADDGENE) (Trono Lab Packaging and Envelope Plasmids): plasmid which bares the env gene, expressing a viral envelope which performs a docking to hosting cells and (3) 25 µg construct of interest PGK-H2BmCherry (#21217 ADDGENE) viral vector expressing the H2B histone which is attached to mCherry through the PGK promoter (phosphoglycerate kinase) (192), using CaCl2 (Sigma – 223506)/ HBS (50mM NaCl Acros Organics – S316065, 1.5mM Na2HPO4 Sigma –30435, 280mM HEPES Sigma – H4034). 2 hours before transfection the medium was changed to DMEM serum free without penicillin/ streptomycin. Plasmid DNA was added dropwise into HBS and stayed for 15 min in room temperature. Then, it was added dropwise to the cells for 24 hours. After 24 hours the medium changed back to full DMEM as previously. The virus was collected at 72 hours from the 293T cells.

**Virus collection:** The culture medium from the transfected 293T cells was collected in a 50ml falcon tube, centrifuged at 2000 rpm for 5 minutes at room temperature to remove cell debris and the

supernatant was filtered using a 0.45µm non-pyrogenic sterile filter (SARSTED, Germany – 83.1826).A 20% sucrose solution was prepared, filtered and added to sterile plastic tubes. 10 mls of the viral supernatant was then layered on top of the sucrose solution. The samples were placed into the Beckman centrifuge and ultracentrifuged at 25,000 rpm for 2 hours using a SW41 Ti Swinging Bucket Rotor (BECKMAN COULTER, USA). The supernatant was discarded and the pellet resuspended in 100-200µls tissue culture PBS, aliquoted in 30µl amounts and stored at -80$^{o}$C.

**Lentivirus Titration in Smooth Muscle Cells**: cSMCs were initially cultured in a 6-well plate, then they were trypsinized counted and evenly distributed in 6 wells of a gelatin-coated 24-well plate. 24 hours later, the 2,5% ADSC medium was removed and replaced with 0,5ml 2,5% ADSC + polybrene (Sigma,28728-55) (4µg/ml in tissue culture water) at a ratio of 1000:1 (2,5% ADSC / polybrene). Then, the plate was placed at 37$^{o}$C for 30 minutes. Lentiviral particles were added in different amounts to every well (0.5, 1, 2, 4, 6µl). One well was kept as a control for the experiment where no virus was added. The wells were observed under fluorescence microscopy 48 hours after the infection with the lentivirus. The percentage of infected cells was calculated in each case and 5µl of the virus (Figure 6.4 in the Appendix section), was used for all subsequent experiments.

### *3.14 Graphene nanoplatelets and graphene oxide*

In the present study, 9 types of graphene platelets (Nanografi, Turkey) were used, showing differences in nanoparticle diameter and specific surface area. Nanoplatelets were weighed and diluted in tissue culture water at a final concentration of 0.5µg/ml and stored in the dark at room temperature. Before each addition to the cells, the graphene solutions were sonicated in the sonication water bath (Elmasonic S 30 H) for 4 minutes and then vortexed.

### *3.15 Internalization of graphene in contractile SMCs*

cSMCs were placed on glass coverslips and 24 hrs later were incubated for 24 hours with 3 different types of graphene (type 2, type 9 and graphene oxide). Coverslips were then washed and cells processed for immunofluorescence as described in the section “Immunofluorescence: Adherent contractile SMCs”

### *3.16 Statistical Analysis*

Data collected from cell growth analysis were collected from IncuCyte ZOOM 2016B, and processed with Microsoft Excel. Continuous data were expressed as mean ± SD. Normality tests were also carried out. The expression of proteins was detected from the visualization of the SDS- PAGE membrane in Azure imaging (Azure Biosystems). Images were collected, converted to grayscale via Photoshop software and then processed in Quantity One Analysis software (BIO-RAD) in order to quantitate the bands’ intensities. Then, the values were analyzed in Microsoft Excel where each value was divided to

its control and final graphs were generated. Standard deviation was also calculated and added to the graphs. Statistics for all the experiments were produced using GraphPad software. Accordingly, paired t-test was performed (comparisons between two conditions – control and each graphene's condition-). The P values obtained were 2-tailed and determined to be significant at $P \leq 0.05$. Statistical significance was also calculated by comparing each condition to each experiment's control, $*P < 0.05$, $**P < 0.01$.

## 4. Results

As the aim of the present study was to assemble vascularised brain organoids containing graphene, we first selected the most suitable size and surface area of graphene and graphene oxide to be used, by addressing the effect on the cell proliferation of all vascular cells to be incorporated in the brain organoid. In addition, we ensured that all cell types that would come into contact with graphene, such as ECs (HUVECs), mural cells (both contractile and synthetic vascular SMCs), and hVPCs differentiated from hESCs (VPC/CD34$^+$ cells) did not show any signs of cell phenotype or cell function alteration. The effects of graphene on neural cells were addressed in a separate study.

### *Establishing experimental conditions to evaluate the effect of graphene on cell proliferation*

To investigate the effect of graphene on vascular cell proliferation, we used the IncuCyte live cell imaging system. However, the graphene was visible in bright field and interfered with the ability of the Incucyte to detect and count cell numbers. Therefore, we decided to visualise the cells using fluorescent protein expression to avoid interference from the graphene. Initially we tested H1 cells constitutively expressing GFP, differentiated to vSMCs. Unfortunately, the fluorescent GFP signal was low and heterogenous, therefore signal quantification was inaccurate and additionally there was extensive background "noise". We therefore generated H1 cells expressing mCherry by targeting the expression construct to the AAVS1 safe harbour locus, to obtain high expression levels. This approach worked well (Manolis Iakovidis' and Maria Markou's unpublished results). A representative example is depicted in Figure 4.1.

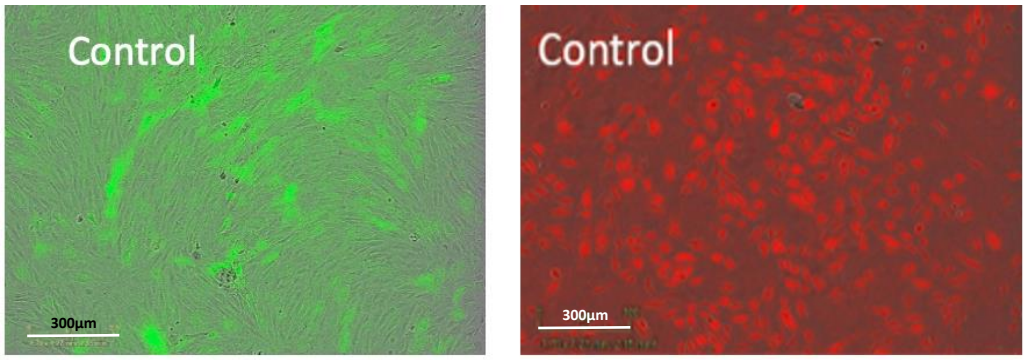


**Figure 4.1.** Representative images of GFP expressing sSMCs (left) and mCherry expressing (right) CD34$^+$VPCs taken from the IncuCyte Live-Cell Analysis

We realised that even though this approach of expressing mCherry was effective and easily detected, as the cells became confluent it was difficult to count individual cells as the mCherry protein diffuses through the entire cell. Therefore, we changed approach and infected the differentiated cells with a

H2B-mCherry lentivirus. The results of the H2B-mCherry lentivirus titration on cSMCs are shown in the Appendix section Figure 6.4. In this way, we obtained a fluorescent nuclear staining allowing us to have a better overview of each independent cell. Quantitation was performed based on the red object count instead of the surface area. The number of red (infected) nuclei at every time point was calculated and after a series of quantitations, the as data of red object count/mm2. Then, data from three independent biological repeats were processed in Excel and final graphs were produced. Graphs were also examined for statistical significance by comparing each condition with the control one.

We have performed cell proliferation assays in HUVECs using 9 types of graphene nanoplatelets with different diameters and surface areas. We chose a wide range of concentrations starting from 1 to 50 μg/ml (1, 5, 10, 25 and 50 μg/ml) in order to determine the optimal concentration for further experiments. (Table 4.1)

***Selection of graphene size, surface area and modification.***

HUVECs were isolated as described in Materials and Methods. Cells were used at passage P2. We performed a cell growth assay in HUVECs where we used 9 types of graphene with different diameter and surface area (Table 4.1). We chose a wide range of concentrations starting from 50 to 1 μg/ml (1-5-10-25-50 μg/ml) in order to determine the optimal concentration devoid of proliferative effect. According to our results, graphene type two (G2), which has the larger diameter compared to the others, does not affect cell proliferation at 1, 5 and 10 μg/ml concentrations as the cell proliferation levels were almost the same as the control (cells without graphene). In addition, there is no statistically significant difference between these lower concentrations and the control. However, 25 and 50 μg/ml had a cytostatic effect with the number of cells remaining at seeding density throughout the time course.

**Table 4.1**. Total types of graphene nanoplatelets used for a screening in the present study along with their diameter and specific surface area

| Graphene nanoplatelets | | |
|---|---|---|
| | Diameter (μm) | S.A: Specific Surface Area ($m^2/g$) |
| 2 | 30 | 135 |
| 3 | 18 | 135 |
| 4 | 18 | 170 |
| 5 | 7 | 170 |
| 6 | 7 | 135 |
| 7 | 1.5 | 320 |
| 8 | 1.5 | 530 |
| 9 | 1.5 | 800 |
| Graphene oxide | 1-5 μm | |

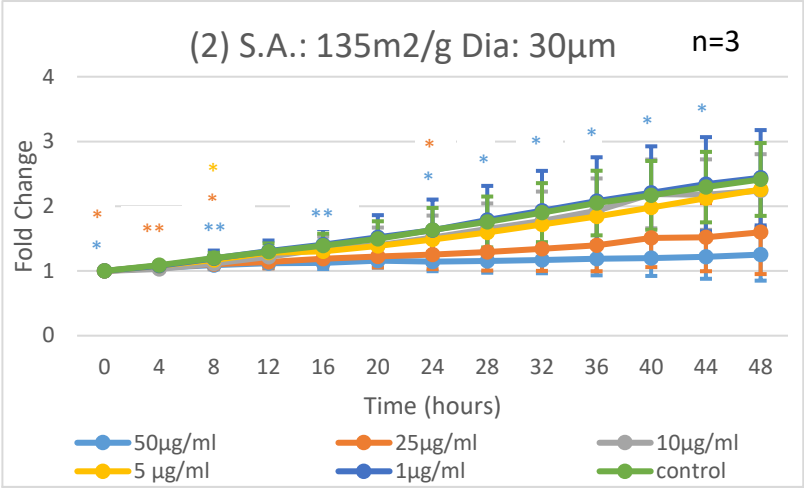
(2) S.A.: 135m2/g Dia: 30µm
n=3
Fold Change
Time (hours)
50µg/ml
25µg/ml
10µg/ml
5 µg/ml
1µg/ml
control

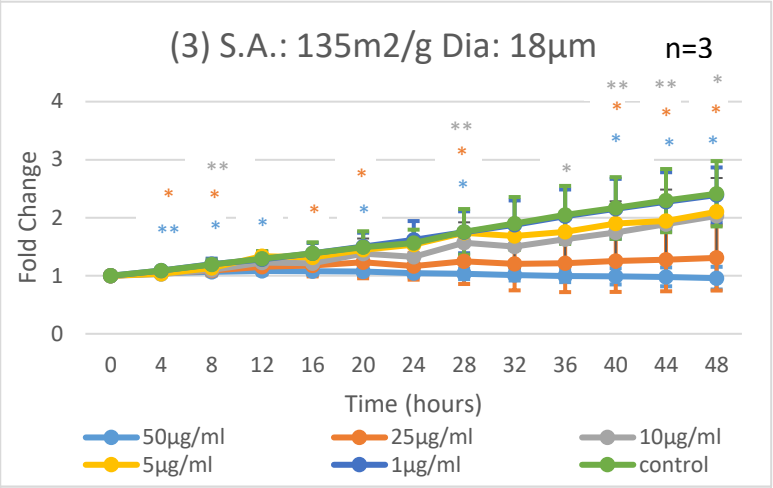
(3) S.A.: 135m2/g Dia: 18µm
n=3
Fold Change
Time (hours)
50µg/ml
25µg/ml
10µg/ml
5µg/ml
1µg/ml
control

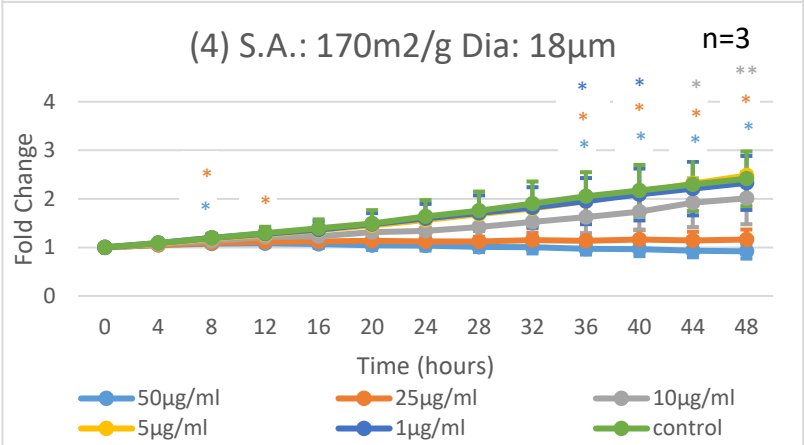
(4) S.A.: 170m2/g Dia: 18µm
n=3
Fold Change
Time (hours)
50µg/ml
25µg/ml
10µg/ml
5µg/ml
1µg/ml
control

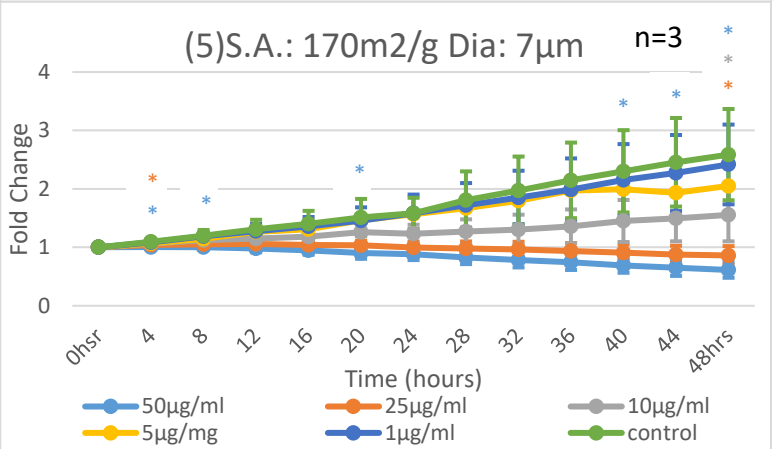
(5)S.A.: 170m2/g Dia: 7µm
n=3
Fold Change
0hsr
48hrs
Time (hours)
50µg/ml
25µg/ml
10µg/ml
5µg/mg
1µg/ml
control

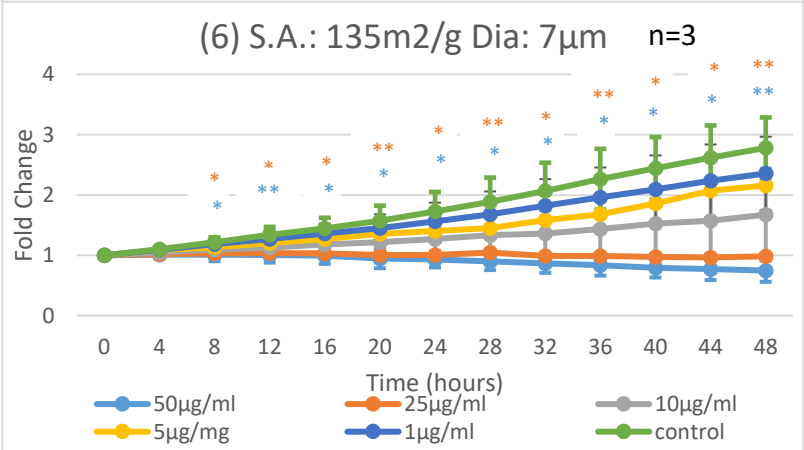
(6) S.A.: 135m2/g Dia: 7µm
n=3
Fold Change
Time (hours)
50µg/ml
25µg/ml
10µg/ml
5µg/mg
1µg/ml
control

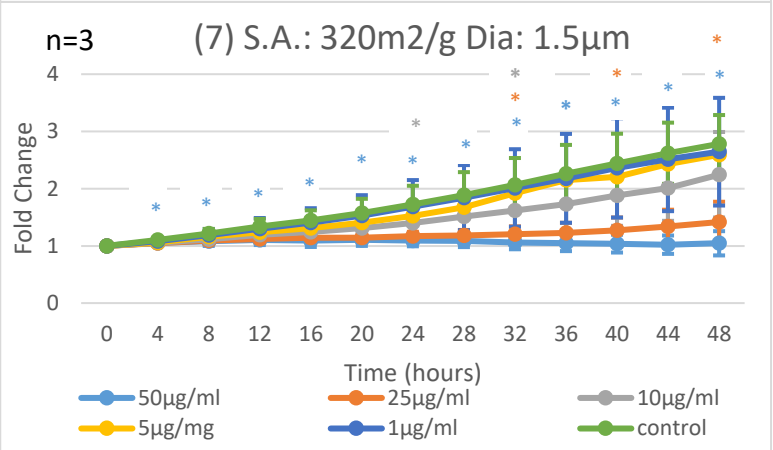
n=3
(7) S.A.: 320m2/g Dia: 1.5µm
Fold Change
Time (hours)
50µg/ml
25µg/ml
10µg/ml
5µg/mg
1µg/ml
control

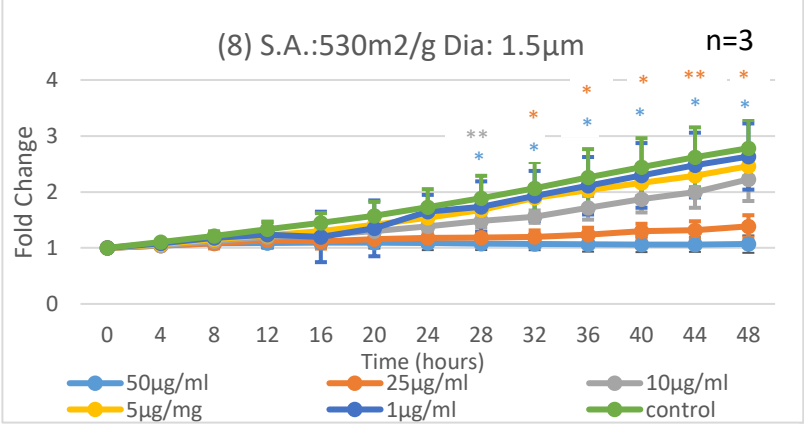
(8) S.A.:530m2/g Dia: 1.5µm
n=3
Fold Change
Time (hours)
50µg/ml
25µg/ml
10µg/ml
5µg/mg
1µg/ml
control

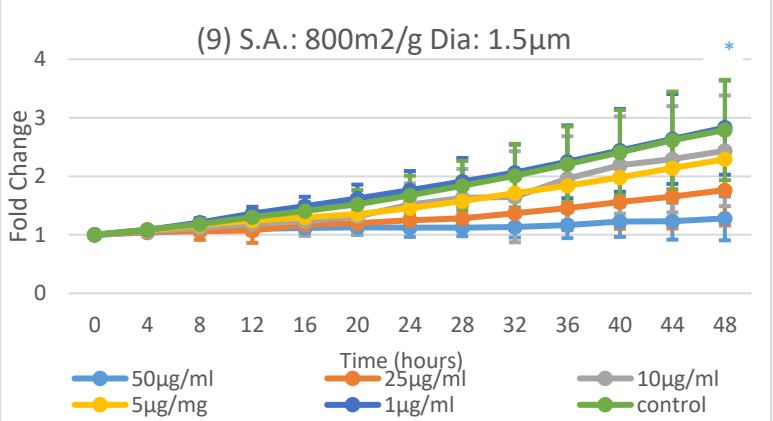
(9) S.A.: 800m2/g Dia: 1.5µm
Fold Change
Time (hours)
50µg/ml
25µg/ml
10µg/ml
5µg/mg
1µg/ml
control

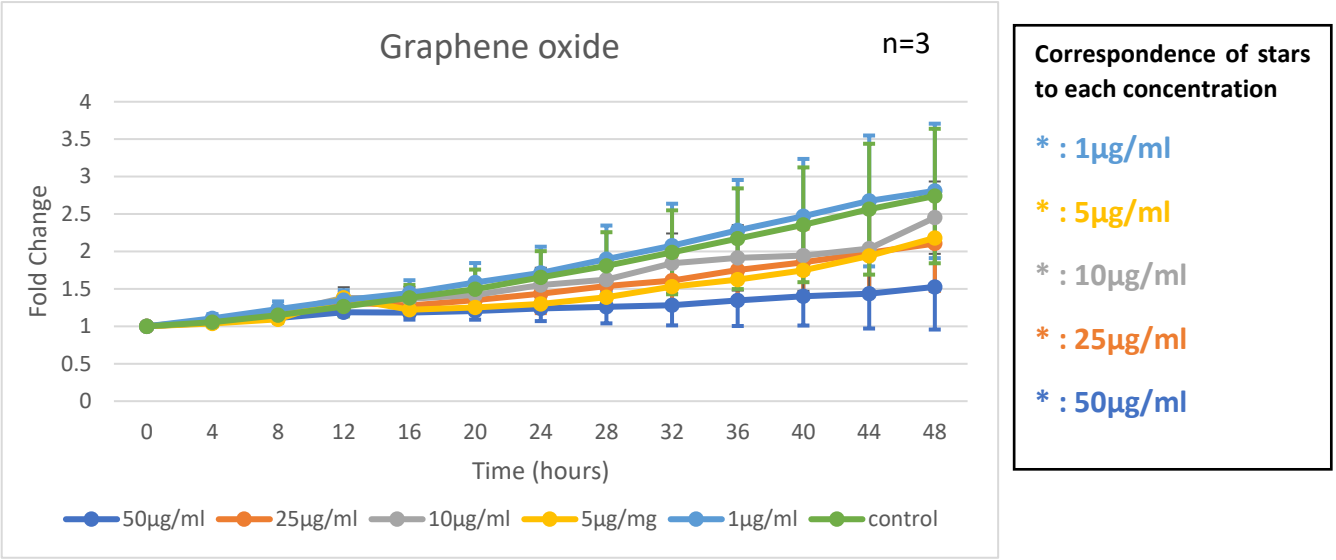


**Figure 4.2**. Schematic diagrams showing the screening of the effect of 9 types of graphene when introduced in cell culture of HUVECs. Graphene nanoplatelets differed in specific surface area and diameter. HUVECs were infected with H2B-mcherry lentivirus and 7000 cells were placed in a collagen coated 96-well plate for 24 hours at 37°C. The next day, the diluted graphene was added to the medium in 5 concentrations (1- 5-10-25-50 µg/ml) in triplicates. The plates were incubated in the IncuCyte Live-Cell Analysis system and 4 images were taken per well every 4 hours for 48 hours in total. The bars show ± SD. The graphs are produced by calculating three independent experiments. Statistical significance was also calculated by comparing each condition to each experiment's control, *P < 0.05, **P < 0.01.

However, 25 and 50 µg/ml had a cytostatic effect with the number of cells remaining at seeding density throughout the time course. This observation is supported by the statistically significant difference at almost every time point between 25 and 50 $\mu$g/ml and control. G3 and G4, both have the same diameter (18 µm), and showed a similar proliferation pattern to G2. G5 and G6, both 7µm diameter, have similar effects on cell proliferation. At high concentrations 25 and 50ug/ml, the cell numbers, at late time points, drop below the seeding density, suggesting cytotoxicity. G5 at 1 ug/ml did not alter cell proliferation but at all other concentrations cell proliferation was inhibited to various degrees, while G6 had an inhibitory effect on cell proliferation at all concentrations. G7, G8 and G9 belong to the subgroup of the smaller diameter graphene types (1.5 µm). Concentrations of 25 and 50 µg/ml were cytostatic, however in the case of G9 the effect at 25 ug/ml was a little less pronounced. 1 ug/ml was devoid of effects on proliferation in all 3 cases. GO was also tested. 1 µg/ml had the same growth rate as control, however the standard deviation in the GO experiment was high.

After this screening (Figure 4.2) we had enough data to compare proliferation rates, concentrations, and the effect of different graphene types. Therefore, we conclude that the graphene types we are going to further use are G2, G9 and GO. G2 was selected as the nanoparticle that bears the larger diameter (30 µm), and shows no alteration of cell proliferation when applied at 1, 5 and 10 $\mu$ g/ml concentrations. In addition, because of its size at 30um, G2 is unlikely to be internalized into the cells and therefore intracellular damage which might result following uptake would be avoided. G9 had one

of the smallest diameters (1.5 µm) and also had a less inhibitory effect on the proliferation rate. GO was chosen due to its known unique physical and chemical properties when it comes to bio-applications.

### *Effect of Graphene Nanoplatelets on Synthetic Vascular Smooth Muscle Cell Proliferation*

We next addressed the effect of G2, G9 and GO on both contractile and synthetic vSMCs, cSMCs and sSMCs. In sSMCs, G2 was very well tolerated and even higher concentrations of 25 and 50 µg/ml. Statistically significant differences were mostly identified between 25 and 50 µg/ml exhibited minimal cell proliferation effects. G9 and GO on the other hand, did not alter cell proliferation at 1 µg/ml, but higher concentrations showed a concentration-dependent inhibition of proliferation. However, in this case even 10 µg/ml reduced significantly the cell growth compared to control. Raw images taken from the IncuCyte indicate that cells had normal morphology during the experiment, data not shown. Having collected the above results regarding the effect of different concentrations of graphene on sSMCs, we further investigated if concentrations even lower than 1µg/ml, cause a less inhibitory effect on cells' proliferation. For this reason, we introduced 0.25, 0.5 and 1µg/ml of the 3 types of graphene to cell culture of sSMCs and followed the same experimental process for 48hours (Figure 6.3) and suggest that there is decrease in cell proliferation at these low concentrations.

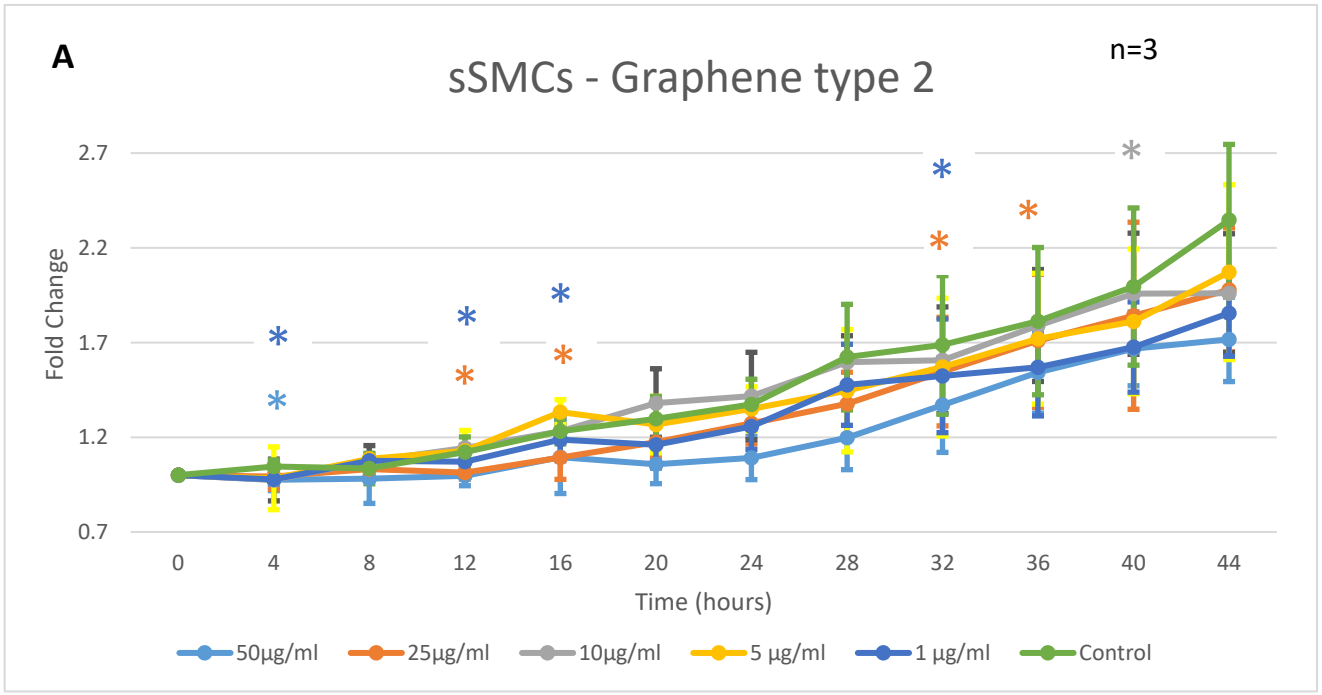

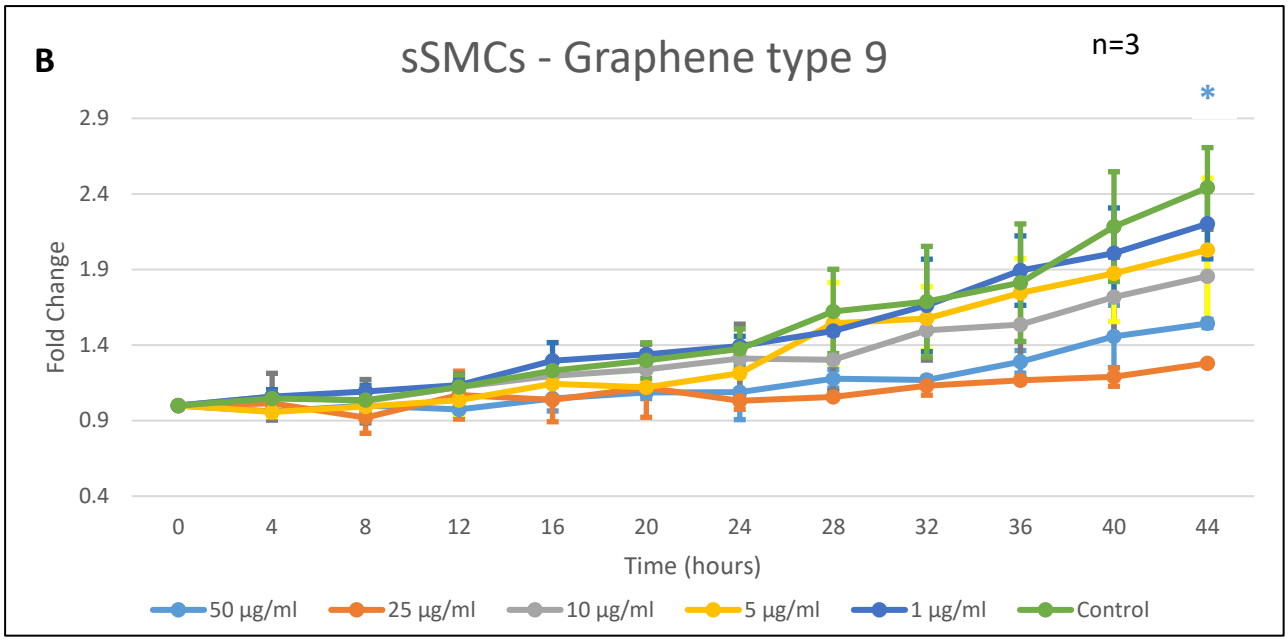


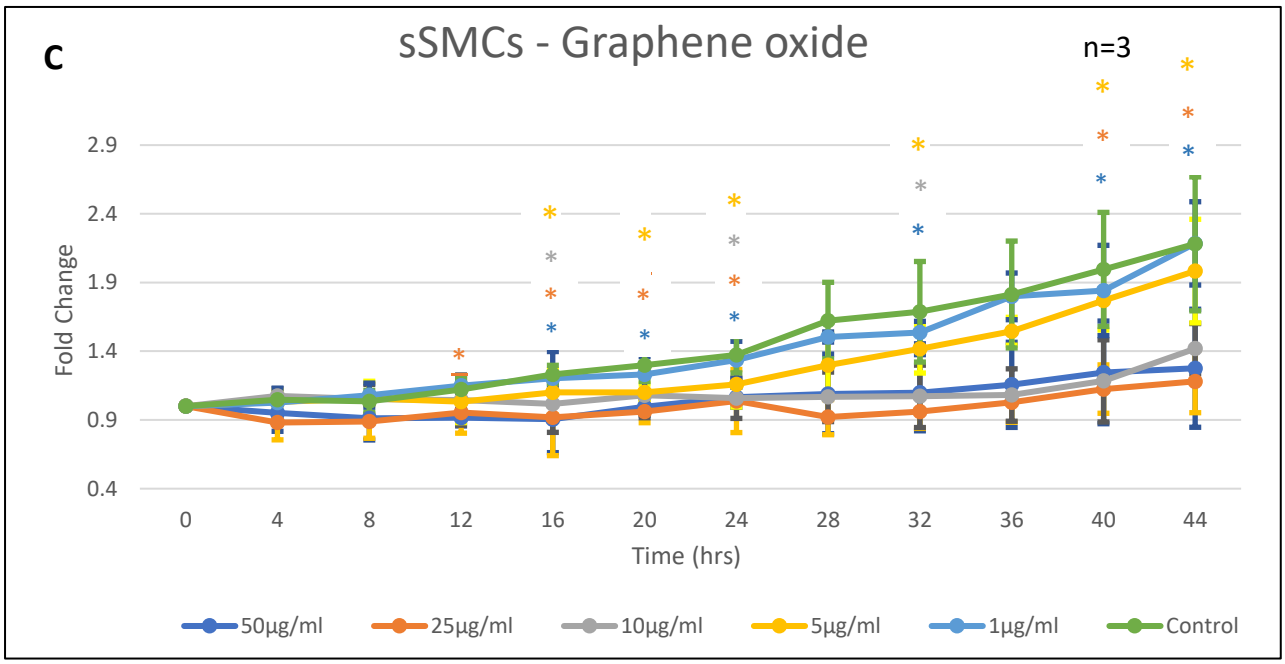


**Figure 4.3** Schematic diagram showing the cell proliferation rate of sSMCs in presence and absence of graphene type 2 (30µm diameter), graphene type 9 (1.5µm diameter) and graphene oxide. sSMCs were infected with H2B-mcherry lentivirus 72 hours after they were splitted and 3.500 cells were seeded into a gelatin coated 96-well plate for 24 hours at 37ºC. The next day, the diluted graphene was added to the cells in Pericytic Medium in 5 concentrations (1- 5-10-25-50µg/ml) in triplicates. The plate was then inserted in the IncuCyte Live-Cell Analysis system and 4 images were taken per well every 4 hours for 44 hours in total. The bars show ± SD. A, B, C) Graphs depict the cell growth throughout the 44-hour period. The results show the means of the three replicates together with their standard deviation. Statistical significance was also calculated by comparing each condition to control, * $P < 0.05$

***Effect of Graphene Nanoplatelets on Contractile Vascular Smooth Muscle Cell Proliferation***

cSMCs are less proliferative compared to sSMCs, as expected, 25 and 50 µg/ml of G2, G9 and GO inhibited cell proliferation, while 1,5 and 10 µg/ml were well tolerated and exhibited minimum inhibition of cell proliferation. Raw images taken from the IncuCyte indicate that cells had normal morphology during the experiment, data not shown.

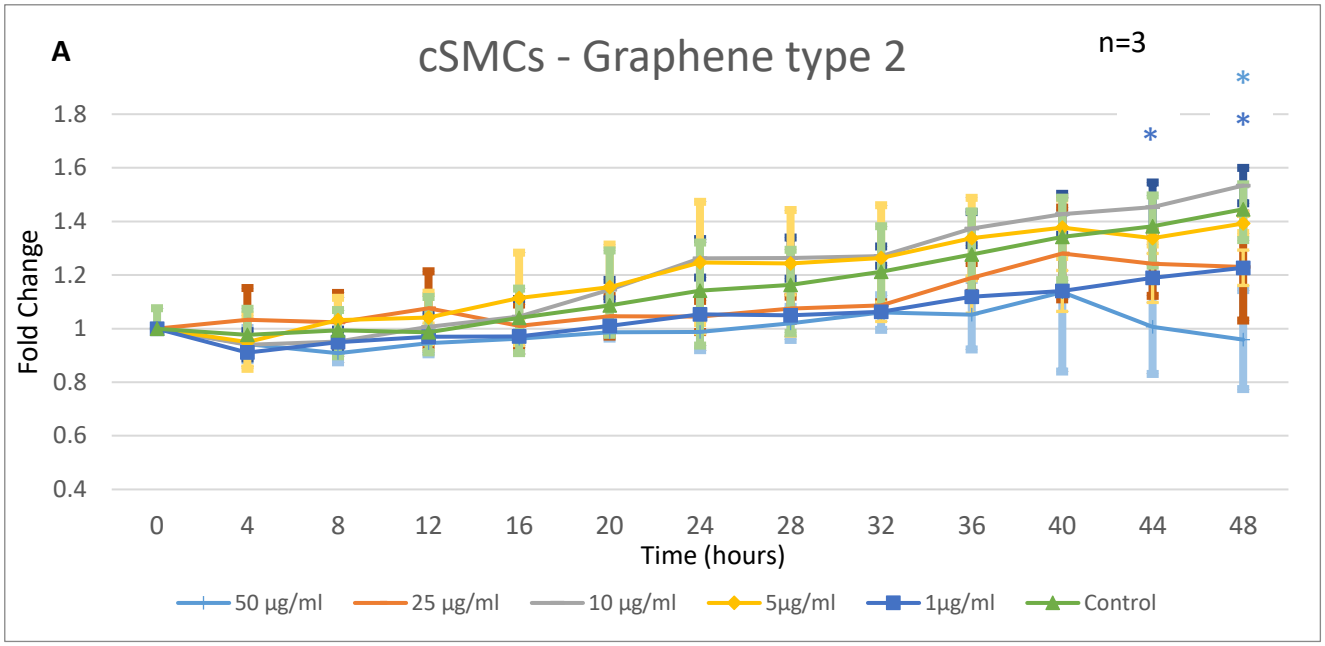


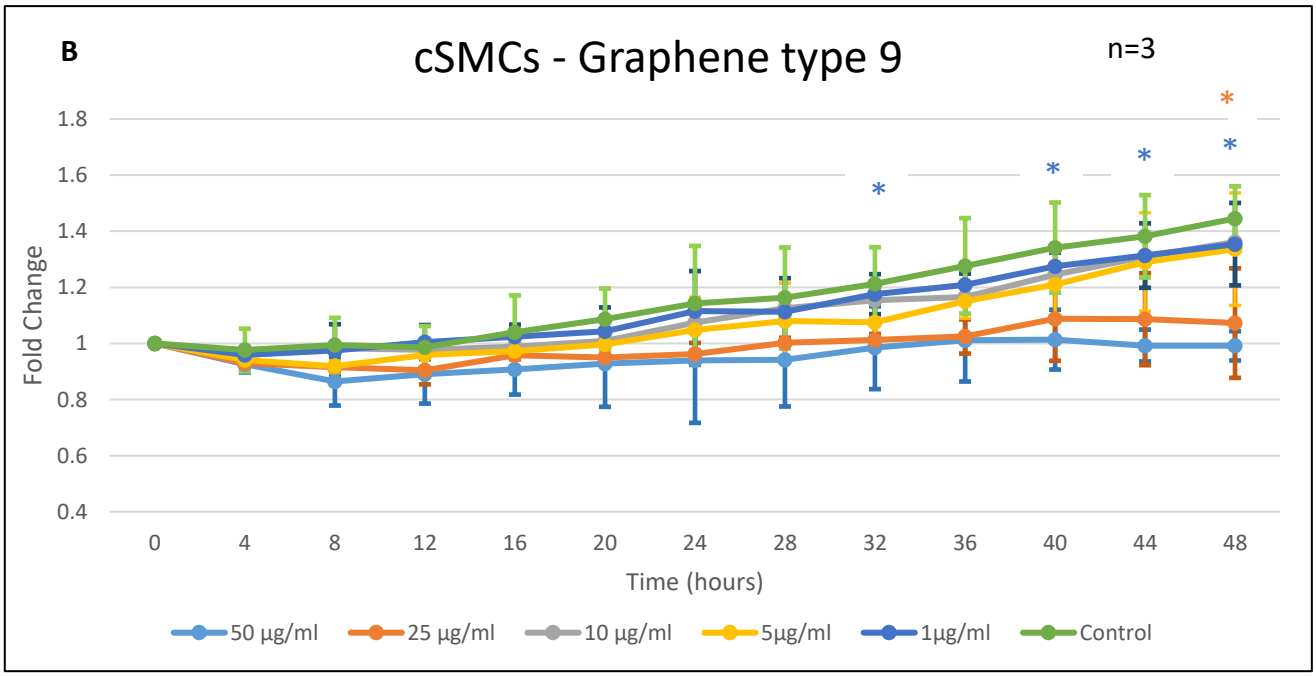

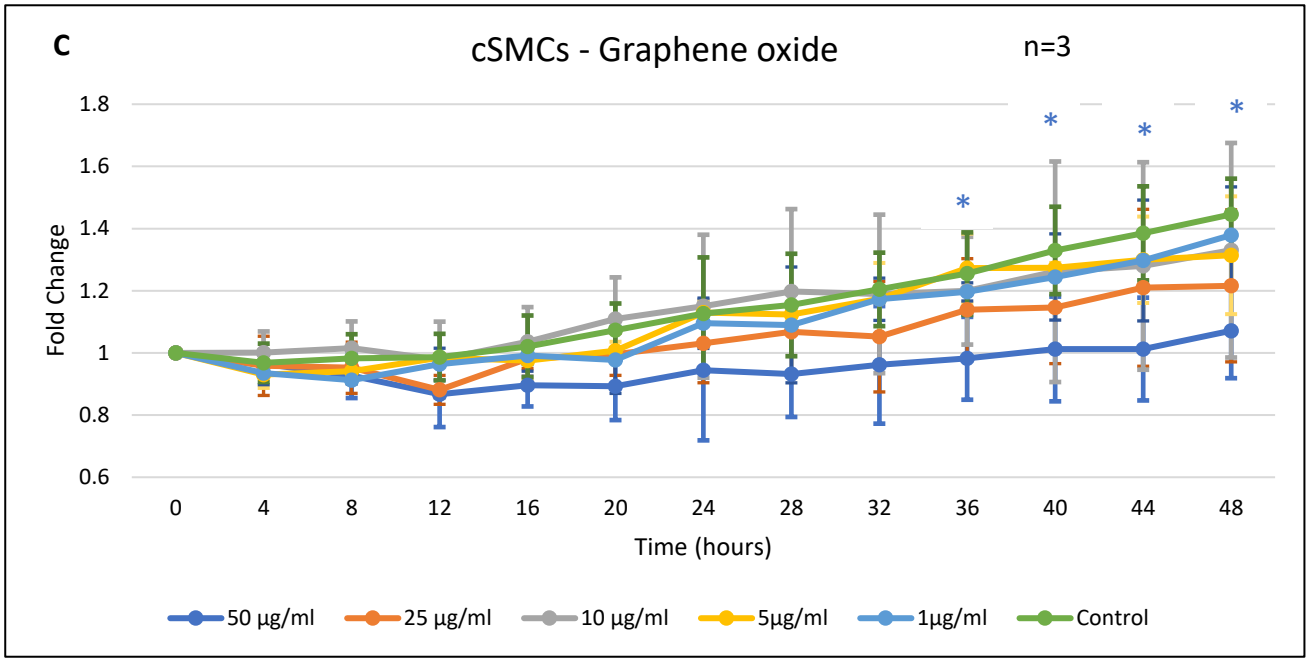


**Figure 4.4.** Schematic diagram showing the cell proliferation rate of contractile SMCs in presence of (A) graphene type 2 (30µm diameter), (B) graphene type 9 (1.5µm diameter) and (C) graphene oxide. sSMCs were infected with H2B virus and 3.500 were seeded per well in gelatin coated 96-well plate for 24 hours at 37°C. The next day, the diluted graphene was added into 2,5% ADSC and the mixture was introduced to the cells in 5 concentrations (1,5,10,25 and 50µg/ml) in triplicates. The plate was then inserted in the IncuCyte Live-Cell Analysis system and 4 images were taken per well per 4 hours for 48 hours in total. The bars show ± SD. The results show the means of the three replicates together with their standard deviation. The screening process was performed by Maria Markou and the analysis was conducted by Athanasia Zoi Pappa. Statistical significance was also calculated by comparing each condition to control, *P < 0.05

### *The effect of graphene on the phenotypic plasticity of VSMCs*

In order to investigate if the presence of graphene plays a role in the transition between the synthetic and contractile phenotype, we evaluated the expression levels of three typical smooth muscle phenotype markers SM22, a-SMA and calponin, known to be downregulated as contractile cells transition to the synthetic phenotype. Based on our results, the expression pattern of SMA seems to remain mainly unaffected by the presence of all 4 conditions of graphene in sSMCs. In cSMCs SMA levels seemed to be decreased by G9 at 1µg/ml (Fig. 4.5 panel c), however due to the low level of SMA expression in the cells, this needs to be further verified. Calponin levels are low in sSMCs, as expected, however levels seem elevated in G2, G9 and GO at 1µg/ml, while 10 ug/ml G2 has no effect. In cSMCs, calponin levels are unaffected by G2, G9 and GO, the variation in the GO experiments needs to be readdressed and clarified. SM22 is also unaffected in sSMCs but in cSMCs G9 1 µg/ml decreases the level of the protein. From the above, we cannot accurately conclude. The experiments need to be repeated to be sure of the result.

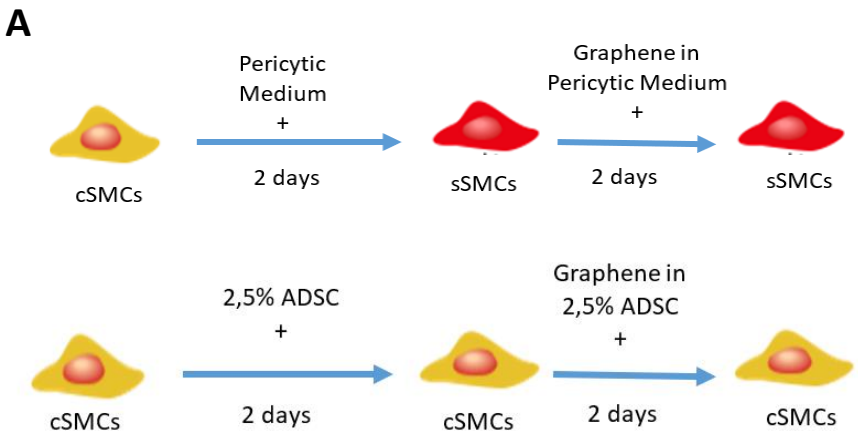
A
Pericytic
Medium
+
2 days
Graphene in
Pericytic Medium
+
2 days
cSMCs
sSMCs
sSMCs
2,5% ADSC
+
2 days
Graphene in
2,5% ADSC
+
2 days
cSMCs
cSMCs
cSMCs

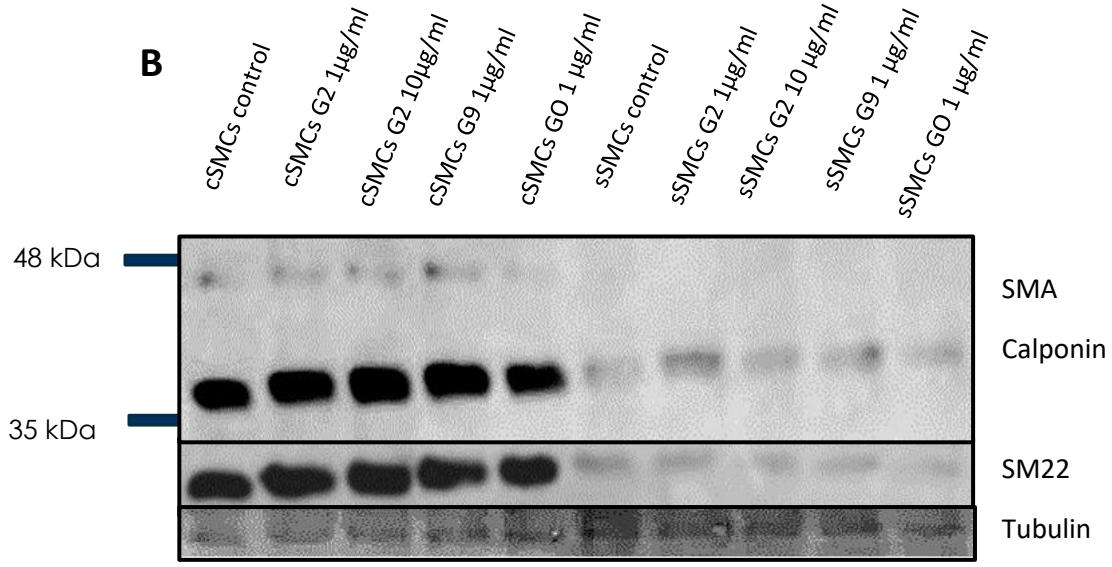
B
cSMCs control
cSMCs G2 1µg/ml
cSMCs G2 10µg/ml
cSMCs G9 1µg/ml
cSMCs GO 1 µg/ml
sSMCs control
sSMCs G2 1µg/ml
sSMCs G2 10 µg/ml
sSMCs G9 1 µg/ml
sSMCs GO 1 µg/ml
48 kDa
35 kDa
SMA
Calponin
SM22
Tubulin

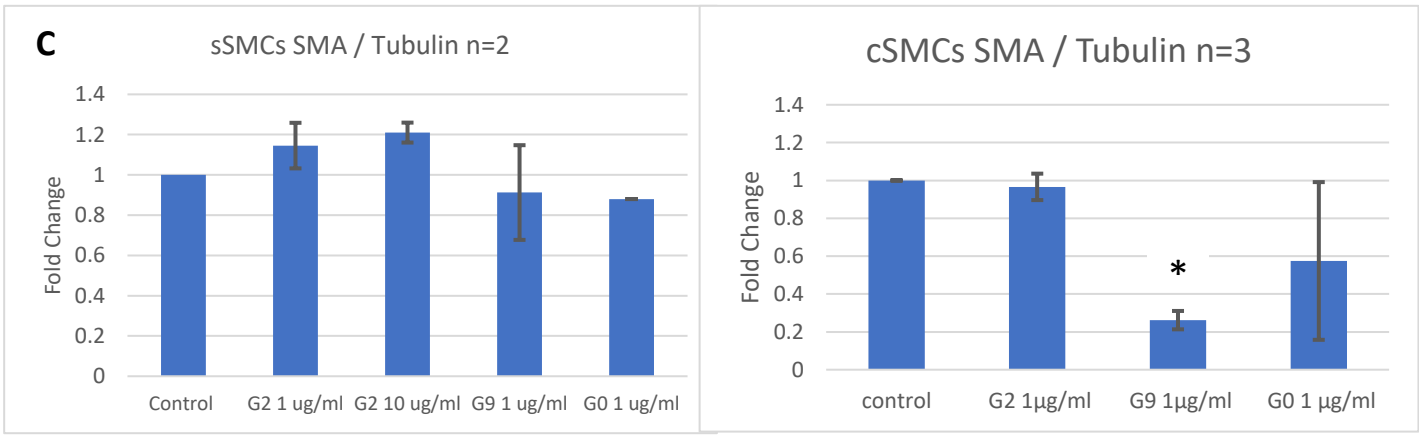
C
sSMCs SMA / Tubulin n=2
Fold Change
1.4
1.2
1
0.8
0.6
0.4
0.2
0
Control
G2 1 ug/ml
G2 10 ug/ml
G9 1 ug/ml
G0 1 ug/ml
cSMCs SMA / Tubulin n=3
Fold Change
1.4
1.2
1
0.8
0.6
0.4
0.2
0
*
control
G2 1µg/ml
G9 1µg/ml
G0 1 µg/ml

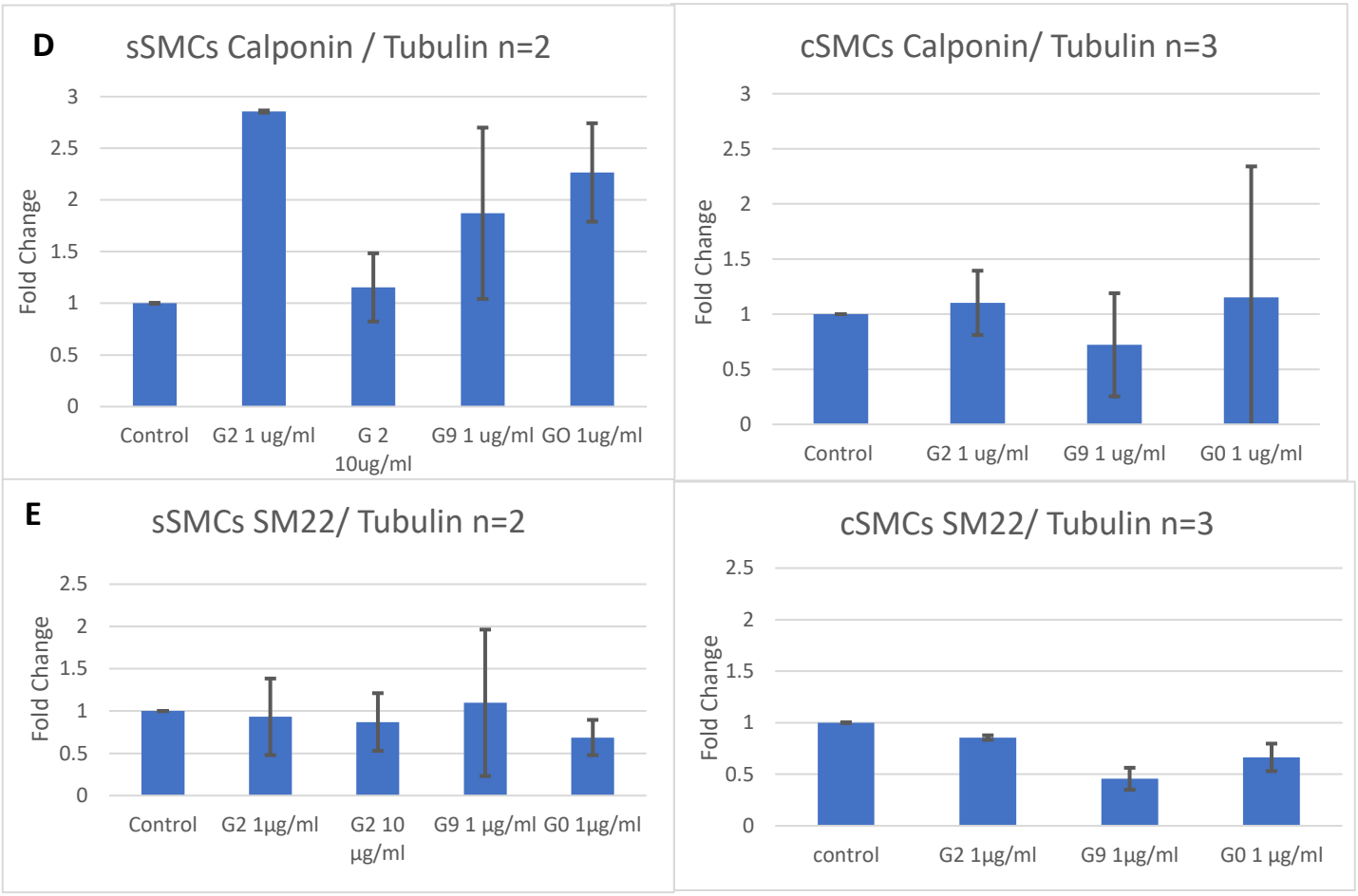


**Figure 4.5**. Schematic diagram of the experimental process followed for the investigation of graphene's role on the expression of SM markers (A). After generating both subtypes of SMCs, we incubated them with G2, G9 and GO at 1 µg/ml for two days. (B) A representative image of a western blotting experiment showing the levels of SMA, Calponin and SM22 expression in the presence and absence of G2, G9 and GO in both cSMCs and sSMCs. Quantitation of the western blotting experiments are shown in (c) SMA (D)Calponin levels and (E) SM22 levels, all normalized to Tubulin. Bands were visualised using Azure Biosystems. Data were collected and processed by Quantity One Analysis software (BIO-RAD) and graphs were produced in Excel. Statistical significance was applied only to n=3 cSMCs results and was calculated by comparing each condition to control, *P < 0.05

***Effect of graphene on the expression of pluripotency marker Oct 3/4 in H1 stem cells***

After investigating the effect of graphene nanoplatelets on vascular cell lines used in the present study, we also addressed the effect of graphene on pluripotent stem cells, as these cells would be used to generate the brain organoid. We approached this issue by checking the pluripotency state of these cells through the expression of OCT 3/4, a widely used pluripotency marker. Nanoplatelets were added to the culture medium for 4 days. Two days after their introduction the medium was changed according to the manipulations described in Materials and Methods section (Figure 3.1).

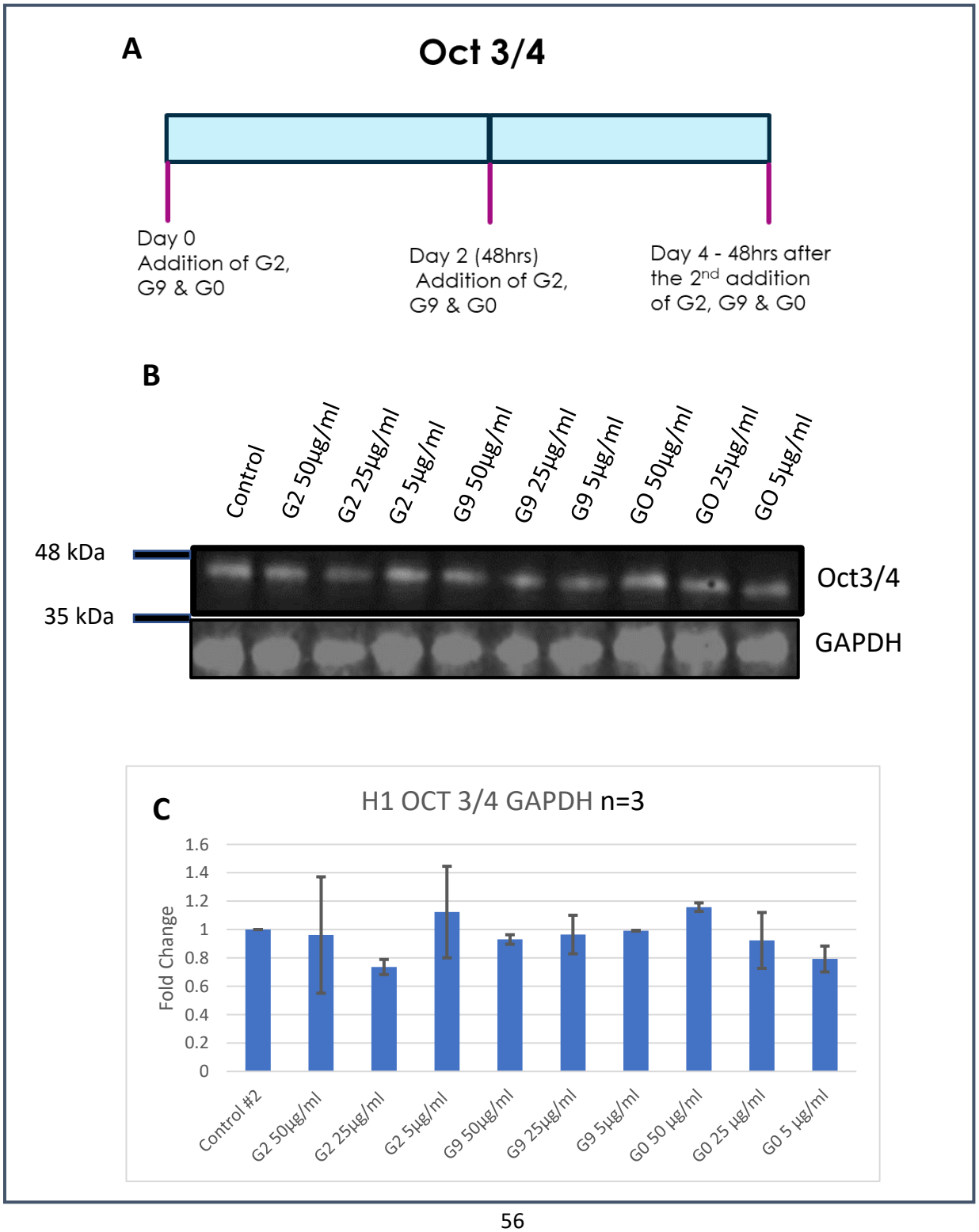

**Figure 4.6**. OCT 3/4 pluripotency marker levels of expression when G2, G9 & GO was introduced in cell culture. We introduced concentrations of 5, 25, 50 μg/ml Graphene in the culture medium for 4 days. As a loading protein we used GAPDH. Cell lysates were prepared, western blot analysis performed and membranes probed with an anti-OCT3/4 antibody. Bands were visualised using Azure Biosystems. Data were collected and processed by Quantity One Analysis (BIO-RAD) software and graphs were produced in Excel. Statistical significance was also calculated for graphs with n=3 by comparing each condition to control.

The results of the effect of G2, G9 and GO on the levels of OCT3/4 show no statistically significant effect of graphene at 5, 25 and 50 ug/ml. The effect of graphene on H1 hESCs proliferation was also addressed at 1, 5 and 10μg/ml, G9 and GO. However, these results belong to one independent experiment and need to be repeated, in addition we need to address the effect of G2. However, 1 and 5 ug/ml of G9 and GO had not effect on the H1 cell proliferationn (Appendix Fig. 6.1).

### *Effect of graphene on the ability of VSMCs and ECs to form vascular organoids*

Having established that graphene G2, G9 and G0 at 1μg/ml and G2 also at 10μg/ml did not alter HUVEC and SMC proliferation, we next addressed whether the presence of graphene affects the ability of these cell types to form a 3D vascular organoid. The assembly of the vascular organoids including both ECs and SMCs, was performed using the hanging drop technique with methylcellulose and EGM-2 (see Materials and Methods). The effect of graphene in the vascular organoid was examined by using 4 different conditions as shown in Table 4.1

**Table 4.2** Types and concentrations of graphene nanoplatelets introduced into the process of vascular organoid generation

| No | Graphene type | Concentration |
|---|---|---|
| Control | - | - |
| 1 | G2 | 1μg/ml and 10 μg/ml |
| 2 | G9 | 1μg/ml |
| 3 | GO | 1μg/ml |

As expected from our previous work (Markou, et al., 2020) in control vascular organoids, ECs are located at the exterior layer of vascular organoids as identified by staining with VE-Cadherin and SMCs were identified in the interior part stained by SM22 (Markou et al., 2020), Figure 4.5 panels VE-cadherin and SM22. In the vascular organoids containing graphene, the graphene accumulated in the interior of each organoid, creating a dark background in brightfield, Figure 4.7 panel Brightfield. Each staining is shown separately and as a merged image. Maximum projection was also included for better visualisation.

Vascular organoids containing graphene nanoplatelets at 1μg/ml have no significant differences compared to the control condition. Their size, shape and structure remain the same, with ECs located on the exterior part covering the sSMCs in the interior. However, when G2 is introduced at a higher concentration (10μg/ml) there is a disruptive effect on vascular organoids. More specifically, their accumulation causes irregular shapes as well as problems in the structural integrity of the organoid. For this reason, only few survived until the end of the experiment.

In conclusion we show that G2, G9 and GO at 1 μg/ml caused no adverse effects on the viability and structural integrity of the vascular organoids. This experiment was performed 1 time analysing 3 vascular organoids per condition.

**Vascular organoid formation sSMCs / HUVECs**

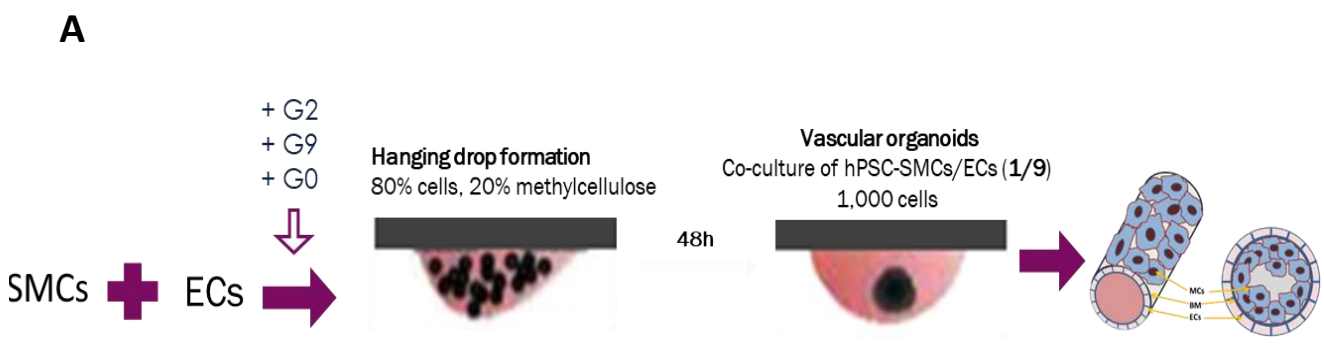

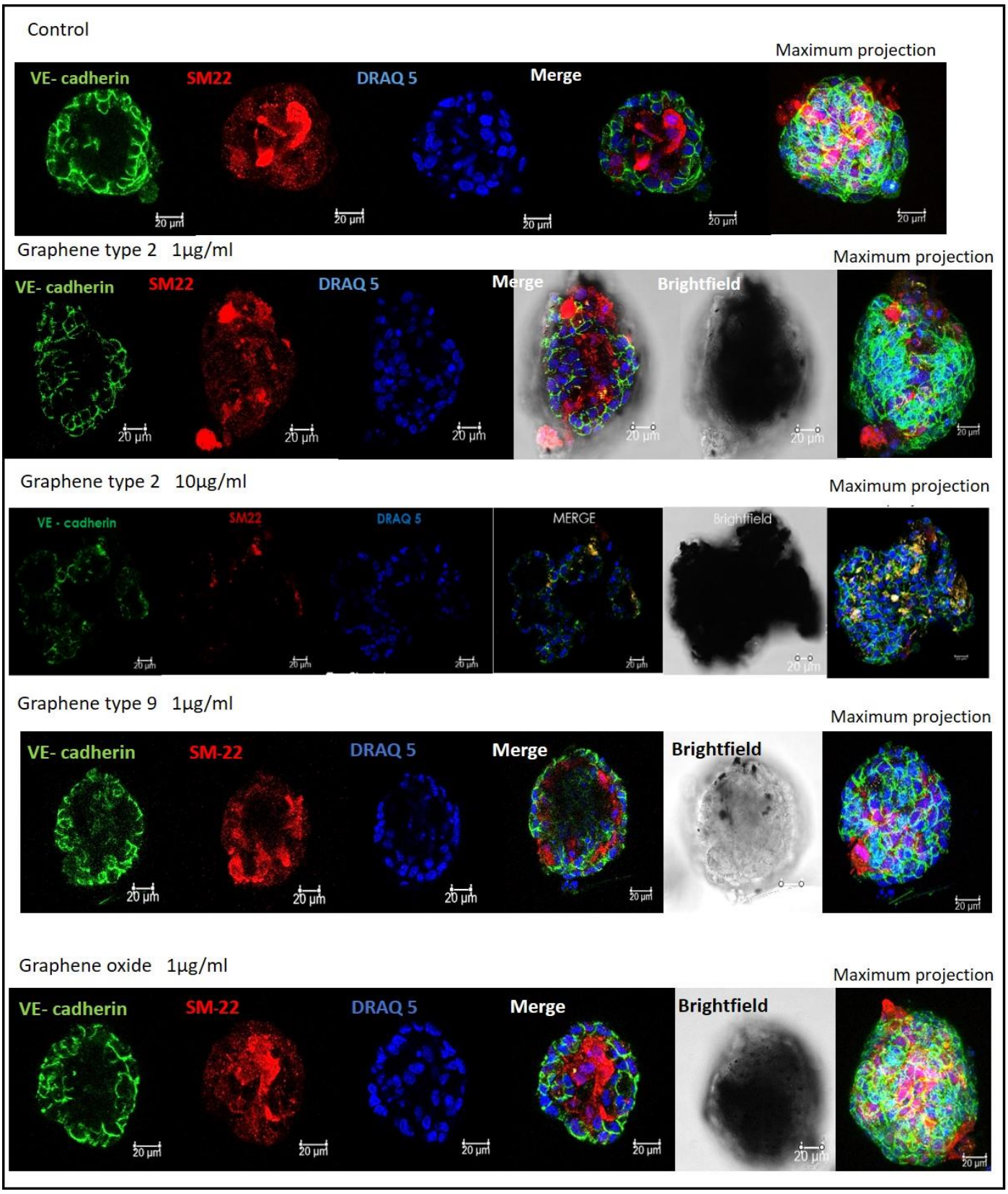


**Figure 4.7.** B, C, D, E, F) Vascular organoids generated form mixed cell populations of sSMCs and HUVECs. G9 and GO were added at 1µg/ml whereas G2 was used in both 1 & 10 µg/ml. 2 days after the hanging drop technique, organoids were collected, fixed and stained with antibodies specific for each cell type. SM22 stains the sSMCs and VE-cadherin labels the ECs. DRAQ5 was used for nuclear staining. Images were taken in Leica TCS SP5 Confocal microscope using HCX PL APO CS 40.0x1.25 OIL UV obiective.

### *Effect of graphene on the ability of VSMCs and CD34$^{+}$ VPCs differentiated from hPSCs to form vascular organoids*

Having established that graphene has no detrimental effect on the generation of CD34$^{+}$ VPCs from hPSCs, we investigated the effect of graphene on vascular organoids formed from this cell population with VSMCs. The H1 mCherry expressing cells were produced by Manolis Iakovidis and Maria Markou. They were differentiated to CD34+ VPCs and isolated as described in Materials and Methods. H1-GFP expressing cells were differentiated to VSMCs as described in Materials and Methods. In this way we generated ECs with red fluorescence and VSMCs with green fluorescence, enabling the vascular organoids generated from these two cell populations to be imaged without antibody staining.

Vascular organoids generated from GFP-cSMCs and mcherry-CD34$^{+}$ VPCs cells presented the same characteristics as the sSMCs /HUVEC organoids. They were structurally and functionally even, having no alterations in terms of size, shape and viability. In this experiment, we omitted the higher concentration of 10μg/ml G2 and tested only 1μg/ml for every different type of graphene. Graphenes' accumulation in the interior is obvious in brightfield at all conditions. This experiment was performed one time and 3 vascular organoids per condition were imaged except for the control which were 2. Therefore, we conclude that G2, G9 and GO at 1μg/ml concentration allow the generation of viable, structurally stable and properly layered vascular organoids. This experiment needs now to be repeated analysing the location of VE-cadherin to ensure tight EC-EC contacts.

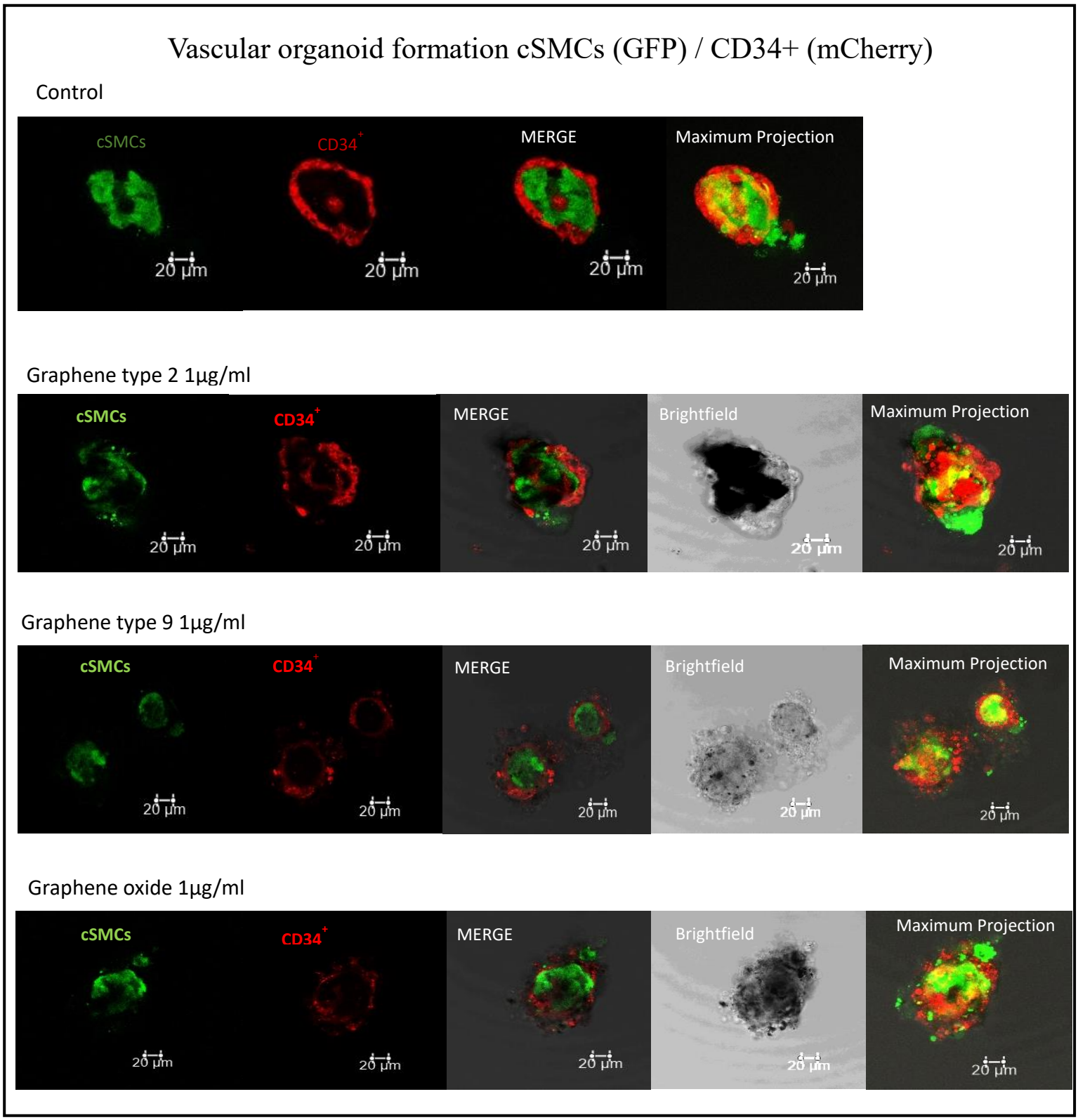


**Figure 4.8.** Vascular organoids generated form mixed populations of GFP-cSMCs and mcherry-CD34$^{+}$ VPCs. G2, G9 and GO were added at 1µg/ml concentration. 2 days after the hanging drop technique, organoids were collected, fixed and imaged by Confocal microscopy. Images were taken in Leica TCS SP5 Confocal microscope using HCX PL APO CS 40.0x1.25 OIL UV objective.

***Functional analysis of cSMCs/ CD34+ VPC vascular organoids in the presence and absence of graphene***

We generated vascular organoids from cSMCs and CD34+VPCs differentiated from H1 cells. As described in the vascular organoids' formation section, both vascular cells express fluorescent proteins and this enabled us to distinguish each cell types contribution in the sprouts. The first observations mainly pertained to the organoids' intense growth in every direction with plenty of new sprouts. G2 and GO increased the number of sprouts at a concentration of 1μg/ml (Figure 4.9 panel A). The length of the sprouts a decreased the depth of the sprouts into Matrigel as presented in Figure 4.9 panel G.

To sum up, 1 μg/ml constitutes a concentration which does not inhibit vascular organoid sprouting, and invasion. Whether there is a stimulatory effect requires repetition of the experiment and analysis of increased number of vascular organoids.

A

**Control**

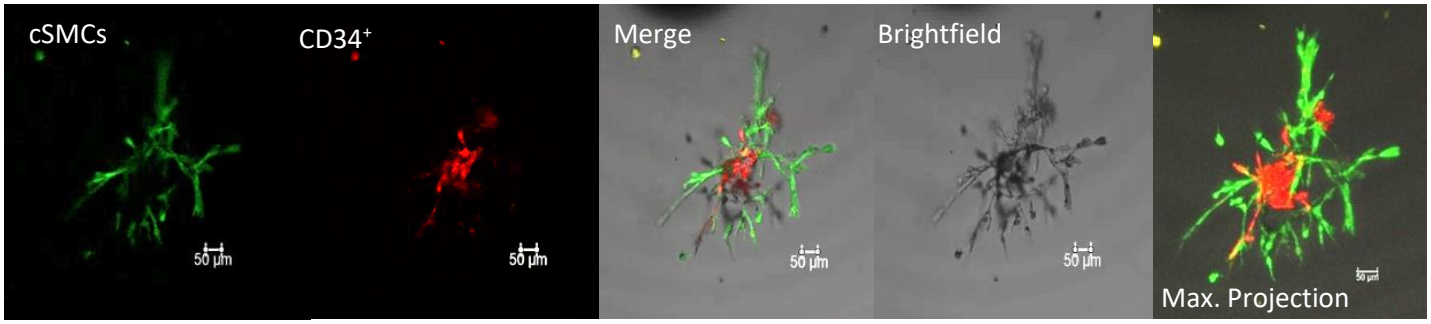


B

**Graphene type 2 1ul/ml**

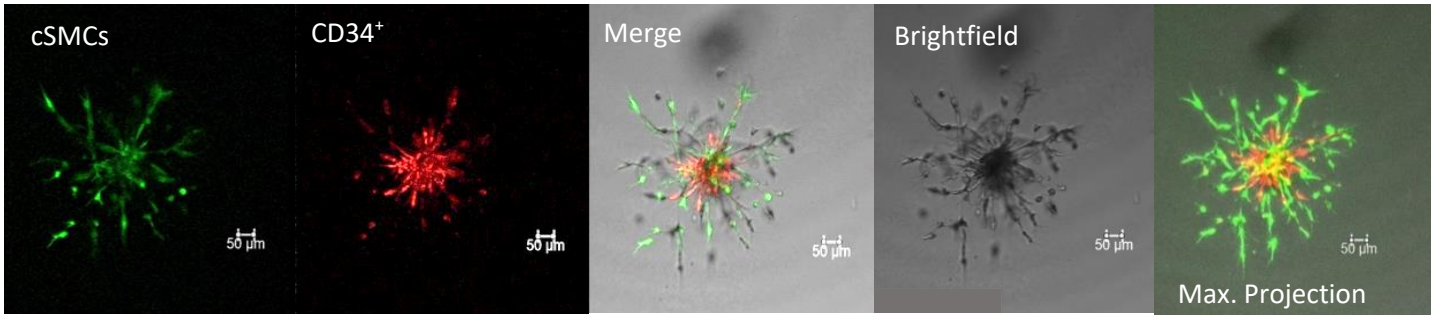


C

**Graphene type 9 1ul/ml**

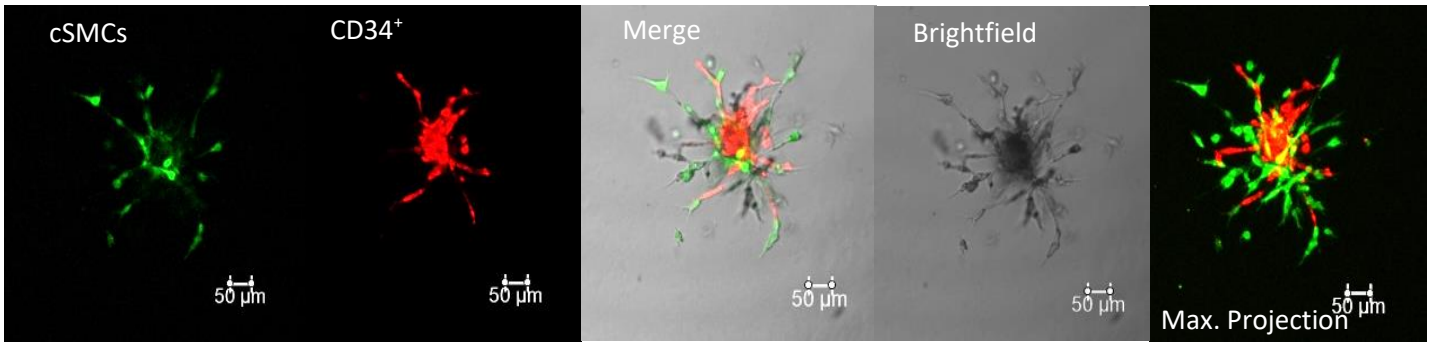


D

**Graphene oxide 1ul/ml**

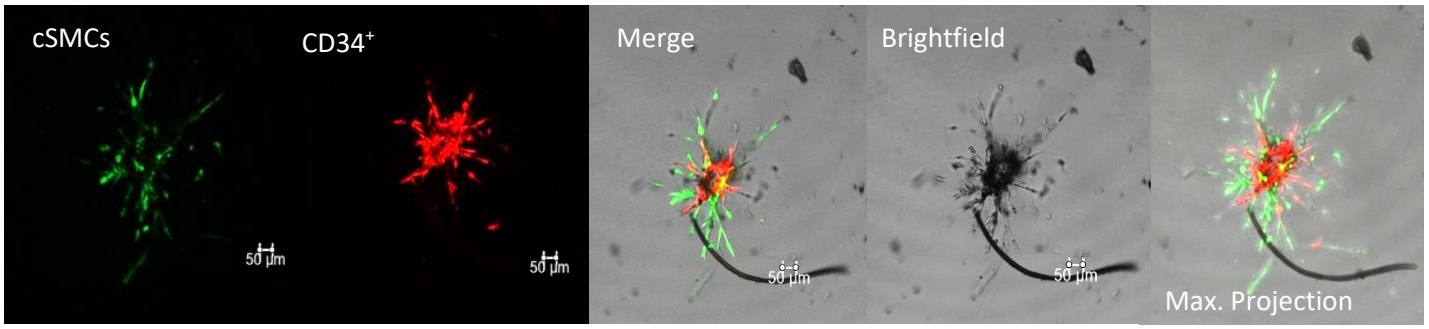

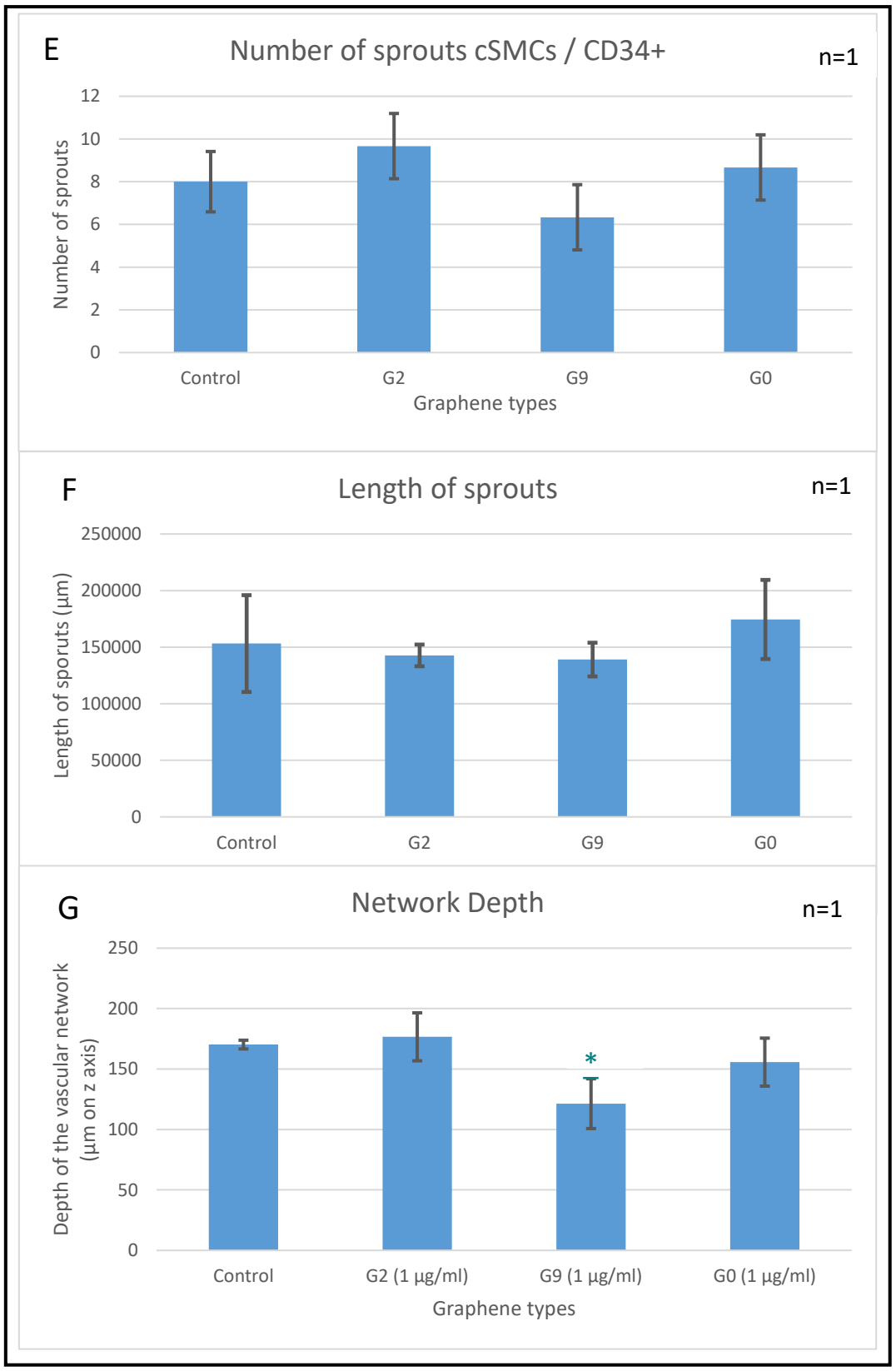
E
Number of sprouts cSMCs / CD34+
n=1
Number of sprouts
12
10
8
6
4
2
0
Control
G2
G9
G0
Graphene types
F
Length of sprouts
n=1
Length of sporuts (µm)
250000
200000
150000
100000
50000
0
Control
G2
G9
G0
G
Network Depth
n=1
Depth of the vascular network (µm on z axis)
250
200
150
100
50
0
*
Control
G2 (1 µg/ml)
G9 (1 µg/ml)
G0 (1 µg/ml)
Graphene types

**Figure 4.9** (A) hPSC- cSMC /CD34+ vascular organoids generated using the hanging drop method, were added on matrigel for two days and allowed to develop sprouts. Representative images of cSMC/ $CD34^+$ VPCs were taken on Leica TCS SP5 confocal microscope and are representative of one independent experiment. Scale bar, 50 μm. (E) The number of sprouts (up), (F) length of sprouts (middle) and (G) network depth (down) were illustrated by counting 3 organoids per condition. The results were quantified using LAS X and imageJ software and they are expressed as means ± SD from one independent experiment. 3 organoids were used to generate the graphs except from the control where we calculated 2. Statistical significance was also calculated by comparing each condition to control *$P < 0.05$

### *Differentiation of CD34+VPCs in the presence of graphene*

We have shown in Figure 4.7 and 4.8 that G2, G9 and GO at 1ug/ml do not inhibit vascular organoid formation. The ECs used in this series of experiments were both HUVECs and $CD34^+$VPCs. As the long-term goal of the project is to generate a vascularised graphene containing organoids using patient specific hiPSCs, we needed to address whether graphene affects VPCs differentiated from hiPSCs and test their performance in vascular organoids containing graphene. We have previously established a method to differentiate VPCs from hESCs (Materials and Methods and (Tsolis et al., 2016). CD34 marker constitutes a transmembrane glycoprotein that is expressed in specified ECs and is used to identify and isolate the EC population by FACs.

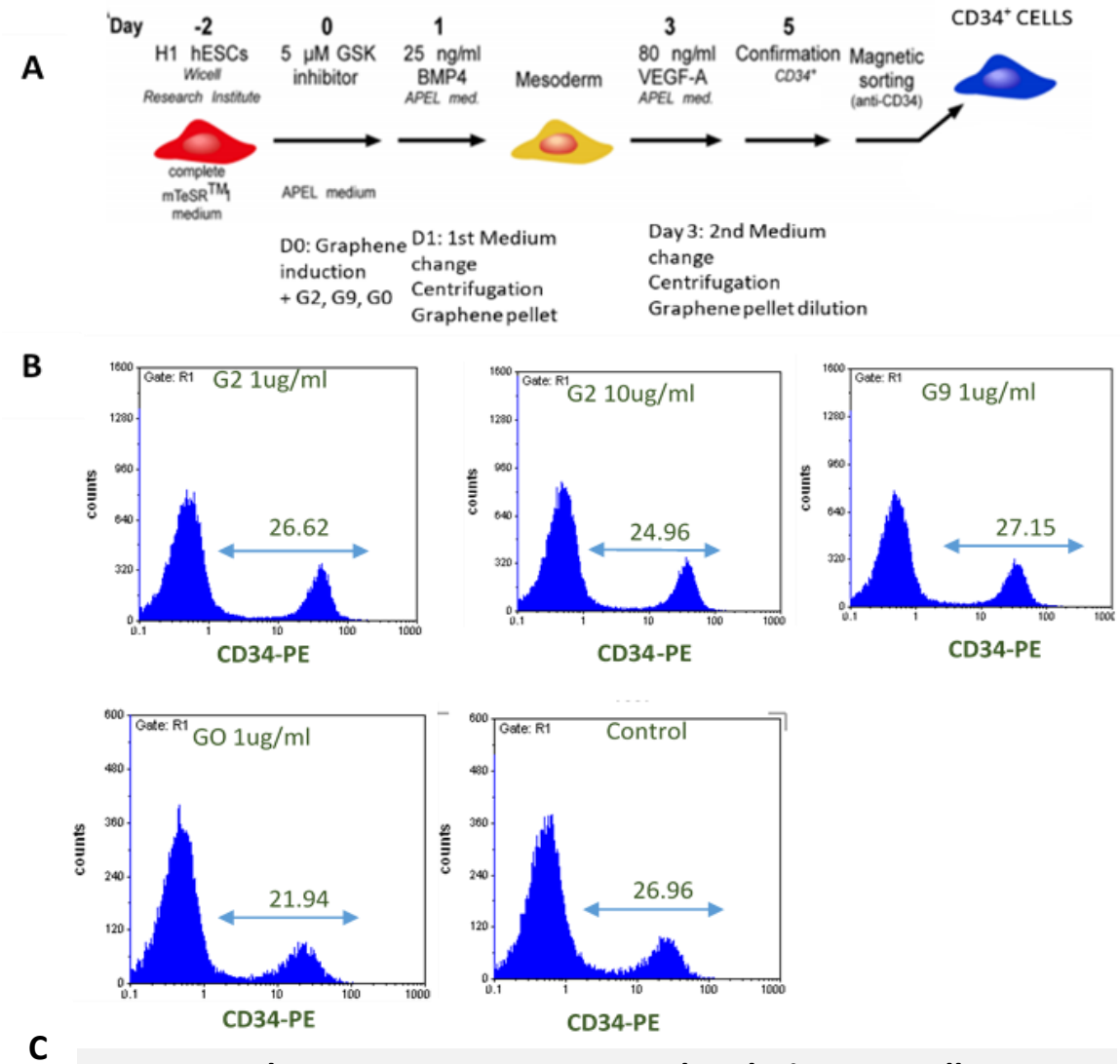


**Figure 4.10.** Investigation of the effect of graphene on the differentiation H1 PSCs to CD34+ VPCs. H1 pluripotent stem cells underwent the differentiation protocol described in Methods (Tsolis et al, 2016) in presence of graphene. At day 5 of the protocol the cells were labeled with CD34-PE antibody and analysed by FACS. A) Representative histogram showing the differentiation protocol and differentiated populations of every condition from one independent experiment. B) Graph showing the results of 3 independent biological repeats. Black bars indicate the ±SD. Statistical significance was also calculated by comparing each condition to control, *P < 0.05

Based on the graphs above, graphene nanoplatelets have no significant effect on the final percentage of the differentiated $CD34^+$VPCs. Even when added at a higher concentration (10µg/ml), G2 had no inhibitory effect on the production of $CD34^+$VPCs. Therefore, we conclude that graphene at the concentrations used neither affects cell viability nor interferes with the differentiation to $CD34^+$ VPCs. Statistical analysis revealed that there are no significant differences between the conditions used.

We also determined whether graphene altered the proliferation of the CD34+VPCs. This experiment was carried out only once and needs to be repeated, therefore we placed it in the Appendix Fig. 6.2. We found that CD34+VPCs were sensitive to G9 and GO at all concentrations while G2 exerted less inhibition of proliferation at all concentrations tested. This experiment needs to be repeated, however there is an indication that G2 1 ug/ml may be the best choice to avoid any toxic effects.

### *Internalisation of graphene nanoplatelets on contractile SMCs*

Finally, to address whether the types of graphene used in our experiments could be internalised and alter cell function by accumulating in an intracellular compartment or indeed perhaps causing intracellular damage, we addressed whether we could visualize the graphene intracellularly and, if so, in which intracellular compartment. Our initial speculation was that, like other nanoplatelets, graphene may accumulate in lysosomes following internalisation by one of several endocytic pathways (Gu et al., 2011).

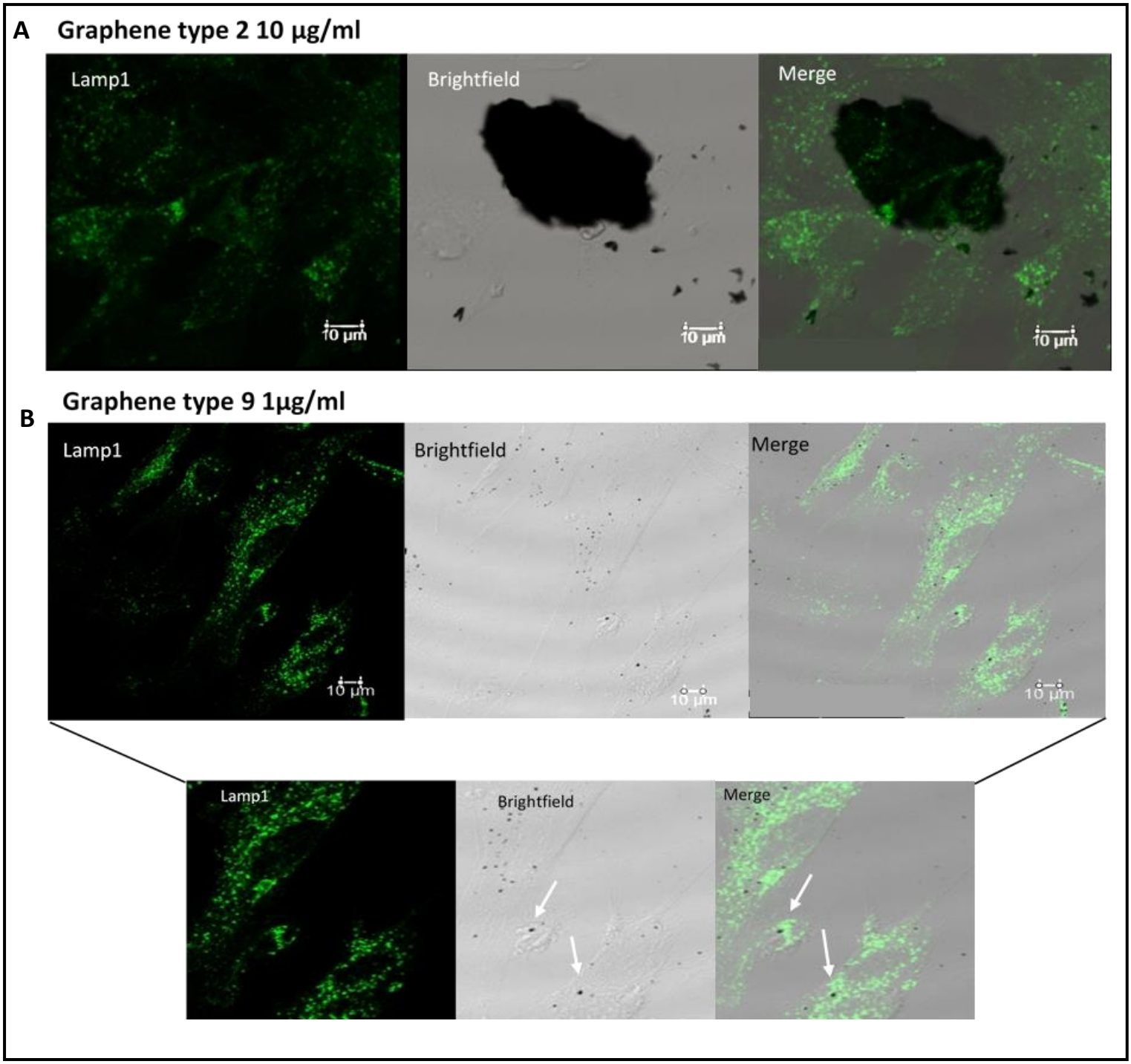
A
Graphene type 2 10 µg/ml
Lamp1
Brightfield
Merge
10 µm
B
Graphene type 9 1µg/ml
Lamp1
Brightfield
Merge
10 µm

C

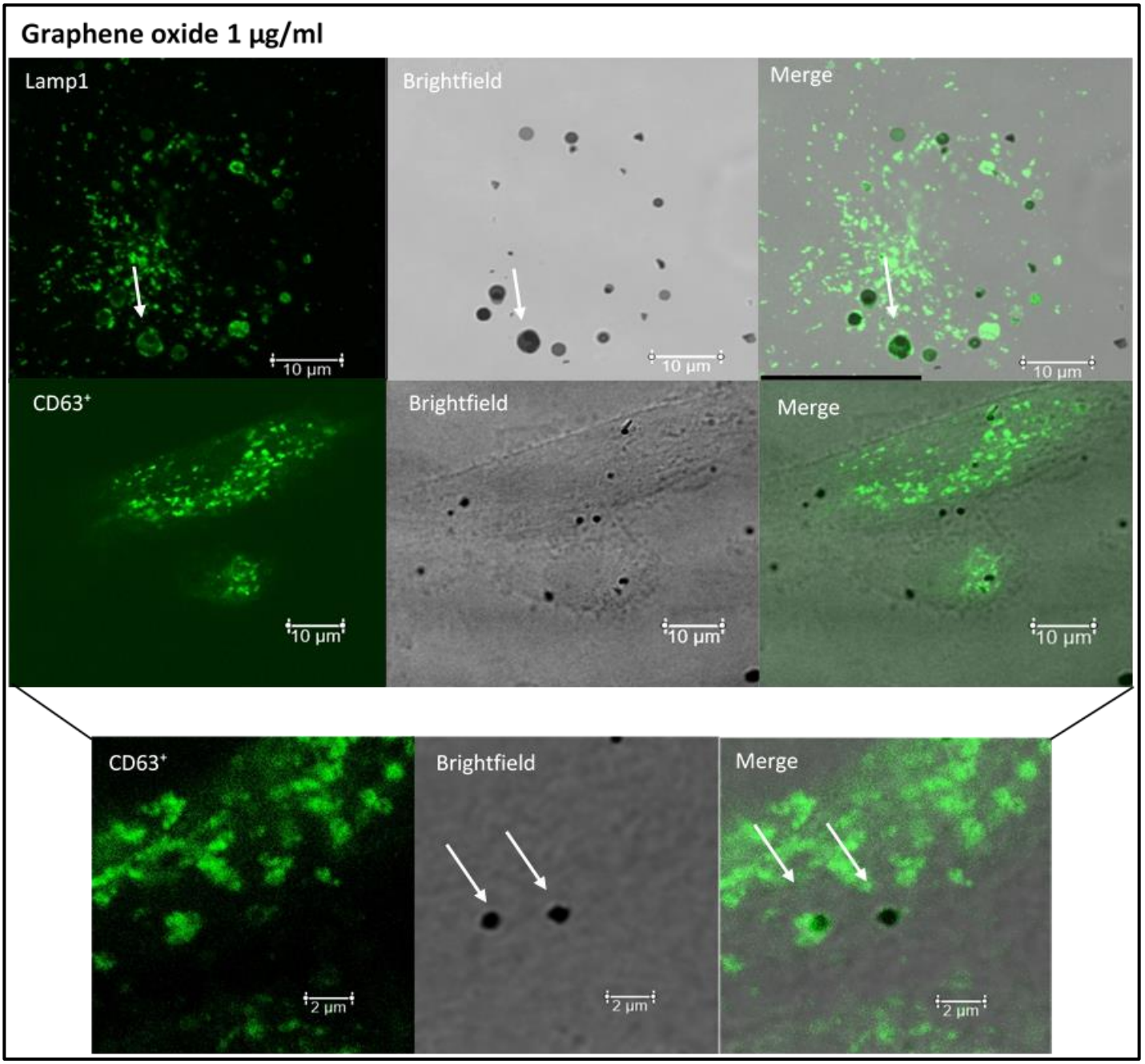


**Figure 4.11.** Images showing the internalisation pattern of G2, G9 & GO in cSMCs. cSMCs were enzymically detached and placed on coverslips. When they attached and were 60-70% confluent, graphene diluted in 2,5% ADSC was introduced into the cell culture for 24 hours. Then, medium was washed away, cells were permeabilised and incubated with either anti-Lamp1 or CD63 antibodies. Graphene nanoplatelets located inside the cells are indicated with the white arrows. Images were taken on a Leica TCS SP5 Confocal microscope where HCX PL APO CS 63.0x1.40 OIL UV objective was used.

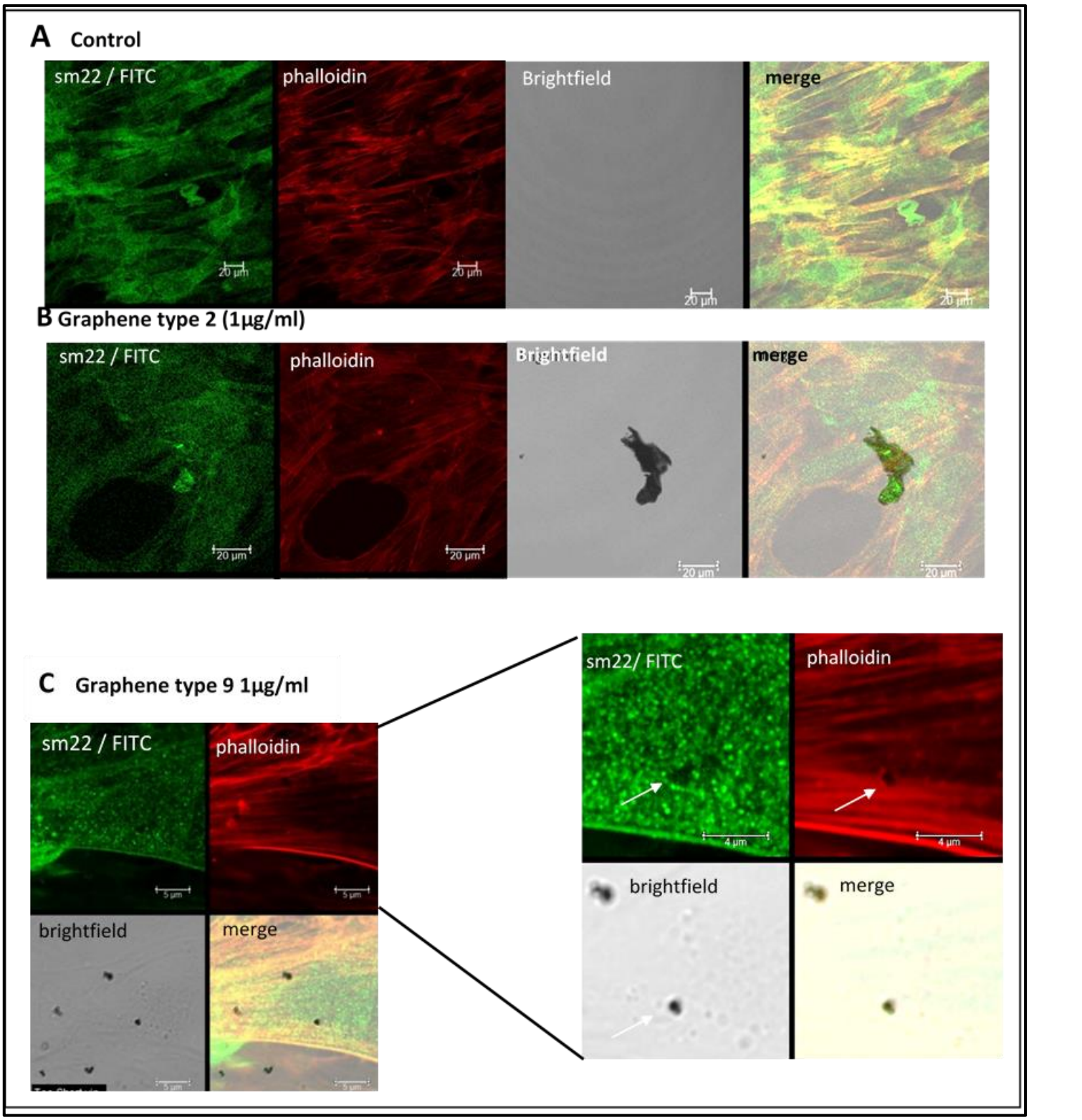
A Control
sm22 / FITC
phalloidin
Brightfield
merge
20 µm
B Graphene type 2 (1µg/ml)
sm22 / FITC
phalloidin
Brightfield
merge
20 µm
C Graphene type 9 1µg/ml
sm22 / FITC
phalloidin
brightfield
merge
5 µm
sm22/ FITC
phalloidin
brightfield
merge
4 µm

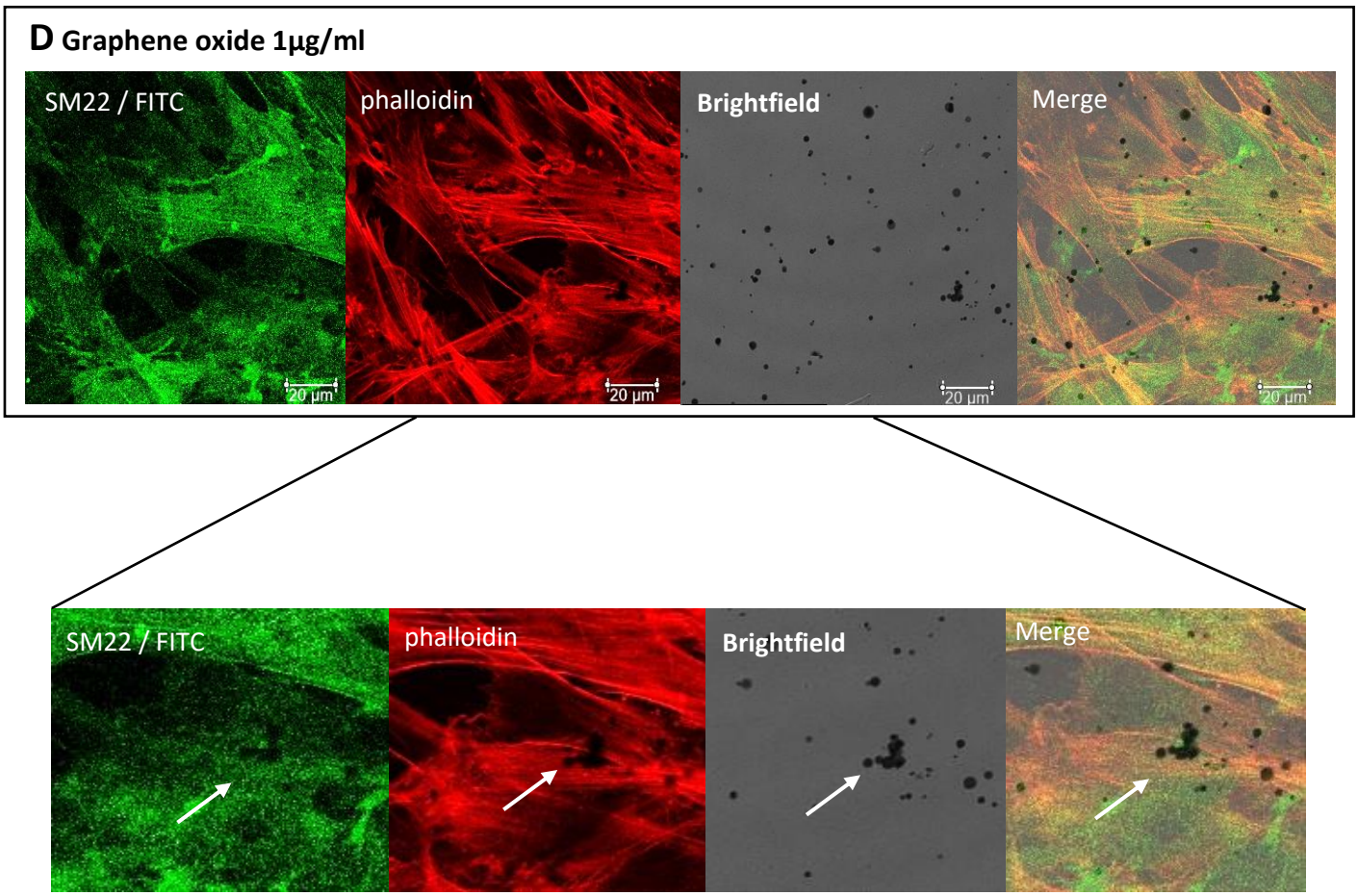


**Figure 4.12** Images showing the internalisation pattern of G2, G 9 and GO in contractile cSMCs. cSMCs were enzymically detached and placed on coverslips. When they attached and were 60-70% confluent, graphene diluted in 2,5% ADSC was introduced into cell culture for 24 hours. Then, medium was washed away, cells were permealised and stained with anti-SM22 antibody (green)and Rhodamine phalloidin. Images were taken in Leica TCS SP5 Confocal microscope where objective HCX PL APO CS 63.0x1.40 OIL UV oil was used.

To address this, we used cSMCs and incubated them with G2, G9 or GO. We used concentrations that we have previously concluded have the least cytotoxic effect (1µg/ml for G2, G9 and GO and 10µg/ml for G2). G2 was not internalised, the size is too big (30 microns) as can be seen from Figure 4.11 & 4.12. G9 and GO were internalised into Lysosomal-associated membrane protein 1 (Lamp1) and/or CD63 positive vesicles (Figure 4.11). In order to confirm our findings and investigate whether graphene is indeed internalised and not just attached to the cell surface, we tested G2, G2 and G9 at 1 ug/ml and used phalloidin and anti-SM22 antibody staining. G2 was not internalised, as expected. G9 and GO were both internalised, this can be seen by the disruption or "holes" in the phalloidin and antiSM22 staining (Figure 4.12).

Therefore, based on our findings about the colocalization of both G9 and GO with the lysosomal markers Lamp1 and CD63, we conclude that they are localised in the lysosomal compartment of the cSMCs.

## *5. Discussion, Future goals*

Recent advances in stem cell research have led to the development of tissue engineering and regenerative medicine, which are now reaching new heights. The scientific field of tissue engineering combines the knowledge of cell biology and biomaterials toward regenerating a functional tissue. Key to the progress in this field is the development of substrates that mimic the cellular microenvironment and provide physico-biochemical properties to enable cell attachment, proliferation, and differentiation. Given the well-described physicochemical properties of graphene and graphene oxide (GO), numerous applications for this novel nanomaterial have been recently envisioned to improve the performance of biomedical devices.

The use of organoids has emerged as a novel research approach due to their ability to partially mimic early embryonic development and represent a tool for drug testing and disease modelling. Recently, vascularisation of brain organoids has been found to increase the nutrient supply and decrease hypoxia and cell death and of establishing a communication between the vasculature and neuronal cells for their proper differentiation, neuronal migration and maturity(Tang et al., 2022). Nanoplatelets of graphene and graphene oxide (GO) have gained broad interest due to their unique properties and advantages such as biocompatibility, flexibility and electrical conductivity (Kumar et al, 2015). In addition, graphene has been shown to act as an excellent substrate for neuronal and vascular cells promoting neurogenesis and angiogenesis (Kumar et al, 2015; Zhang et al., 2018). Therefore, we set out to generate vascularised, graphene containing brain organoids. The focus of the present study was to elucidate the effect of graphene nanomaterials on vascular cells, some of which we differentiate from PSCs. Therefore, we investigated the effect of a wide range of graphene types on pluripotent and vascular cells (hPSCs, ECs, sSMCs, cSMCs) either separately or as vascular organoids.

While many studies have been performed to assess the cytotoxicity of graphene-based nanomaterials on human stem cells (Kenry et al., 2018), it is important to note that their full toxicological profile is still far from being established. We performed cell growth assays on HUVECs introducing a wide range of graphene nanoplatelets with different diameter size groups. The results from the screening of graphene nanoplatelets showed that the inhibition of EC proliferation seemed to be dependent on concentration and diameter. At low concentrations (1 and 5 ug/ml) graphene nanoplatelets of all diameter sizes were without effects on cell proliferation. (Table 5.1). However, at higher concentrations (25 and 50 ug/ml) cytotoxicity was more apparent in nanoplatelets with a diameter of 7 microns (G5 and 6). At first sight this appears difficult to explain, however we speculate that perhaps nanoplatelets of 7 microns might be uptaken by the cell and as they are very large may negatively affect cell function. Particles of 30 and 18 microns are not uptaken into the cell. Smaller particles of 1.5 micron are uptaken but may not alter cell function. This theory needs to be tested experimentally.

Our results are in agreement with studies using graphene or GO on ECs. Indeed, it has been shown that bovine serum albumin-capped graphene oxide (BSA-GO) exhibits ultrastrong binding affinity towards VEGF-A 165 [(Kd ) – 3 x $10^{-12}$ M] inhibiting the proliferation, migration and tube formation of HUVECs, but also blocking strongly angiogenesis in chick chorioallantoic membrane and VEGF-induced blood vessel formation in rabbit cornea (Lai et al., 2016). The VEGF-A was shown to bind directly to the GO particles (lateral size approx. 240nm) however, the authors did not consider any other mechanism of toxicity from the GO – other than VEGF-A binding and inhibition of angiogenesis by removing available VEGF-A from the endothelial cell milieu. At low concentrations the GO was devoid of anti-antiangiogenic effects but at higher concentrations angiogenesis was inhibited *in vitro* and *in vivo*. The results agree with our findings that at low concentrations of 1 ug/ml GO is nontoxic in HUVECs but higher concentrations inhibit HUVEC cell proliferation. Further experiments are required here to see if the effect we observe with GO is due to VEGF-A sequestration, this can be addressed by investigating the phosphorylation of VEGFR2, induced by VEGF-A addition, to see if indeed if there is less phosphorylation in the presence of GO compared to controls.

Pristine graphene (PG) has also been shown to negatively affect the survival of brain microvascular endothelial cells (BMVECs) in an *in vitro* model of blood-brain-barrier (BBB) (Rosas-Hernandez et al., 2019). In this study 10 ug/ml PG was nontoxic but higher concentrations of 50 and 100 ug/ml decreased cell viability and function. The size of graphene used in this study was between 50 nm to 1.7 um, in the range of G7, 8 and 9 in our study. These results agree with our findings in HUVECs, at a concentration of 10 ug/ml graphene does not affect cell function, but higher concentrations are toxic.

The lateral GO size influence on GO-mediated vascular cytotoxicity was determined by constructing i) micrometer-sized GO (MGO: 1089 nm), ii) submicrometer-sized GO (SGO: 390.2 nm), iii) nanometer-sized GO (NGO: 65.5 nm), and iv) graphene qu3 dots (GODs). SGO and NGO bind and activate the G protein-coupled receptor (GPCR) inducing PLC β3 activation, which hydrolyses PIP2 to DAG and IP3. The latter upon binding to its receptor (IP3 R) releases Ca 2+ from the ER leading to JNK phosphorylation, that phosphorylates Bcl-2 dissociating it from Beclin-1. Activated Beclin-1 induces autophagy via LC3 and ultimately to apoptotic cell death via caspase-3 activation and DNA fragmentation . The authors show that this induction of autophagy is concentration dependent and 10ug/ml in the case of SGO and NGO being sufficient to induce the effect. Due to time constraints, we have not investigated the cause of toxicity in our experimental models and indeed it would be interesting to see if autophagy is involved.

There are also publications reporting the angiogenic effect of graphene. Graphene oxide (GO) and reduced graphene oxide (rGO) have been shown to induce angiogenesis via the intracellular formation

of reactive oxygen and nitrogen species as well as activation of phospho-eNOS and phospho-Akt (Mukherjee et al-9361). The concentration of GO used in this study was between 1ng/ml to 5 ug/ml. In serum starved HUVECs proliferation, wound healing and tube formation were enhanced by 10ng/ml GO (204nm) in the absence of VEGF-A. The concentrations in this study showing an angiogenic effect are much lower than those used in our study, so direct comparison is difficult. In agreement, a gelatin-methacryloyl (GelMA) hydrogel containing 0.002% w/w rGO was biocompatible with fibroblasts, keratinocytes and endothelial cells and induced proliferation and migration of the cells. Moreover, it strongly stimulated angiogenesis in the chick embryo model (Raza ur Rehman et al-9392). Likewise, polyvinyl alcohol/carboxymethyl cellulose (PVA/CMC) scaffolds containing 0.005 and 0,0075% rGO induced EC (EA. hy926) proliferation in vitro and significantly increased angiogenesis in the chick chorioallantoic membrane model (Chakraborty et al-9393).

In conclusion, from our results and in agreement with the literature, HUVECs are sensitive to concentration and size of graphene. At 1 ug/ml there is no alteration of cell proliferation, and 10ug of G2 is also well tolerated. G2 (30 microns) and G9 (1.5 microns) also showed lower toxicity compared to other sizes, so these two size extremes, and GO, were selected for further experiments.

It is well known that a vessel contains not only ECs but also mural cells, including VSMCs. Therefore, we also addressed whether G2, G9 and GO had the same profile in this cell type as in HUVECs. We have developed a protocol to obtain both contractile and synthetic vSMCs, differentiated from PSCs, and needed to be sure that both phenotypes were stable in final graphene condition selected. Our results clearly show that the proliferation of cSMCs and sSMCs are unaffected by G2, G9 and GO at 1, 5 and 10 ug/ml. However, at higher concentrations cell proliferation of both cell types was decreased(Lim et al., 2016). The phenotypes of both cell types were not altered by G2 and G9 at the concentrations tested (1 and 10ug/ml G2, 1 ug/ml for G9 and GO). In the only other study in the literature regarding VSMCs and graphene, Ren and his research team investigated the effect of GO on VSMCs. Even though we cannot directly compare our study to that of Ren as they used GO coated coverslips to attach the VSMCs, nevertheless their results agree with ours in that they did not observe any toxicity or phenotype alteration. In fact, GO favoured the proliferation of VSMCs (Ren et al., 2021).

As our intention is to combine the ECs and VSMC with PSCs to generate vascularised brain organoids, we also addressed the effect of graphene on PSCs. We added G2, G9 and GO at high concentrations to H1 stem cells (5, 25 and 50 ug/ml) for 4 days. We did not observe any decrease in OCT3/4 key pluripotency marker. This experiment needs further characterisation and other markers of pluripotency need to be addressed. Chen et al., 2012 found that mouse iPSCs cultured on glass and graphene had no alteration of OCT3/4 levels but at day9 (but not day 5) OCT3/4 levels had dramatically

decreased (Chen et al., 2012). In this experiment Chen plated the iPSCs on graphene or GO coated coverslips so we cannot directly compare our results, however we cannot rule out that at 9 days our cells may also have lost OCT3/4 staining. In agreement with Chen, Heo and coworkers also investigated the effect of GO on hiPSCs pluripotency marker OCT3/4. They found a strong decrease in the expression of OCT3/4 by western in hiPSCs exposed to GO at 100ug/ml for 96 hrs https://www.ncbi.nlm.nih.gov/pubmed/33640729. Nevertheless, as our intention is to take the hiPSCs, add graphene or GO and then begin the embryoid body formation for subsequent brain organoid formation, we do not envisage the cells remaining in the pluripotent stage for 9 days in the presence of graphene.

In order to vascularise the brain organoids, we intend to use both HUVECs and a source of ECs differentiated from hESCs/hiPSCs, these cells are called $CD34^+$ Vascular Progenitor Cells ($CD34^+$VPCs). These VPCs are ideal to use in this context as they are more plastic and may develop more easily a brain vasculature signature. Therefore, we investigated the effect of graphene and GO on the differentiation of hPSCs to VPCs. We used G2 (1 and 10ug/ml) and G9(1ug/ml) and GO (1ug/ml). Our results show that there is no effect of the graphene or GO on the differentiation efficiency. This is in contrast to the findings of Garcia-Alegria and coworkers who found that GO assists directed differentiation to ECs(Garcia-Alegria et al., 2016). The reason for the lack of effect in our system may well be attributed to the fact that the Garcia-Alegria lab used GO coated coverslips and in addition their differentiation protocol differs significantly from ours.

We further tested the effect of G2, G9 and GO in the generation and sprouting of vascular organoids. This system allows us to address whether the graphene or GO effect vessel formation and sprouting angiogenesis. We found perhaps a slight stimulation of angiogenesis under these conditions, however low number of organoids allow only an initial overview and increased number of vascular organoids need to be analysed.

Finally, we considered that internalisation of graphene or GO may cause intracellular damage. In fact, it has been shown that GO internalisation is toxic in astrocyte-like F98 cells, by triggering apoptosis through inhibition of autophagy (Wei et al., 2019). In agreement with this publication is the work of Wei and coworkers who show that GO causes autophagy-lysosomal dysfunction at concentrations of 5ug/ml (Dai et al., 2022). These findings are important as autophagy plays a significant role in maintaining cellular homeostasis and can be induced by various stimuli including oxidative stress, starvation, aging, and infection. During autophagy induction, misfolded or aggregated proteins and intracellular organelles are sequestered in double- membrane vesicles (autophagosomes), which then fuse with lysosomes to form autolysosomes (H. Zhang & Baehrecke, 2015). The association of autophagy and several disease conditions, neurodegeneration, cancer, metabolic diseases etc,

underlines the fundamental role of autophagy in cellular homeostasis (Klionsky et al., 2021). Further work on GO found damaged lysosomal and mitochondrial membranes – however mg amounts of GO were uptaken into the cell undermining the relevance of the findings (L. Liu et al., 2020). There are limited publications on the internalisation of graphene nanoplatelets, and none on VSMC. Our results on graphene type2, 9 and GO internalisation in cSMCs are in agreement with the literature in that we see accumulation of both G9 and GO in intracellular LAMP1 and CD63 positive late endosomes/lysosomes. G2 is not internalised, as expected due to its large size (30 microns). Whether there is damage to the lysosomal compartment remains to be addressed.

So, in conclusion we suggest G2 at 1 ug/ml is optimal for use in vascularised brain organoids. There is no alteration of endothelial or VSM cell proliferation, no negative effects on vascular cell differentiation, vascular organoid formation, angiogenic sprouting, pluripotency of stem cells. In addition, G2 is not internalised into the cells thereby avoiding any effect on lysosomal or mitochondria function and autophagy.

***Future Goals***

The wide spectrum of approaches that we used to validate the effect of graphene nanoplatelets on the vascular component of a vascularised brain organoid, has shed light on several key parameters, EC and VSMC proliferation, sprouting angiogenesis, differentiation of ECs and the phenotypic stability of VSMCs. A promising future plan of the present research is to identify any alterations on the transcriptome of each vascular cell line caused by the presence of graphene. In this way, we will acquire the knowledge on the expression pattern of specific mechanisms underlying the embryonic development. For this reason, we have already started a series of experiment where we incubated cSMCs, sSMCs, H1 hESCs and $CD34^+$ VPCs with and without 1μg/ml of G2 for 48 hours. Then, we extracted the pellets and stored them at -80$^o$C for future RNA sequencing.

As already mentioned in the text, we need to proceed with some repetitions of the experiments presented, in order to solidify our experiments and apply statistics on them. We should repeat the western blotting for the pluripotent marker Oct 3/4 in presence of graphene at low concentrations of 1μg/ml to have n = 3 experiments. Moreover, we need to repeat the vascular organoid sprouting assay by using cSMCs/ $CD34^+$ VPCs and sSMCs/ $CD34^+$ VPCs endothelial cells for the investigation of the effect of graphene. We can also evaluate the contribution of each cell type to the developing sprouts.

After the assessment of cell growth in all cell lines used in the present study, we found that higher concentrations of graphene lead to the inhibition of the cell proliferation or even the cell death. In the second case, it would be crucial to know whether cell death is a result of apoptosis, necrosis, autophagy etc. In addition, as referred to in the text, it would be very interesting to address whether the effect of GO on EC proliferation, is due to VEGF-A binding by investigating phosphorylation of VEGFR.

Furthermore, the discovery of G9's and G0's internalisation in cSMCs constitutes a building block for the research on the endocytic pathway graphene nanoplatelets follow when they are internalised(Goenka et al., 2014). It is important to investigate if graphene is also accumulated into endothelial cells and which types are internalised.

Regarding the general aim of the project, once we have concluded in the optimal concentration and graphene type on the vascular part of the vascularised brain organoid assembly, we should incorporate it in brain organoid culture. Speaking about brain organoids is particularly challenging to generate them in a biomimetic microenvironment favorable for proceeding brain development. In the process of brain organoid formation, the embryoid bodies- EBs are initially formed (M. A. Lancaster et al., 2017) Then, they are transferred into Petri dishes for suspended culture to generate brain organoids. The major issue with the EBs is the lack of nutrient supply, which still limits the growth and maturation of organoids. Since the brain organoids grow more days in cell culture and their dimensions expand it

would be necessary to connect the developing vascularised brain organoids into a microfluidics flow (device).

Finally, the present study highlights the importance of nanomaterials applications in the field of tissue engineering. The in vitro generation of 3-D organ models by differentiating hESCs has brought broad interest to the discovery of their applications. An increasing number of studies have been published in the recent years analysing their potential application for gene and drug delivery and tissue engineering, which lead us to believe that these materials hold promise for solving future medical problems(Tonelli et al., 2015). Graphene derivatives have shown remarkable properties on cell maturity and proliferation. 1µg/ml of G2 is proved to be a proper concentration to continue with our experiments and expand to others previously described. However, graphene substrates form various shapes, sizes and dimensions. It would be promising to investigate the presence of graphene as sheets on coverslips or even as 3-d scaffolds for the development of vascularised organoid models.

## *6. Appendix*

### Investigation of the effect of graphene nanoplatelets on human pluripotent stem cell (H1- mcherrry) cell proliferation

To address the effect of graphene on pluripotent stem cells we first evaluated H1 hESC - mcherry cell proliferation with/ without the presence of graphene nanoplatelets using the Incucyte live cell imaging system. We selected 1 graphene nanoparticle size 1.5 (G9) and also GO and evaluated concentrations of 1, 5 and 10μg/ml for 48hrs. G9 showed no statistically significant alteration of cell proliferation at 1 and 5 μg /ml, however the 10 μg /ml concentration had a moderate inhibitory effect. Similarly,

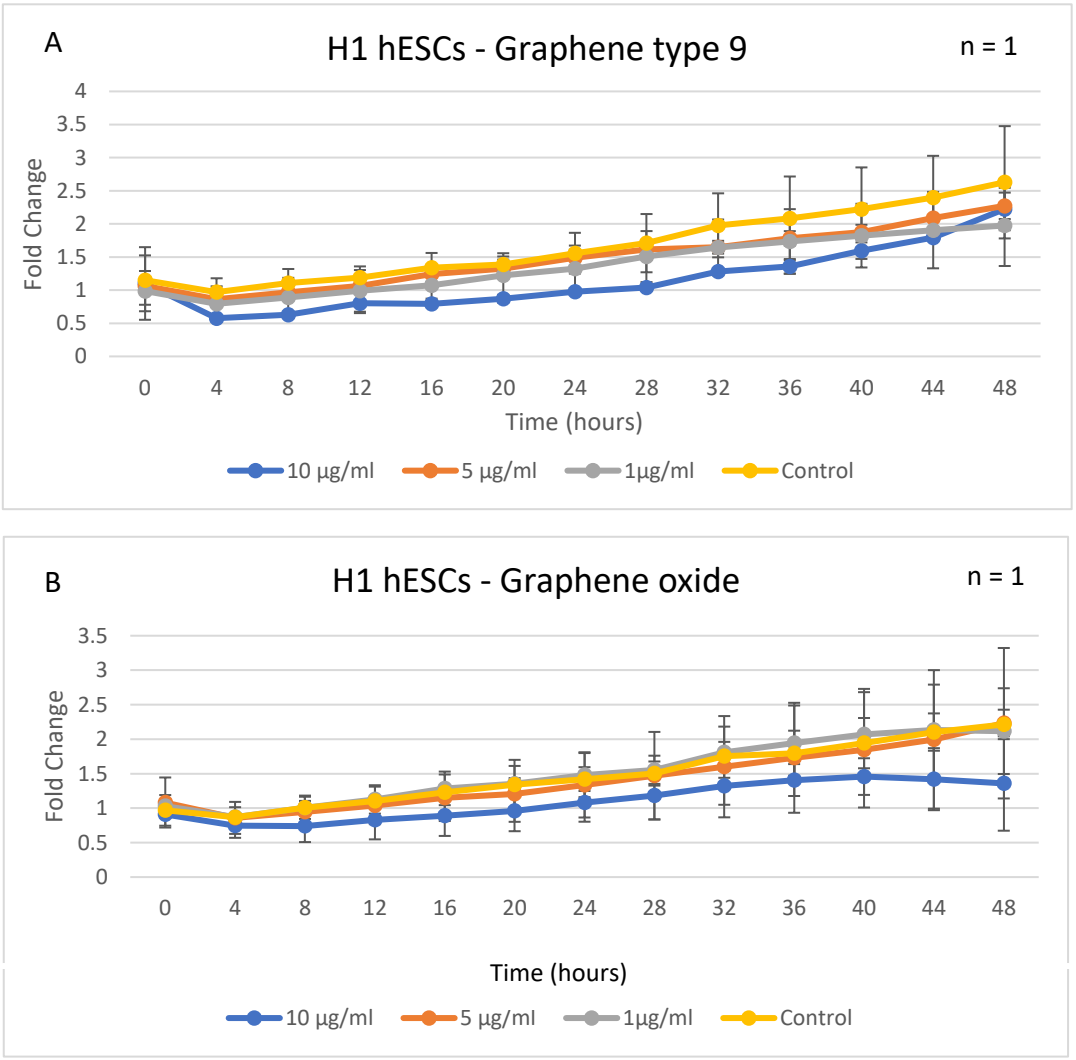


**Figure 6.1**. Schematic diagram showing the cell proliferation rate of hESCs in presence of graphene type 9 and graphene oxide. Pluripotent stem cells were passaged in a ratio of 1:20 and placed in matrigel coated 96-well plate for 24 hours at 37°C. The next day, the diluted graphene was added into the mTESR medium and the mixture was introduced to the cells in 3 concentrations (1-5-10μg/ml). Each condition was represented in triplicates. Right after that, the plate was inserted in the proper space of the IncuCyte Live-Cell Analysis system and 4 images were taken per well per 4 hours. A, B) Graphs depict the fluctuation of cell growth through a 40-hour period. 1, 5 and 10 μg/ml of each graphene type caused almost none effect, with 10μg/ml of graphene oxide causing a minor decrease on cell proliferation. The results show the means of the three replicates together with their standard deviation

graphene oxide had no effect on the proliferation rate at 1 and 5 μg /ml but at 10μg/ml the proliferation was significantly reduced.

## Investigation of the effect of graphene nanoplatelets on the proliferation of CD34⁺VPCs differentiated from H1 hESCs.

We generated and isolated CD34⁺VPCs cells from H1 cells according to Materials and Methods and investigated the effect of graphene on their proliferation. For this experiment we used 5 different concentrations of graphene from 50μg/ml to 1 μg/ml (1, 5,10, 25 and 50 ug/ml). The y axis shows the fold change on the proliferation rate and the x axis depicts the different time points during the 40-hour cell growth assay.

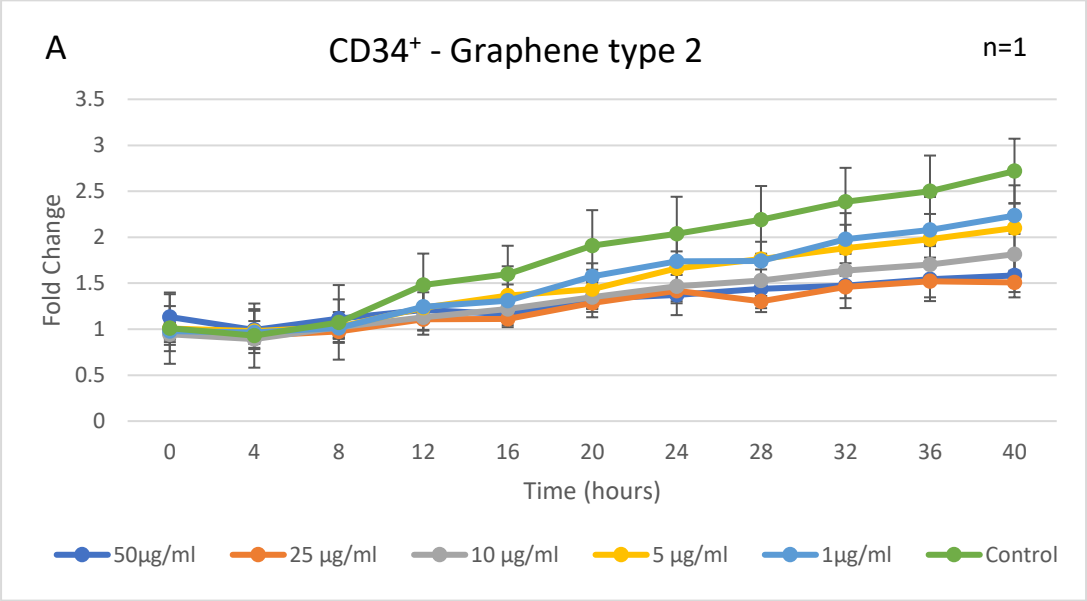

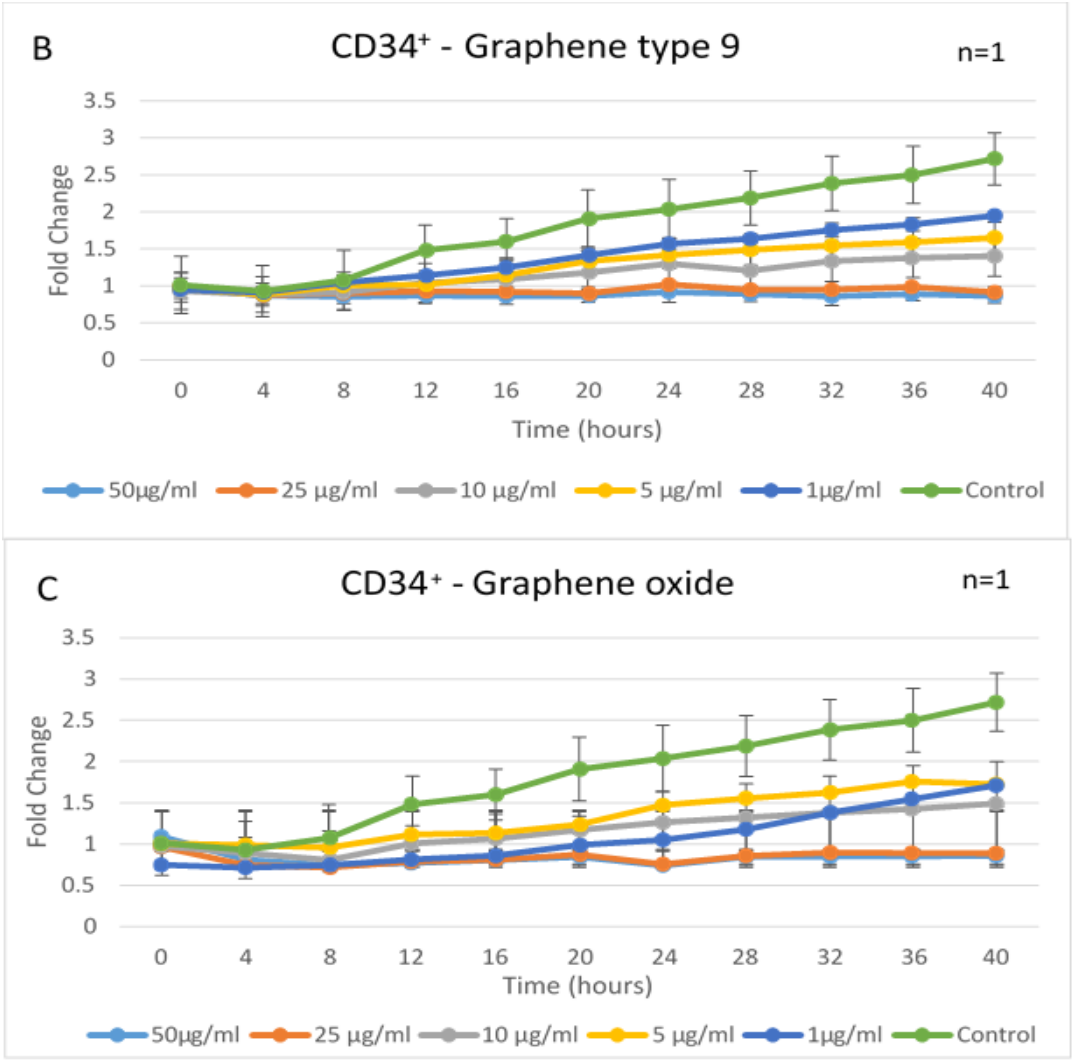


**Figure 6.2**. Schematic diagram showing the cell proliferation rate of CD34+VPCs in presence of G2, G9 and GO. 7,000 CD34+VPCs were placed in fibronectin coated 96-well plates for 24 hours at 37ºC. The next day, the diluted graphene was added into the APEL medium and the mixture was introduced to the cells in 5 concentrations (1,5,10,25 and 50µg/ml). Each condition was represented in triplicates. The plate was inserted into the IncuCyte Live-Cell Analysis system and 4 images were taken per well every 4 hours. A, B) Graphs depict the fluctuation of cell growth through the 40-hour period. The results show the means of the three replicates together with their standard deviation.

### *Effect of lower concentrations of Graphene Nanoplatelets on Synthetic Vascular Smooth Muscle Cell Proliferation*

According to the results of the cell growth on the sSMCs, 1µg/ml seems to be a concentration with least effect on cell proliferation (Figure 4.3). However, GO had a slight inhibitory effect even at 1 ug/ml. Therefore, we further examined 3 lower concentrations of G2, G9 and GO (0.25, 0.5 and 1 µg/ml) to address whether they might be devoid of effects on proliferation. The results show that these lower concentrations indeed do not alter cell proliferation. The y axis shows the fold change on the proliferation rate and the x axis depicts the different time points during the 40-hour cell growth assay. Raw images taken from the IncuCyte indicate that cells had normal morphology during the experiment,

data not shown. The experiment was conducted once and more repetitions are required for their validation.

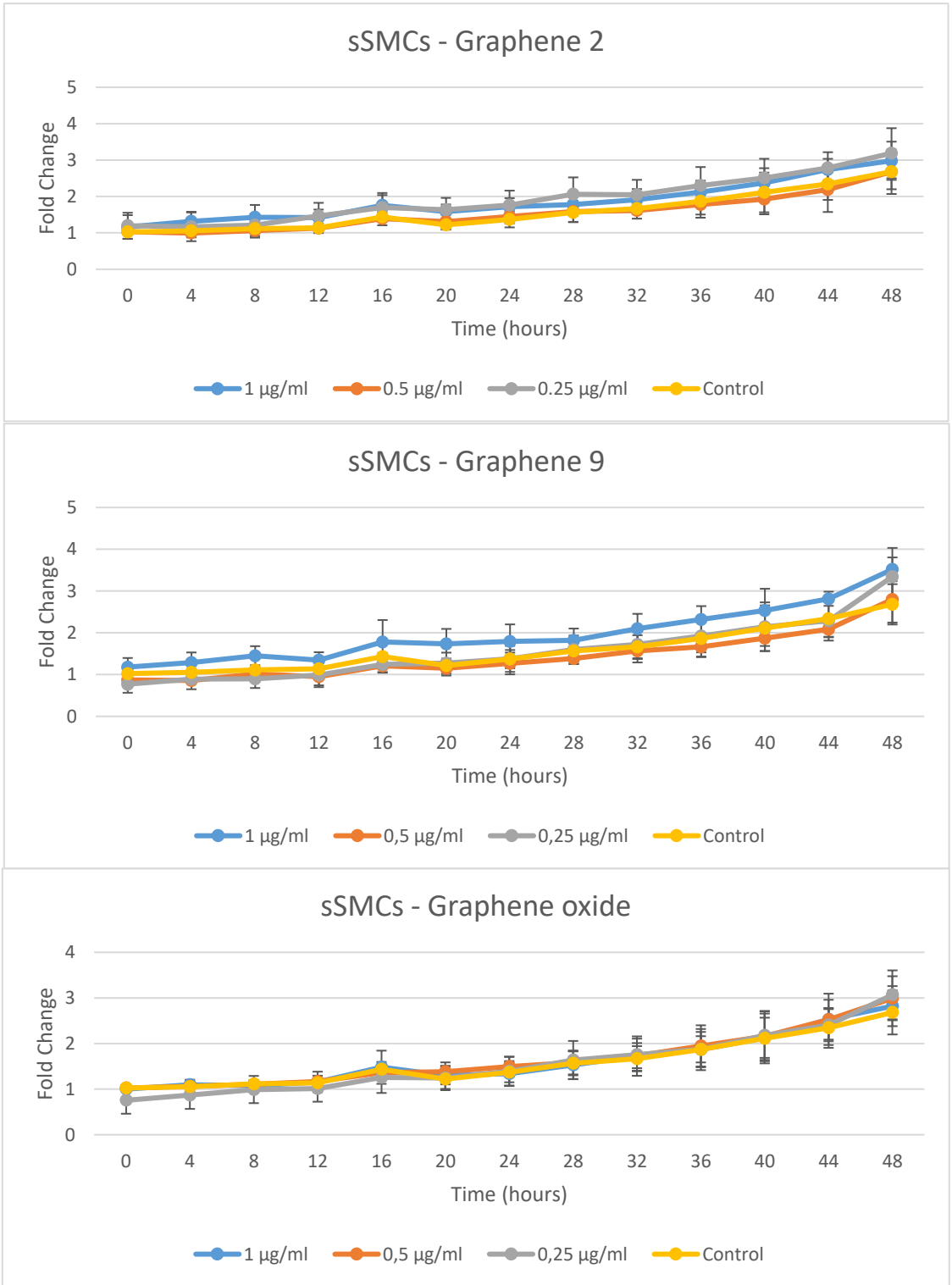


**Figure 6.3** Schematic diagram showing the cell proliferation rate of sSMCs in presence of graphene type 2, 9 and graphene oxide. sSMCs cells were splitted 3.500 cells/ well were placed in gelatin coated 96-well plate for 24 hours at 37ºC. The next day, the diluted graphene was added into the Pericytic Medium medium and the mixture was introduced to the cells in 3 concentrations (0.25-.05-1 μg/ml). Each condition was represented in triplicates. Black bars indicate ±SD. Right after that, the plate was inserted in the proper space of the IncuCyte Live-Cell Analysis system and 4 images were taken per well per 4 hours. A, B, C) Graphs depict the fluctuation of cell growth through a 48-hour period. The results show the means of the three replicates together with their standard deviation

### *Lentiviral infection of the cSMCs*

After the production and collection of the H2B-mcherry lentivirus, we tested various amounts of the virus to determine the optimal concentration for the infection of cSMCs. The results are shown in Figure 4.14 and we conclude that the most efficient infection was observed between 4 and 6 ul of the virus, 79 and 84% respectively. All the percentages were calculated using both images of brightfield and fluorescence using ImageJ software. We chose to use 5ul (in a 24-well) of the virus.

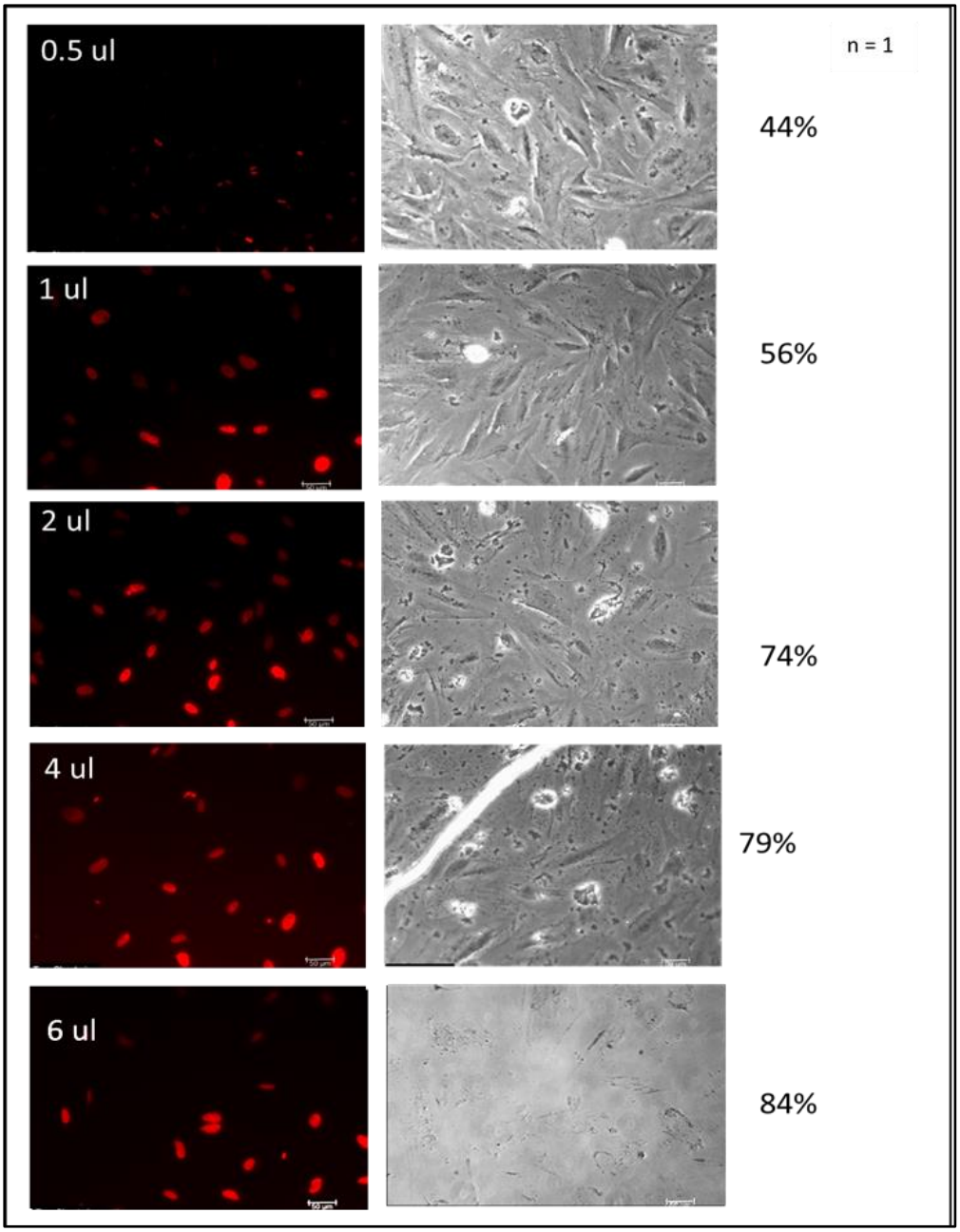


**Figure 6.4.** Lentivirus H2B titration on cSMCs. On a 24-well plate cSMCs were plated on 6 wells and 5 different amounts of the lentivirus were introduced into cell culture (0.5, 1, 2, 4 & 6ul) plus a control without virus. Infection's efficiency was calculated 3 days after the addition of the virus. Images were collected from a fluorescent microscope and the efficiency percentages were calculated via the ImageJ software. Virus production was performed by Maria Markou and Manolis Iakovidis

## *7.References*


Agboola, O. S., Hu, X., Shan, Z., Wu, Y., & Lei, L. (2021a). Brain organoid: a 3D technology for investigating cellular composition and interactions in human neurological development and disease models in vitro. Stem Cell Research & Therapy 2021 12:1, 12(1), 1–16. https://doi.org/10.1186/S13287-021-02369-8

Ahn, J. K., Chebotaryov, S., Choi, J. H., Choi, S., Choi, W., Choi, Y., Jang, H. I., Jang, J. S., Jeon, E. J., Jeong, I. S., Joo, K. K., Kim, B. R., Kim, B. C., Kim, H. S., Kim, J. Y., Kim, S. B., Kim, S. H., Kim, S. Y., Kim, W., … Yu, I. (2012). Observation of reactor electron antineutrinos disappearance in the RENO experiment. Physical Review Letters, 108(19). https://doi.org/10.1103/PHYSREVLETT.108.191802

Akay, M. (Ed.). (2006). Wiley Encyclopedia of Biomedical Engineering. https://doi.org/10.1002/9780471740360

Akhavan, O., Ghaderi, E., & Akhavan, A. (2012). Size-dependent genotoxicity of graphene nanoplatelets in human stem cells. Biomaterials, 33(32), 8017–8025. https://doi.org/10.1016/j.biomaterials.2012.07.040

Alison, M. R., & Islam, S. (2009). Attributes of adult stem cells. The Journal of Pathology, 217(2), 144–160. https://doi.org/10.1002/PATH.2498

Atala, A. (2012). The Jay and Margie Grosfeld lecture Regenerative medicine strategies. https://doi.org/10.1016/j.jpedsurg.2011.10.013

Bagley, J. A., Reumann, D., Bian, S., Lévi-Strauss, J., & Knoblich, J. A. (2017). Fused cerebral organoids model interactions between brain regions. Nature Methods 2017 14:7, 14(7), 743–751. https://doi.org/10.1038/nmeth.4304

Bahal, R., Ali McNeer, N., Quijano, E., Liu, Y., Sulkowski, P., Turchick, A., … Glazer, P. M. (2016). In vivo correction of anaemia in $\beta$ -thalassemic mice by $\gamma$ PNA-mediated gene editing with nanoparticle delivery. Nature Communications 2016 7:1, 7(1), 1–14. https://doi.org/10.1038/ncomms13304

Baptista, P. M., Siddiqui, M. M., Lozier, G., Rodriguez, S. R., Atala, A., & Soker, S. (2011). The use of whole organ decellularization for the generation of a vascularized liver organoid. Hepatology, 53(2), 604–617. https://doi.org/10.1002/HEP.24067

Bai, R. G., Muthoosamy, K., Manickam, S., & Hilal-Alnaqbi, A. (2019). Graphene-based 3D scaffolds in tissue engineering: fabrication, applications, and future scope in liver tissue engineering. International Journal of Nanomedicine, 14, 5753–5783. https://doi.org/10.2147/IJN.S192779

Bellin, M., Marchetto, M. C., Gage, F. H., & Mummery, C. L. (2012). Induced pluripotent stem cells: the new patient? Nature Reviews Molecular Cell Biology 2012 13:11, 13(11), 713–726. https://doi.org/10.1038/nrm344

Blau, H. M., Brazelton, T. R., & Weimann, J. M. (2001). The evolving concept of a stem cell: entity or function? Cell, 105(7), 829–841. https://doi.org/10.1016/S0092-8674(01)00409-3

Bolotin, K. I., Sikes, K. J., Hone, J., Stormer, H. L., & Kim, P. (2008). Temperature-Dependent Transport in Suspended Graphene. Physical Review Letters, 101(9). https://doi.org/10.1103/physrevlett.101.096802

Bolotin, K. I., Sikes, K. J., Jiang, Z., Klima, M., Fudenberg, G., Hone, J., … Stormer, H. L. (2008). Ultrahigh electron mobility in suspended graphene. Solid State Communications, 146(9–10), 351–355. https://doi.org/10.1016/J.SSC.2008.02.024

Burridge, P. W., & Zambidis, E. T. (2013). Highly efficient directed differentiation of human induced pluripotent stem cells into cardiomyocytes. Methods in Molecular Biology (Clifton, N.J.), 997, 149–161. https://doi.org/10.1007/978-1-62703-348-0_12

Carletti, E., Motta, A., & Migliaresi, C. (2011). Scaffolds for tissue engineering and 3D cell culture. Methods in Molecular Biology (Clifton, N.J.), 695, 17–39. https://doi.org/10.1007/978-1-60761-984-0_0

Castro Neto, A. H., Guinea, F., Peres, N. M. R., Novoselov, K. S., & Geim, A. K. (2009a). The electronic properties of graphene. Reviews of Modern Physics, 81(1), 109–162. https://doi.org/10.1103/REVMODPHYS.81.109

Carlsson, J., Nilsson, K., Westermark, B., Pontén, J., Sundström, C., Larsson, E., Bergh, J., Påhlman, S., Busch, C., & Collins, V. P. (1983). Formation and growth of multicellular spheroids of human origin. International Journal of Cancer, 31(5), 523–533. https://doi.org/10.1002/IJC.2910310502

Carr, C. M., & Rizo, J. (2010). Molecules, mechanisms, and cellular roles of clathrin-independent endocytosis. Current Opinion in Cell Biology, 22(4), 488–495. https://doi.org/10.1016/J.CEB.2010.04.001

Chang, Y., Yang, S. T., Liu, J. H., Dong, E., Wang, Y., Cao, A., … Wang, H. (2011). In vitro toxicity evaluation of graphene oxide on A549 cells. Toxicology Letters, 200(3), 201–210. https://doi.org/10.1016/J.TOXLET.2010.11.016

Chen, H., Müller, M. B., Gilmore, K. J., Wallace, G. G., & Li, D. (2008). Mechanically strong, electrically conductive, and biocompatible graphene paper. Advanced Materials, 20(18), 3557–3561. https://doi.org/10.1002/ADMA.200800757

Chen, G. Y., Pang, D. W. P., Hwang, S. M., Tuan, H. Y., & Hu, Y. C. (2012). A graphene-based platform for induced pluripotent stem cells culture and differentiation. Biomaterials, 33(2), 418–427. https://doi.org/10.1016/J.BIOMATERIALS.2011.09.071

Cheng, C. J., Tietjen, G. T., Saucier-Sawyer, J. K., & Saltzman, W. M. (2015). A holistic approach to targeting disease with polymeric nanoplatelets. Nature Reviews Drug Discovery 2015 14:4, 14(4), 239–247. https://doi.org/10.1038/nrd4503

Choudhury, D., Mo, X., Iliescu, C., Tan, L. L., Tong, W. H., & Yu, H. (2011). Exploitation of physical and chemical constraints for three-dimensional microtissue construction in microfluidics. Biomicrofluidics, 5(2). https://doi.org/10.1063/1.3593407

Contreras-Torres, F. F., Rodríguez-Galván, A., Guerrero-Beltrán, C. E., Martínez-Lorán, E., Vázquez-Garza, E., Ornelas-Soto, N., & García-Rivas, G. (2017b). Differential cytotoxicity and internalization of graphene family nanomaterials in myocardial cells. Materials Science and Engineering C, 73, 633–642. https://doi.org/10.1016/J.MSEC.2016.12.080

Chung, C., Kim, Y. K., Shin, D., Ryoo, S. R., Hong, B. H., & Min, D. H. (2013). Biomedical applications of graphene and graphene oxide. Accounts of Chemical Research, 46(10), 2211–2224. https://doi.org/10.1021/AR300159F

Clevers, H. (2016). Modeling Development and Disease with Organoids. Cell, 165(7), 1586–1597. https://doi.org/10.1016/J.CELL.2016.05.082

Damle, A., Sundaresan, R., Rajwade, J. M., Srivastava, P., & Naik, A. (2022). A concise review on implications of silver nanoplatelets in bone tissue engineering. Biomaterials Advances, 141, 213099. https://doi.org/10.1016/J.BIOADV.2022.213099

Dai, D., Chen, Y., Wang, Q., Wang, C., & Zhang, C. (2022). Graphene oxide induced dynamic changes of autophagy-lysosome pathway and cell apoptosis via TFEB dysregulation in F98 cells. Ecotoxicology and Environmental Safety, 246. https://doi.org/10.1016/J.ECOENV.2022.114172

Dawson, E., Mapili, G., Erickson, K., Taqvi, S., & Roy, K. (2008). Biomaterials for stem cell differentiation. Advanced Drug Delivery Reviews, 60(2), 215–228. https://doi.org/10.1016/J.ADDR.2007.08.037

Dhandayuthapani, B., Yoshida, Y., Maekawa, T., & Kumar, D. S. (2011). Polymeric scaffolds in tissue engineering application: A review. International Journal of Polymer Science, 2011.

di Lullo, E., & Kriegstein, A. R. (2017). The use of brain organoids to investigate neural development and disease. Nature Reviews Neurosci, 18(10), 573–584. https://doi.org/10.1038/nrn.2017.107

Doherty, G. J., & McMahon, H. T. (2009). Mechanisms of endocytosis. Annual Review of Biochemistry, 78, 857–902. https://doi.org/10.1146/ANNUREV.BIOCHEM.78.081307.110540

Dreyer, D. R., Park, S., Bielawski, C. W., & Ruoff, R. S. (2010). The chemistry of graphene oxide. Chemical Society Reviews, 39(1), 228–240. https://doi.org/10.1039/B917103G

Engler, A. J., Sen, S., Sweeney, H. L., & Discher, D. E. (2006). Matrix Elasticity Directs Stem Cell Lineage Specification. Cell, 126(4), 677–689. https://doi.org/10.1016/J.CELL.2006.06.044

Fan, W., Sun, Y., Shi, Z., Wang, H., Letters, J. D.-N., (2019). Mouse induced pluripotent stem cells-derived Alzheimer's disease cerebral organoid culture and neural differentiation disorders. Elsevier. Neurosci Lett 15;711:134433. doi: 10.1016/j.neulet.2019.134433. Epub 2019 Aug 14. PMID: 31421155.

Farokhzad, O. C., & Langer, R. (2009). Impact of nanotechnology on drug delivery. ACS Nano, 3(1), 16–20. https://doi.org/10.1021/NN900002M

Feng, L., Zhang, S., & Liu, Z. (2011). Graphene based gene transfection. Nanoscale, 3(3), 1252–1257. https://doi.org/10.1039/C0NR00680G

Fisichella, M., Dabboue, H., Bhattacharyya, S., Lelong, G., Saboungi, M. L., Warmont, F., Midoux, P., Pichon, C., Guérin, M., Hevor, T., & Salvetat, J. P. (2010). Uptake of functionalized mesoporous silica nanoparticles by human cancer cells. Journal of Nanoscience and Nanotechnology, 10(4), 2314–2324. https://doi.org/10.1166/JNN.2010.1917

Fujita, J., & Fukuda, K. (2014). Future prospects for regenerated heart using induced pluripotent stem cells. Journal of Pharmacological Sciences, 125(1), 1–5. https://doi.org/10.1254/JPHS.14R01CP

Garcia-Alegria, E., Iluit, M., Stefanska, M., Silva, C., Heeg, S., Kimber, S. J., Kouskoff, V., Lacaud, G., Vijayaraghavan, A., & Batta, K. (2016). Graphene Oxide promotes embryonic stem cell

differentiation to haematopoietic lineage. Scientific Reports, 6. https://doi.org/10.1038/SREP25917

Geim, A. K., & Novoselov, K. S. (2007). The rise of graphene. Nature Materials 2007 6:3, 6(3), 183–191. https://doi.org/10.1038/nmat1849

Gerstner, E. (2010). Nobel Prize 2010: Andre Geim & Konstantin Novoselov. Nature Physics 2009 6:11, 6(11), 836–836. https://doi.org/10.1038/nphys1836

Ghosal, K., Pal, S., Ghosh, D., Jana, K., & Sarkar, K. (2022). In vivo biocompatible shape memory polyester derived from recycled polycarbonate e-waste for biomedical application. Biomaterials Advances, 138. https://doi.org/10.1016/j.bioadv.2022.212961

Goenka, S., Sant, V., & Sant, S. (2014). Graphene-based nanomaterials for drug delivery and tissue engineering. Journal of Controlled Release, 173(1), 75–88. https://doi.org/10.1016/j.jconrel.2013.10.017

Graf, T. (2002). Differentiation plasticity of hematopoietic cells. Blood, 99(9), 3089–3101. https://doi.org/10.1182/BLOOD.V99.9.3089

Guinea, F., Castro Neto, A. H., & Peres, N. M. R. (2006). Electronic states and Landau levels in graphene stacks. Physical Review B - Condensed Matter and Materials Physics, 73(24). https://doi.org/10.1103/PHYSREVB.73.245426

Halim, A., Luo, Q., Ju, Y., & Song, G. (2018). A Mini Review Focused on the Recent Applications of Graphene Oxide in Stem Cell Growth and Differentiation. Nanomaterials 2018, Vol. 8, Page 736, 8(9), 736. https://doi.org/10.3390/NANO8090736

Hall, P. A., & Watt, F. M. (1989). Stem cells: the generation and maintenance of cellular diversity. Development, 106(4), 619–633. https://doi.org/10.1242/DEV.106.4.619

Hasetine, W. (1999). A brave new medicine. A conversation with William Haseltine. Interview by Joe Flower. Health Forum Journal, 42(4), 28–30, 61. https://europepmc.org/article/med/10539016

Heo, C., Yoo, J., Lee, S., Jo, A., Jung, S., Yoo, H., Suh, M. (2011). The control of neural cell-to-cell interactions through non-contact electrical field stimulation using graphene electrodes. Biomaterials, 32(1), 19–27. https://doi.org/10.1016/J.BIOMATERIALS.2010.08.095

Hedin, U., & Thyberg, J. (1987). Plasma fibronectin promotes modulation of arterial smooth-muscle cells from contractile to synthetic phenotype. Differentiation, 33(3), 239–246. https://doi.org/10.1111/J.1432-0436.1987.TB01563.X

Hernández, D., Rooney, L. A., Daniszewski, M., Gulluyan, L., Liang, H. H., Cook, A. L., Hewitt, A. W., & Pébay, A. (2021). Culture Variabilities of Human iPSC-Derived Cerebral Organoids Are a Major Issue for the Modelling of Phenotypes Observed in Alzheimer's Disease. Stem Cell Reviews and Reports 2021 18:2, 18(2), 718–731. https://doi.org/10.1007/S12015-021-10147-5

Hinderer, S., Layland, S. L., & Schenke-Layland, K. (2016). ECM and ECM-like materials - Biomaterials for applications in regenerative medicine and cancer therapy. Advanced Drug Delivery Reviews, 97, 260–269. https://doi.org/10.1016/J.ADDR.2015.11.019

Ho, Y. C., Lee, H. P., Hwang, S. M., Lo, W. H., Chen, H. C., Chung, C. K., & Hu, Y. C. (2006). Baculovirus transduction of human mesenchymal stem cell-derived progenitor cells: variation of transgene expression with cellular differentiation states. Gene Therapy 2006 13:20, 13(20), 1471–1479. https://doi.org/10.1038/sj.gt.3302796

Hollister, S. J., Maddox, R. D., & Taboas, J. M. (2002). Optimal design and fabrication of scaffolds to mimic tissue properties and satisfy biological constraints. Biomaterials, 23(20), 4095–4103. https://doi.org/10.1016/S0142-9612(02)00148-5

Hu, W., Peng, C., Lv, M., Li, X., Zhang, Y., Chen, N., Huang, Q. (2011). Protein corona-mediated mitigation of cytotoxicity of graphene oxide. ACS Nano, 5(5), 3693–3700. https://doi.org/10.1021/NN200021J

Huang, S., Sultan, C., & Ingber, D. E. (2007). Tensegrity, Dynamic Networks, and Complex Systems Biology: Emergence in Structural and Information Networks Within Living Cells. Complex Systems Science in Biomedicine, 283–310. https://doi.org/10.1007/978-0-387-33532-2_11

Huh, D., Matthews, B. D., Mammoto, A., Montoya-Zavala, M., Yuan Hsin, H., & Ingber, D. E. (2010). Reconstituting organ-level lung functions on a chip. Science (New York, N.Y.), 328(5986), 1662–1668. https://doi.org/10.1126/SCIENCE.1188302

Hwang, N. S., Varghese, S., & Elisseeff, J. (2008). Controlled differentiation of stem cells. Advanced Drug Delivery Reviews, 60(2), 199–214. https://doi.org/10.1016/J.ADDR.2007.08.036

Jang, K. J., Mehr, A. P., Hamilton, G. A., McPartlin, L. A., Chung, S., Suh, K. Y., & Ingber, D. E. (2013). Human kidney proximal tubule-on-a-chip for drug transport and nephrotoxicity assessment. Integrative Biology: Quantitative Biosciences from Nano to Macro, 5(9), 1119–1129. https://doi.org/10.1039/C3IB40049B

Jeong, H., Hwang, J., Lee, H., Hammond, P. T., Choi, J., & Hong, J. (2017). In vitro blood cell viability profiling of polymers used in molecular assembly. Scientific Reports 2017 7:1, 7(1), 1–13. https://doi.org/10.1038/s41598-017-10169-5

Jo, J., Xiao, Y., Sun, A., Cukuroglu, E., Tran, H., cell, J. G.-C. (2014) Midbrain-like organoids from human pluripotent stem cells contain functional dopaminergic and neuromelanin-producing neurons. Elsevier. 4;19(2):248-257. doi: 10.1016/j.stem.2016.07.005. (2014). Design of advanced porous graphene materials: from graphene nanomesh to 3D architectures. Nanoscale, 6(4), 1922–1945. https://doi.org/10.1039/C3NR04555B

Kadoshima, T., Sakaguchi, H., Nakano, T., Soen, M., Ando, S., Eiraku, M., & Sasai, Y. (2013). Self-organization of axial polarity, inside-out layer pattern, and species-specific progenitor dynamics in human ES cell–derived neocortex. Proceedings of the National Academy of Sciences, 110(50), 20284–20289. https://doi.org/10.1073/PNAS.1315710110

Kadzik, R. S., & Morrisey, E. E. (2012). Directing lung endoderm differentiation in pluripotent stem cells. Cell Stem Cell, 10(4), 355–361. https://doi.org/10.1016/J.STEM.2012.03.013

Kang, H. J., Kawasawa, Y. I., Cheng, F., Zhu, Y., Xu, X., Li, M., Sousa, A. M. M., Pletikos, M., Meyer, K. A., Sedmak, G., Guennel, T., Shin, Y., Johnson, M. B., Krsnik, Ž., Mayer, S., Fertuzinhos, S., Umlauf, S., Lisgo, S. N., Vortmeyer, A., … Šestan, N. (2011a). Spatio-temporal transcriptome of the human brain. Nature, 478(7370), 483–489. https://doi.org/10.1038/NATURE10523

Kang, H. J., Kawasawa, Y. I., Cheng, F., Zhu, Y., Xu, X., Li, M., Sousa, A. M. M., Pletikos, M., Meyer, K. A., Sedmak, G., Guennel, T., Shin, Y., Johnson, M. B., Krsnik, Ž., Mayer, S., Fertuzinhos, S., Umlauf, S., Lisgo, S. N., Vortmeyer, A., Šestan, N. (2011b). Spatio-temporal transcriptome of the human brain. Nature, 478(7370), 483–489. https://doi.org/10.1038/NATURE10523

Kenry, Lee, W. C., Loh, K. P., & Lim, C. T. (2018). When stem cells meet graphene: Opportunities and challenges in regenerative medicine. Biomaterials, 155, 236–250. https://doi.org/10.1016/J.BIOMATERIALS.2017.10.004

Keyoumu, Y., Huo, Q., Cheng, L., Ma, H., Zhang, M., Ma, Y., & Ma, X. (2019). The detailed biological investigations about combined effects of novel polyphenolic and photo-plasmonic nanoparticles loaded graphene nanosheets on coronary endothelial cells and isolated rat aortic rings. Undefined, 202. https://doi.org/10.1016/J.JPHOTOBIOL.2019.111666

Kim, J., Kim, Y. R., Kim, Y., Lim, K. T., Seonwoo, H., Park, S., Cho, S. P., Hong, B. H., Choung, P. H., Chung, T. D., Choung, Y. H., & Chung, J. H. (2013). Graphene-incorporated chitosan substrata for

adhesion and differentiation of human mesenchymal stem cells. Journal of Materials Chemistry B, 1(7), 933–938. https://doi.org/10.1039/C2TB00274D

Kimbrel, E. A., & Lanza, R. (2015). Current status of pluripotent stem cells: moving the first therapies to the clinic. Nature Reviews. Drug Discovery, 14(10), 681–692. https://doi.org/10.1038/NRD4738

Klionsky, D. J., Petroni, G., Amaravadi, R. K., Baehrecke, E. H., Ballabio, A., Boya, P., Bravo-San Pedro, J. M., Cadwell, K., Cecconi, F., Choi, A. M. K., Choi, M. E., Chu, C. T., Codogno, P., Colombo, M. I., Cuervo, A. M., Deretic, V., Dikic, I., Elazar, Z., Eskelinen, E. Pietrocola, F. (2021). Autophagy in major human diseases. The EMBO Journal, 40(19). https://doi.org/10.15252/EMBJ.2021108863

Kommireddy, D. S., Sriram, S. M., Lvov, Y. M., & Mills, D. K. (2006). Stem cell attachment to layer-by-layer assembled TiO2 nanoparticle thin films. Biomaterials, 27(24), 4296–4303. https://doi.org/10.1016/J.BIOMATERIALS.2006.03.042

Körbling, M., & Estrov, Z. (2003). Adult Stem Cells for Tissue Repair — A New Therapeutic Concept? Https://Doi.Org/10.1056/NEJMra022361, 349(6), 570–582. https://doi.org/10.1056/NEJMRA022361

Kumar, S., & Chatterjee, K. (2015). Strontium eluting graphene hybrid nanoplatelets augment osteogenesis in a 3D tissue scaffold. Nanoscale, 7(5), 2023–2033. https://doi.org/10.1039/C4NR05060F

Lammel, T., Boisseaux, P., Fernández-Cruz, M. L., & Navas, J. M. (2013). Internalization and cytotoxicity of graphene oxide and carboxyl graphene nanoplatelets in the human hepatocellular carcinoma cell line Hep G2. Particle and Fibre Toxicology, 10(1).

Lancaster, M. A., Corsini, N. S., Burkard, T. R., & Knoblich, J. A. (2016). Guided self-organization recapitulates tissue architecture in a bioengineered brain organoid model. BioRxiv, 049346. https://doi.org/10.1101/049346https://doi.org/10.1186/1743-897

Lancaster, M. A., Corsini, N. S., Wolfinger, S., Gustafson, E. H., Phillips, A. W., Burkard, T. R., Otani, T., Livesey, F. J., & Knoblich, J. A. (2017). Guided self-organization and cortical plate formation in human brain organoids. Nature Biotechnology 2017 35:7, 35(7), 659–666. https://doi.org/10.1038/nbt.3906

Lancaster, M. A., & Knoblich, J. A. (2014). Organogenesis in a dish: modeling development and disease using organoid technologies. Science (New York, N.Y.), 345(6194). https://doi.org/10.1126/SCIENCE.1247125

Lancaster, M. A., & Knoblich, J. A. (2014). Generation of cerebral organoids from human pluripotent stem cells. Nature protocols, 9(10), 2329-2340.

Lee, C., Wei, X., Kysar, J. W., & Hone, J. (2008). Measurement of the elastic properties and intrinsic strength of monolayer graphene. Science (New York, N.Y.), 321(5887), 385–388. https://doi.org/10.1126/SCIENCE.1157996

Lee, W. C., Lim, C. H. Y. X., Shi, H., Tang, L. A. L., Wang, Y., Lim, C. T., & Loh, K. P. (2011). Origin of enhanced stem cell growth and differentiation on graphene and graphene oxide. ACS Nano, 5(9), 7334–7341. https://doi.org/10.1021/NN202190C

Li, N., Zhang, X., Song, Q., Su, R., Zhang, Q., Kong, T., … Cheng, G. (2011). The promotion of neurite sprouting and outgrowth of mouse hippocampal cells in culture by graphene substrates. Biomaterials, 32(35), 9374–9382. https://doi.org/10.1016/J.BIOMATERIALS.2011.08.065

Li, X., Ye, X., Qi, J., Fan, R., Gao, X., Wu, Y., … Guo, G. (2016). EGF and curcumin co-encapsulated nanoparticle/hydrogel system as potent skin regeneration agent. International Journal of Nanomedicine, 11, 3993–4009. https://doi.org/10.2147/IJN.S104350

Li, X., Valadez, A. v., Zuo, P., & Nie, Z. (2012). Microfluidic 3D cell culture: potential application for tissue-based bioassays. Bioanalysis, 4(12), 1509–1525. https://doi.org/10.4155/BIO.12.133

Li, Y., Liu, Y., Fu, Y., Wei, T., le Guyader, L., Gao, G., Liu, R. S., Chang, Y. Z., & Chen, C. (2012). The triggering of apoptosis in macrophages by pristine graphene through the MAPK and TGF-beta signaling pathways. Biomaterials, 33(2), 402–411. https://doi.org/10.1016/J.BIOMATERIALS.2011.09.091

Liang, G., & Zhang, Y. (2012). Embryonic stem cell and induced pluripotent stem cell: an epigenetic perspective. Cell Research 2013 23:1, 23(1), 49–69. https://doi.org/10.1038/cr.2012.175

Liao, K. H., Lin, Y. S., MacOsko, C. W., & Haynes, C. L. (2011b). Cytotoxicity of graphene oxide and graphene in human erythrocytes and skin fibroblasts. ACS Applied Materials and Interfaces, 3(7), 2607–2615. https://doi.org/10.1021/AM200428V

Linares, J., Matesanz, M. C., Vila, M., Feito, M. J., Gonçalves, G., Vallet-Regí, M., Portolés, M. T. (2014). Endocytic mechanisms of graphene oxide nanosheets in osteoblasts, hepatocytes and macrophages. ACS Applied Materials and Interfaces, 6(16), 13697–13706. https://doi.org/10.1021/AM5031598/ASSET/IMAGES/MEDIUM/AM-2014-031598_0011.GIF

Liu, Z., Robinson, J. T., Sun, X., & Dai, H. (2008). PEGylated nanographene oxide for delivery of water-insoluble cancer drugs. Journal of the American Chemical Society, 130(33), 10876–10877. https://doi.org/10.1021/JA803688X

Lo, W. H., Hwang, S. M., Chuang, C. K., Chen, C. Y., & Hu, Y. C. (2009). Development of a hybrid baculoviral vector for sustained transgene expression. Molecular Therapy, 17(4), 658–666. https://doi.org/10.1038/MT.2009.13

Luzio, J. P., Gray, S. R., & Bright, N. A. (2010). Endosome-lysosome fusion. Biochemical Society Transactions, 38(6), 1413–1416. https://doi.org/10.1042/BST0381413

Ma, N., Ma, C., Li, C., Wang, T., Tang, Y., Wang, H., Mou, X., Chen, Z., & He, N. (2013). Influence of nanoparticle shape, size, and surface functionalization on cellular uptake. Journal of Nanoscience and Nanotechnology, 13(10), 6485–6498. https://doi.org/10.1166/JNN.2013.7525

Mansour, A. A., Gonçalves, J. T., Bloyd, C. W., Li, H., Fernandes, S., Quang, D., Johnston, S., Parylak, S. L., Jin, X., & Gage, F. H. (2018). An in vivo model of functional and vascularized human brain organoids. Nature Biotechnology, 36(5), 432–441. https://doi.org/10.1038/NBT.4127

Mao, A. S., & Mooney, D. J. (2015). Regenerative medicine: Current therapies and future directions. Proceedings of the National Academy of Sciences of the United States of America, 112(47), 14452–14459. https://doi.org/10.1073/PNAS.1508520112

Markou, M., Kouroupis, D., Badounas, F., Katsouras, A., Kyrkou, A., Fotsis, T., Murphy, C., & Bagli, E. (2020). Tissue Engineering Using Vascular Organoids From Human Pluripotent Stem Cell Derived Mural Cell Phenotypes. Frontiers in Bioengineering and Biotechnology, 8. https://doi.org/10.3389/FBIOE.2020.00278

Marsano, A., Conficconi, C., Lemme, M., Occhetta, P., Gaudiello, E., Votta, E., Cerino, G., Redaelli, A., & Rasponi, M. (2016). Beating heart on a chip: a novel microfluidic platform to generate functional 3D cardiac microtissues. Lab on a Chip, 16(3), 599–610. https://doi.org/10.1039/C5LC01356A

Martinelli, V., Bosi, S., Penã, B., Baj, G., Long, C. S., Sbaizero, O., … Mestroni, L. (2019). 3D Carbon Nanotube-Based Composites for Cardiac Tissue Engineering. ACS Applied Bio Materials, 1(5), 1530–1537. https://doi.org/10.1021/ACSABM.8B00440

Marx, V. (2015). Tissue engineering: Organs from the lab. Nature, 522(7556), 373–377. https://doi.org/10.1038/522373A

Mi, P., Kokuryo, D., Cabral, H., Wu, H., Terada, Y., Saga, T., … Kataoka, K. (2016). A pH-activatable nanoparticle with signal-amplification capabilities for non-invasive imaging of tumour malignancy. Nature Nanotechnology 2016 11:8, 11(8), 724–730. https://doi.org/10.1038/nnano.2016.72

Minami, K., Kasuya, Y., Yamazaki, T., Ji, Q., Nakanishi, W., Hill, J. P., … Ariga, K. (2015). Highly Ordered 1D Fullerene Crystals for Concurrent Control of Macroscopic Cellular Orientation and Differentiation toward Large-Scale Tissue Engineering. Advanced Materials (Deerfield Beach, Fla.), 27(27), 4020–4026. https://doi.org/10.1002/ADMA.201501690

Morozov, S. V., Novoselov, K. S., Katsnelson, M. I., Schedin, F., Elias, D. C., Jaszczak, J. A., & Geim, A. K. (2008). Giant intrinsic carrier mobilities in graphene and its bilayer. Physical Review Letters, 100(1). https://doi.org/10.1103/PHYSREVLETT.100.016602

Mu, Q., Su, G., Li, L., Gilbertson, B. O., Yu, L. H., Zhang, Q., … Yan, B. (2012). Size-dependent cell uptake of protein-coated graphene oxide nanosheets. ACS Applied Materials & Interfaces, 4(4), 2259–2266. https://doi.org/10.1021/AM300253C

Mücksch, C., & Urbassek, H. M. (2011). Adsorption of BMP-2 on a hydrophobic graphite surface: A molecular dynamics study. Chemical Physics Letters, 510(4–6), 252–256. https://doi.org/10.1016/J.CPLETT.2011.05.036

Mueller-Klieser, W. (1987). Multicellular spheroids A review on cellular aggregates in cancer research. J Cancer Res Clin Oncol, 113, 101–122.

Nair, M., Nancy, D., Krishnan, A. G., Anjusree, G. S., Vadukumpully, S., & Nair, S. V. (2015). Graphene oxide nanoflakes incorporated gelatin-hydroxyapatite scaffolds enhance osteogenic differentiation of human mesenchymal stem cells. Nanotechnology, 26(16). https://doi.org/10.1088/0957-4484/26/16/161001

Ng, Elizabeth S., Davis, R., Stanley, E. G., & Elefanty, A. G. (2008). A protocol describing the use of a recombinant protein-based, animal product-free medium (APEL) for human embryonic stem cell differentiation as spin embryoid bodies. Nature Protocols, 3(5), 768–776. https://doi.org/10.1038/NPROT.2008.42

Ng, Elizabeth Stadler, Azzola, L., Sourris, K., Robb, L., Stanley, E. G., & Elefanty, A. G. (2005). The primitive streak gene Mixl1 is required for efficient haematopoiesis and BMP4-induced ventral mesoderm patterning in differentiating ES cells. Development, 132(5), 873–884. https://doi.org/10.1242/DEV.01657

Nishikawa, S. I., Jakt, L. M., & Era, T. (2007). Embryonic stem-cell culture as a tool for developmental cell biology. Nature Reviews Molecular Cell Biology 2007 8:6, 8(6), 502–507. https://doi.org/10.1038/nrm2189

Novoselov, K. S., Geim, A. K., Morozov, S. v., Jiang, D., Katsnelson, M. I., Grigorieva, I. v., Dubonos, S. v., & Firsov, A. A. (2005). Two-dimensional gas of massless Dirac fermions in graphene. Nature 2005 438:7065, 438(7065), 197–200. https://doi.org/10.1038/nature04233

Novoselov, K. S., Geim, A. K., Morozov, S. v., Jiang, D., Zhang, Y., Dubonos, S. v., Grigorieva, I. v., & Firsov, A. A. (2004). Electric field in atomically thin carbon films. Science, 306(5696), 666–669. https://doi.org/10.1126/SCIENCE.1102896/SUPPL_FILE/NOVOSELOV.SOM.PDF

Ohnuki, M., & Takahashi, K. (2015). Present and future challenges of induced pluripotent stem cells. Philosophical Transactions of the Royal Society of London. Series B, Biological Sciences, 370(1680). https://doi.org/10.1098/RSTB.2014.0367

Oldershaw, R. A., Baxter, M. A., Lowe, E. T., Bates, N., Grady, L. M., Soncin, F., … Kimber, S. J. (2010). Directed differentiation of human embryonic stem cells toward chondrocytes. Nature Biotechnology, 28(11), 1187–1194. https://doi.org/10.1038/NBT.1683

Owens, G. K., Kumar, M. S., & Wamhoff, B. R. (2004). Molecular regulation of vascular smooth muscle cell differentiation in development and disease. Physiological Reviews, 84(3), 767–801. https://doi.org/10.1152/PHYSREV.00041.2003/ASSET/IMAGES/LARGE/Z9J0030403131003.JPEG

Park, J., Wrzesinski, S. H., Stern, E., Look, M., Criscione, J., Ragheb, R., … Fahmy, T. M. (2012). Combination delivery of TGF- $\beta$ inhibitor and IL-2 by nanoscale liposomal polymeric gels enhances tumour immunotherapy. Nature Materials 2012 11:10, 11(10), 895–905. https://doi.org/10.1038/nmat3355

Pérez, R. A., Won, J. E., Knowles, J. C., & Kim, H. W. (2013). Naturally and synthetic smart composite biomaterials for tissue regeneration. Advanced Drug Delivery Reviews, 65(4), 471–496. https://doi.org/10.1016/J.ADDR.2012.03.009

Pelham, R. J., & Wang, Y. L. (1997). Cell locomotion and focal adhesions are regulated by substrate flexibility. Proceedings of the National Academy of Sciences of the United States of America, 94(25), 13661–13665. https://doi.org/10.1073/PNAS.94.25.13661/ASSET/29B06AAA-EF44-464A-91B5-8ED8DEB779BC/ASSETS/GRAPHIC/PQ2571755004.JPEG

Peyrin, J. M., Deleglise, B., Saias, L., Vignes, M., Gougis, P., Magnifico, S., Betuing, S., Pietri, M., Caboche, J., Vanhoutte, P., Viovy, J. L., & Brugg, B. (2011). Axon diodes for the reconstruction of

oriented neuronal networks in microfluidic chambers. Lab on a Chip, 11(21), 3663–3673. https://doi.org/10.1039/C1LC20014C

Qian, X., Song, H., & Ming, G. L. (2019). Brain organoids: Advances, applications and challenges. Development (Cambridge), 146(8). https://doi.org/10.1242/DEV.166074/19861

Quesenberry, P. J., Colvin, G. A., & Lambert, J. F. (2002). The chiaroscuro stem cell: a unified stem cell theory. Blood, 100(13), 4266–4271. https://doi.org/10.1182/BLOOD-2002-04-1246

Quint, C., Arief, M., Muto, A., Dardik, A., & Niklason, L. E. (2012). Allogeneic human tissue-engineered blood vessel. Journal of Vascular Surgery, 55(3), 790–798. https://doi.org/10.1016/j.jvs.2011.07.098

Raffaini, G., & Ganazzoli, F. (2010). Protein adsorption on a hydrophobic surface: a molecular dynamics study of lysozyme on graphite. Langmuir: The ACS Journal of Surfaces and Colloids, 26(8), 5679–5689. https://doi.org/10.1021/LA903769C

Raiborg, C., & Stenmark, H. (2009). The ESCRT machinery in endosomal sorting of ubiquitylated membrane proteins. Nature, 458(7237), 445–452. https://doi.org/10.1038/NATURE07961

Rao, C. N. R., Sood, A. K., Subrahmanyam, K. S., & Govindaraj, A. (2009). Graphene: The New Two-Dimensional Nanomaterial. Angewandte Chemie International Edition, 48(42), 7752–7777. https://doi.org/10.1002/ANIE.200901678

Rashid, S. T., & Alexander, G. J. M. (2013). Induced pluripotent stem cells: From Nobel Prizes to clinical applications. Journal of Hepatology, 58(3), 625–629. https://doi.org/10.1016/J.JHEP.2012.10.026

Ren, J., Braileanu, G., Gorgojo, P., Valles, C., Dickinson, A., Vijayaraghavan, A., & Wang, T. (2021). On the biocompatibility of graphene oxide towards vascular smooth muscle cells. Nanotechnology, 32(5). https://doi.org/10.1088/1361-6528/ABC1A3

Rong, P., Yang, K., Srivastan, A., Kiesewetter, D. O., Yue, X., Wang, F., Nie, L., Bhirde, A., Wang, Z., Liu, Z., Niu, G., Wang, W., & Chen, X. (2014). Photosensitizer Loaded Nano-Graphene for Multimodality Imaging Guided Tumor Photodynamic Therapy. Theranostics, 4(3), 229. https://doi.org/10.7150/THNO.8070

Rosas-Hernandez, H., Escudero-Lourdes, C., Ramirez-Lee, M. A., Cuevas, E., Lantz, S. M., Imam, S. Z., Majeed, W., Bourdo, S. E., Paule, M. G., Biris, A. S., & Ali, S. F. (2019). Cytotoxicity profile of pristine graphene on brain microvascular endothelial cells. Journal of Applied Toxicology : JAT, 39(7), 966–973. https://doi.org/10.1002/JAT.3786

Rossi, G., Manfrin, A., & Lutolf, M. P. (2018). Progress and potential in organoid research. Nature Reviews Genetics 2018 19:11, 19(11), 671–687. https://doi.org/10.1038/s41576-018-0051-9

Ryoo, S. R., Kim, Y. K., Kim, M. H., & Min, D. H. (2010). Behaviors of NIH-3T3 fibroblasts on graphene/carbon nanotubes: proliferation, focal adhesion, and gene transfection studies. ACS Nano, 4(11), 6587–6598. https://doi.org/10.1021/NN1018279

Ryu, J. H., Lee, Y., Kong, W. H., Kim, T. G., Park, T. G., & Lee, H. (2011). Catechol-functionalized chitosan/pluronic hydrogels for tissue adhesives and hemostatic materials. Biomacromolecules, 12(7), 2653–2659. https://doi.org/10.1021/BM200464X/SUPPL_FILE/BM200464X_SI_001.PDF

Ryu, S., & Kim, B. S. (2013). Culture of neural cells and stem cells on graphene. Tissue Engineering and Regenerative Medicine 2013 10:2, 10(2), 39–46. https://doi.org/10.1007/S13770-013-0384-6

Sales, V. L., Engelmayr, G. C., Mettler, B. A., Johnson, J. A., Sacks, M. S., & Mayer, J. E. (2006). Transforming growth factor-beta1 modulates extracellular matrix production, proliferation, and apoptosis of endothelial progenitor cells in tissue-engineering scaffolds. Circulation, 114(1 Suppl). https://doi.org/10.1161/CIRCULATIONAHA.105.001628

Sanchez, C., Arribart, H., & Guille, M. M. G. (2005). Biomimetism and bioinspiration as tools for the design of innovative materials and systems. Nature Materials 2005 4:4, 4(4), 277–288. https://doi.org/10.1038/nmat1339

Sasidharan, A., Panchakarla, L. S., Chandran, P., Menon, D., Nair, S., Rao, C. N. R., & Koyakutty, M. (2011a). Differential nano-bio interactions and toxicity effects of pristine versus functionalized graphene. Nanoscale, 3(6), 2461–2464. https://doi.org/10.1039/C1NR10172B

Settembre, C., Fraldi, A., Medina, D. L., & Ballabio, A. (2013). Signals from the lysosome: a control centre for cellular clearance and energy metabolism. Nature Reviews. Molecular Cell Biology, 14(5), 283–296. https://doi.org/10.1038/NRM3565

Shadjou, N., Hasanzadeh, M., & Khalilzadeh, B. (2017). Graphene-based scaffolds on bone tissue engineering. Https://Doi.Org/10.1080/21655979.2017.1373539, 9(1), 38–47. https://doi.org/10.1080/21655979.2017.1373539

Shah, S., Yin, P. T., Uehara, T. M., Chueng, S. T. D., Yang, L., & Lee, K. B. (2014). Guiding stem cell differentiation into oligodendrocytes using graphene-nanofiber hybrid scaffolds. Advanced Materials (Deerfield Beach, Fla.), 26(22), 3673–3680.https://doi.org/10.1002/ADMA.201400523

Sheng, Y., Wang, W., & Chen, P. (2010). Interaction of an ionic complementary peptide with a hydrophobic graphite surface. Protein Science: A Publication of the Protein Society, 19(9), 1639–1648. https://doi.org/10.1002/PRO.444

Shi, Y., Inoue, H., Wu, J. C., & Yamanaka, S. (2016b). Induced pluripotent stem cell technology: a decade of progress. Nature Reviews Drug Discovery 2016 16:2, 16(2), 115–130. https://doi.org/10.1038/nrd.2016.245

Simon, K. A., Mosadegh, B., Minn, K. T., Lockett, M. R., Mohammady, M. R., Boucher, D. M., … Whitesides, G. M. (2016). Metabolic response of lung cancer cells to radiation in a paper-based 3D cell culture system. Biomaterials, 95, 47–59. https://doi.org/10.1016/J.BIOMATERIALS.2016.03.002

Spence, J. R., Mayhew, C. N., Rankin, S. A., Kuhar, M. F., Vallance, J. E., Tolle, K., … Wells, J. M. (2011). Directed differentiation of human pluripotent stem cells into intestinal tissue in vitro. Nature, 470(7332), 105–110. https://doi.org/10.1038/NATURE09691

Takahashi, K., Tanabe, K., Ohnuki, M., Narita, M., Ichisaka, T., Tomoda, K., & Yamanaka, S. (2007). Induction of pluripotent stem cells from adult human fibroblasts by defined factors. Cell, 131(5), 861–872. https://doi.org/10.1016/J.CELL.2007.11.019

Takahashi, K., & Yamanaka, S. (2006). Induction of pluripotent stem cells from mouse embryonic and adult fibroblast cultures by defined factors. Cell, 126(4), 663–676. https://doi.org/10.1016/J.CELL.2006.07.024

Tang, X. Y., Wu, S., Wang, D., Chu, C., Hong, Y., Tao, M., Hu, H., Xu, M., Guo, X., & Liu, Y. (2022). Human organoids in basic research and clinical applications. Signal Transduction and Targeted Therapy, 7(1). https://doi.org/10.1038/S41392-022-01024-9

Temple, S. (2001). The development of neural stem cells. Nature, 414(6859), 112–117. https://doi.org/10.1038/35102174

Terraciano, V., Hwang, N., Moroni, L., Park, H. Bin, Zhang, Z., Mizrahi, J., … Park, H. (2007). Differential Response of Adult and Embryonic Mesenchymal Progenitor Cells to Mechanical Compression in Hydrogels. Stem Cells, 25(11), 2730–2738. https://doi.org/10.1634/STEMCELLS.2007-0228

Thibault, M. M., Hoemann, C. D., & Buschmann, M. D. (2007). Fibronectin, vitronectin, and collagen I induce chemotaxis and haptotaxis of human and rabbit mesenchymal stem cells in a

standardized transmembrane assay. Stem Cells and Development, 16(3), 489–502. https://doi.org/10.1089/SCD.2006.0100

Tonelli, F. M., Goulart, V. A., Gomes, K. N., Ladeira, M. S., Santos, A. K., Lorençon, E., Ladeira, L. O., & Resende, R. R. (2015). Graphene-based nanomaterials: biological and medical applications and toxicity. Nanomedicine (London, England), 10(15), 2423–2450. https://doi.org/10.2217/NNM.15.65

Tomioka, I., Maeda, T., Shimada, H., Kawai, K., Okada, Y., Igarashi, H., Okano, H. (2010). Generating induced pluripotent stem cells from common marmoset (Callithrix jacchus) fetal liver cells using defined factors, including Lin28. Genes to Cells: Devoted to Molecular & Cellular Mechanisms, 15(9), 959–969. https://doi.org/10.1111/J.1365-2443.2010.01437.X

Tsolis, K. C., Bagli, E., Kanaki, K., Zografou, S., Carpentier, S., Bei, E. S., Economou, A. (2016). Proteome changes during transition from human embryonic to vascular progenitor cells. Journal of Proteome Research, 15(6), 1995–2007. https://doi.org/10.1021/ACS.JPROTEOME.6B00180/SUPPL_FILE/PR6B00180_SI_003.PDF

Treuel, L., Jiang, X., & Nienhaus, G. U. (2013). New views on cellular uptake and trafficking of manufactured nanoparticles. Journal of the Royal Society, Interface, 10(82). https://doi.org/10.1098/RSIF.2012.0939

Unagolla, J. M., & Jayasuriya, A. C. (2022). Recent advances in organoid engineering: A comprehensive review. https://doi.org/10.1016/j.apmt.2022.101582

Utesch, T., Daminelli, G., & Mroginski, M. A. (2011). Molecular dynamics simulations of the adsorption of bone morphogenetic protein-2 on surfaces with medical relevance. Langmuir, 27(21), 13144–13153. https://doi.org/10.1021/LA202489W

Vander A.J., Sherman J., Luciano D. S., (2001). Human Physiology: The Mechanisms of Body Function.

Velasco, M. A., Narváez-Tovar, C. A., & Garzón-Alvarado, D. A. (2015). Design, materials, and mechanobiology of biodegradable scaffolds for bone tissue engineering. BioMed Research International, 2015. https://doi.org/10.1155/2015/729076

Vogt, N. (2021). Assembloids. Nature Methods 2021 18:1, 18(1), 27–27. https://doi.org/10.1038/s41592-020-01026-x

Wang, L., Tao, T., Su, W., Yu, H., Yu, Y., & Qin, J. (2017). A disease model of diabetic nephropathy in a glomerulus-on-a-chip microdevice. Lab on a Chip, 17(10), 1749–1760. https://doi.org/10.1039/C7LC00134G

Wei, M., Fu, Z., Wang, C., Zheng, W., Li, S., & Le, W. (2019). Graphene Oxide Nanocolloids Induce Autophagy-Lysosome Dysfunction in Mouse Embryonic Stem Cells. Journal of Biomedical Nanotechnology, 15(2), 340–351. https://doi.org/10.1166/JBN.2019.2684

Weissman, I. L. (2000). Stem cells: units of development, units of regeneration, and units in evolution. Cell, 100(1), 157–168. https://doi.org/10.1016/S0092-8674(00)81692-X

Woo, K. M., Jun, J. H., Chen, V. J., Seo, J., Baek, J. H., Ryoo, H. M., Kim, G. S., Somerman, M. J., & Ma, P. X. (2007). Nano-fibrous scaffolding promotes osteoblast differentiation and biomineralization. Biomaterials, 28(2), 335–343. https://doi.org/10.1016/J.BIOMATERIALS.2006.06.013

Wheeler, S. E. (2012). Understanding Substituent Effects in Noncovalent Interactions Involving Aromatic Rings, 14. https://doi.org/10.1021/ar300109n

Wichterle, H., Lieberam, I., Porter, J. A., & Jessell, T. M. (2002). Directed differentiation of embryonic stem cells into motor neurons. Cell, 110(3), 385–397. https://doi.org/10.1016/S0092-8674(02)00835-8

Wu, Z. S., Ren, W., Gao, L., Zhao, J., Chen, Z., Liu, B., … Cheng, H. M. (2009). Synthesis of graphene sheets with high electrical conductivity and good thermal stability by hydrogen arc discharge exfoliation. ACS Nano, 3(2), 411–417. https://doi.org/10.1021/NN900020U

Xu, H., Jiao, Y., Qin, S., Zhao, W., Chu, Q., & Wu, K. (2018). Organoid technology in disease modelling, drug development, personalized treatment and regeneration medicine. Experimental Hematology and Oncology, 7(1), 1–12. https://doi.org/10.1186/S40164-018-0122-9/TABLES/1

Young, H. E., & Black, A. C. (2004). Adult Stem Cells. https://doi.org/10.1002/ar.a.10134

Yu, F., Deng, R., Hao Tong, W., Huan, L., Chan Way, N., Islambadhan, A., Iliescu, C., & Yu, H. (2017a). A perfusion incubator liver chip for 3D cell culture with application on chronic hepatotoxicity testing. Scientific Reports, 7(1). https://doi.org/10.1038/S41598-017-13848-5

Yu, F., Deng, R., Hao Tong, W., Huan, L., Chan Way, N., Islambadhan, A., Iliescu, C., & Yu, H. (2017b). A perfusion incubator liver chip for 3D cell culture with application on chronic hepatotoxicity testing. Scientific Reports, 7(1). https://doi.org/10.1038/S41598-017-13848-5

Yu, F., Hunziker, W., & Choudhury, D. (2019). Engineering Microfluidic Organoid-on-a-Chip Platforms. Micromachines 2019, Vol. 10, Page 165, 10(3), 165. https://doi.org/10.3390/MI10030165

Yu, F., Selva Kumar, N. D., Choudhury, D., Foo, L. C., & Ng, S. H. (2018). Microfluidic platforms for modeling biological barriers in the circulatory system. Drug Discovery Today, 23(4), 815–829. https://doi.org/10.1016/J.DRUDIS.2018.01.036

Yu, F., Zhuo, S., Qu, Y., Choudhury, D., Wang, Z., Iliescu, C., & Yu, H. (2017). On chip two-photon metabolic imaging for drug toxicity testing. Biomicrofluidics, 11(3). https://doi.org/10.1063/1.4983615

Yu, J. (2020). Vascularized Organoids: A More Complete Model. International Journal of Stem Cells, 14(2), 127–137. https://doi.org/10.15283/IJSC20143

Yu, J., Vodyanik, M. A., Smuga-Otto, K., Antosiewicz-Bourget, J., Frane, J. L., Tian, S., Nie, J., Jonsdottir, G. A., Ruotti, V., Stewart, R., Slukvin, I. I., & Thomson, J. A. (2007). Induced pluripotent stem cell lines derived from human somatic cells. Science (New York, N.Y.), 318(5858), 1917–1920. https://doi.org/10.1126/SCIENCE.1151526

Yuan, J., Gao, H., Sui, J., Duan, H., Chen, W. N., & Ching, C. B. (2012). Cytotoxicity evaluation of oxidized single-walled carbon nanotubes and graphene oxide on human hepatoma HepG2 cells: an iTRAQ-coupled 2D LC-MS/MS proteome analysis. Toxicological Sciences: An Official Journal of the Society of Toxicology, 126(1), 149–161. https://doi.org/10.1093/TOXSCI/KFR332

Yuan, Z. (2015). A New Explanation of K. J. Arrow's Impossibility Theorem: On Conditions of Social Welfare Functions. Open Journal of Political Science, 05(01), 26–39. https://doi.org/10.4236/OJPS.2015.51003

Zakrzewski, W., Dobrzyński, M., Szymonowicz, M., & Rybak, Z. (2019). Stem cells: past, present, and future. Stem Cell Research & Therapy, 10(1). https://doi.org/10.1186/S13287-019-1165-5

Zhang, H., & Baehrecke, E. H. (2015). Eaten alive: novel insights into autophagy from multicellular model systems. Trends in Cell Biology, 25(7), 376–387. https://doi.org/10.1016/J.TCB.2015.03.001

Zhang, J., Griesbach, J., Ganeyev, M., Zehnder, A. K., Zeng, P., Schädli, G. N., Leeuw, A. de, Lai, Y., Rubert, M., & Müller, R. (2022). Long-term mechanical loading is required for the formation of 3D bioprinted functional osteocyte bone organoids. Biofabrication, 14(3). https://doi.org/10.1088/1758-5090/AC73B9

Zhang, Y. S., Arneri, A., Bersini, S., Shin, S. R., Zhu, K., Goli-Malekabadi, Z., Aleman, J., Colosi, C., Busignani, F., Dell'Erba, V., Bishop, C., Shupe, T., Demarchi, D., Moretti, M., Rasponi, M., Dokmeci, M. R., Atala, A., & Khademhosseini, A. (2016). Bioprinting 3D microfibrous scaffolds

for engineering endothelialized myocardium and heart-on-a-chip. Biomaterials, 110, 45–59. https://doi.org/10.1016/J.BIOMATERIALS.2016.09.003

Zhang, Y., Ali, S. F., Dervishi, E., Xu, Y., Li, Z., Casciano, D., & Biris, A. S. (2010). Cytotoxicity effects of graphene and single-wall carbon nanotubes in neural phaeochromocytoma-derived pc12 cells. ACS Nano, 4(6), 3181–3186.

Zhao, H., Ding, R., Zhao, X., Li, Y., Qu, L., Pei, H., Yildirimer, L., Wu, Z., & Zhang, W. (2017). Graphene-based nanomaterials for drug and/or gene delivery, bioimaging, and tissue engineering. Drug Discovery Today, 22(9), 1302–1317. https://doi.org/10.1016/j.drudis.2017.04.002

Zhou, J., Zhang, Y., Lin, Q., Liu, Z., Wang, H., Duan, C., … Wang, C. (2010). Embryoid bodies formation and differentiation from mouse embryonic stem cells in collagen/Matrigel scaffolds. Journal of Genetics and Genomics, 37(7), 451–460. https://doi.org/10.1016/S1673-8527(09)60064-3

Zisch, A. H., Lutolf, M. P., & Hubbell, J. A. (2003). Biopolymeric delivery matrices for angiogenic growth factors. Cardiovascular Pathology, 12(6), 295–310. https://doi.org/10.1016/S1054-8807(03)00089-9